A Study on Insulation Problems in Drive Fed Medium Voltage Induction Motors

by

Saeed Ul Haq

A thesis
presented to the University of Waterloo
in fulfillment of the thesis requirement for the degree of
Doctor of Philosophy
in
Electrical and Computer Engineering

Waterloo, Ontario, Canada, 2007

Author’s Declaration

I hereby declare that I am the sole author of this thesis. This is a true copy of the thesis, including any required final revisions, as accepted by my examiners.

I understand that my thesis may be made electronically available to the public.

Abstract

The PWM (pulse-width-modulated) type voltage source converters (VSC) allow a precise speed control of induction motors with maximum achievable energy efficiency. However, the rapid growth of this technology has created quite a concern, as the PWM waveform produces complex transients that stress the motor insulation, to much severe levels, compared to the normal sinusoidal voltage waveforms. As a result, the machine may fail prematurely due to increased dielectric heating; high turn-to-turn stress caused by non-linear potential distributions; increased partial discharge (PD) activities due to overshoots in pulse waveforms; and built-up space charge by high frequency signals. The present work therefore addresses the problems associated with enamelled wires and groundwall insulation in motor stator coil working under PWM-VSC.

In form-wound stator coils, the enamelled wires are meant to operate, mostly, at power frequency (60Hz) voltages. For PWM drive applications, it has been confirmed by using thermally stimulated depolarization current (TSDC) that the interfaces between the magnet wire insulation layers give rise to the accumulation of space charge that produces electric field perturbations inside the wire insulation. Numerical analysis further explored that this hazardous inter-turn electric field can be reduced up to ~48%, if the fewer number of insulation layers with similar over all thickness is used on the magnet wire. This reduction in field can be attributed to a lower accumulation of space charge during the aging duration and likely due to fewer number of trap levels.

To make the motor magnet wires less susceptible to high *dV/dt*, more resistant to PD, and to reduced space charge effects, a solution with new enamels, by adding inorganic nanofillers is suggested. In this regard, the wire specimens having fumed silica as nanofillers shows promising results compare to Al_2O_3 and TiO_2. In wire coatings, a filler concentration up to 1% shows considerable improvement in the life expectancy under PMW waveforms. Also, reduction in the amount of accumulated charges is additionally observed, more than 60%, which is associated with the conduction current that becomes larger for nanostructure materials. Nanofilled materials release trapped charges more rapidly, and thus, the residual charge after long depolarization times is smaller than those with pure materials.

In groundwall, the insulation problems stemming from the use of PWM-VSC with medium voltage motors are mostly associated with the voltage stresses on the surface of the coils. PD erodes the mica layers, aggravating the problem and, perhaps, eventually destroying the whole stator insulation system. At present, there is no industrial standard available to evaluate the groundwall insulation life of motors fed from PWM-VSC. To observe variations in the life expectancy and to understand the degradation mechanisms, accelerated aging of groundwall insulation under steep-front unipolar pulses are carried out, considering the operating temperature range, pulse switching frequency, and voltages. Compared to 60 Hz ac, the maximum drop in the lifetime is observed to be ~58%, when the pulse voltage waveform with switching frequency up to 3 kHz is used under normal ambient temperature. However, with the use of efficient cooling, an improvement in the life expectancy of the groundwall insulation is predicted and the drop in the lifetime is observed to be ~31%.

Furthermore, as hot spots are observed in groundwall insulation with PWM-VSC aging the dominant mechanism is believed to be more thermal than electrical. However, the degradation caused by electrical aging, becomes much faster in the presence of hot spots, when the PWM-VSC is used. The visual examination of groundwall stator bars established that the presence of both thermal and electrical stresses produces much severe effects, leading to delamination, cracking, embitterment, or depolymerisation of the insulation system. In this regard, the obtained results further explored that the characterizing of groundwall insulation for better applications at higher temperatures and frequencies is therefore essential. In order to extend the lifetime of form-wound stator coils under PWM-VSC, this research strongly believes that the changes are required in the processing of the coils at the VPI and enamel coating stages.

Acknowledgements

I would like to thank my supervisors, Dr. Shesha Jayaram and Dr. Edward Cherney for their, assistance, support, and guidance throughout the duration of this work.

I am grateful to the members of my Ph.D. committee for their valuable suggestions and critical comments.

Thanks to both Dr. Gorur G. Raju from University of Windsor, and Dr. Greg Stone from IRIS Power, who provided me a kind support and did a number of discussions on academic and research, during my graduate studies.

Thanks to my friends of the high voltage group: Ali, Alex, Ayman, Chahat, Chitral, Emad, Fermin, Gowri, Isaias, Jason, Luiz, Mostafa, Rocket, Ron, Sarajit, Tilak, and Yushep, for all the nice moments that we shared in the HV lab.

Thanks are due to Dave Messervey, Ramtin Omranipour and Meredith Stranges from GE Peterborough for providing test samples and for their valuable comments during this work.

Also, I would like to thank all our Pakistani, Indian, and Canadian friends in Waterloo for their company during these years.

To my family, especially my wife Qamar Saeed, mother Pukhraj Begum, and my father-in-law Ashfaq Ahmed Paracha, I express my deepest gratitude for the support provided.

I gratefully acknowledge NSERC and the Ontario Ministry of Training, Colleges and Universities for financially supporting my graduate studies and the Water and Power Development Authority (WAPDA), for the X-Pakistan study leave.

To my loving wife Qamar

To my mother, sisters and brother

Table of Contents

List of Tables

List of Figures

Chapter 1 Introduction

1.1 Introduction

The ac induction motor is the dominant motor technology in use today, representing more than 90 percent of installed motor capacity. These motors are available in single-phase and poly-phase configurations, in sizes ranging from fractions of a Watt to tens of thousands of Watts in output. A combination of an adjustable speed drive (ASD) with induction motor results in a high efficiency system, which can cover a wide range of applications. Therefore, due to the advantage of choosing the right-sized, energy efficient motor and to integrate it into an optimized drive-power system, the application of these motors is rapidly increasing [1].

In the early nineties, ASDs have been the linchpin, for precise speed control, which is varied almost continuously at all levels of power. In particular, modern converters implement the pulse width modulation (PWM) technique to produce variable frequency ac voltage waveforms, which are used in drive control. These PWM-type inverter drives allow for a more precise control of motors, than older technologies, which use variable voltage inverters (VVI), and current source inverters (CSI). In addition, such installations increase energy efficiency as much as 50%, improve the power factor and process precision, and provide other performance benefits such as soft starting and over-speed capability [2].

In a motor, the stator winding consists of strand, turn, and groundwall insulation. Typically, they consist of a combination of organic and inorganic materials. The groundwall, or slot insulation, is composed of epoxy-mica flakes on a fibre glass mat with a glass backing that separates the winding from the stator core; whereas, the turn insulation in the stators has an organic coating of polyimide. In windings where the turn and strand insulation differ, the turn insulation is usually a resin rich mica-paper tape.

Typically, this tape consists of small bits of mica flakes that are bonded to a fibreglass tape and wrapped around the insulated copper strands in the turn [3,4].

In medium voltage motors (≥1000 and ≤13800 volts), the form-wound stator coil insulation system is much more complex than the random-wound one (<1000 volts). In addition to the use of mica flakes tape, bonded with epoxy or polyester resin as the groundwall insulation, the insulation system of a coil includes a semi-conducting coating over the slot-section of the groundwall. Also, a special coating is applied at the ends of the slots to grade the electric stress in these regions. Presently, both groundwall and enamelled wire insulation are designed to operate, mostly, at power frequency voltages (60 Hz). Therefore, in PWM drive applications; which has fundamental component of 60 Hz, the fast switching produces complex transients that severely stress the motor insulation. As a result, a machine can fail prematurely due to the increased dielectric heating; high turn-to-turn stress, caused by the nonlinear potential distributions; increased partial discharge (PD) activities, due to overshoots in pulse waveforms; and built-up space charge by the high frequency signals.

As there are continual developments in power electronics, the industry is focusing on devising drives for medium voltage motors with switching devices which can both turn on and off with rapid transitions to reduce switching losses [5]. However, this is at the cost of additionally stressing the motor insulation. The premature failure of motor insulation appears to be associated with an accelerated degradation, caused by the following:

- An increased growth rate in the material's micro-cavities due to the local electro-mechanical energy storage and failure of stress grading due to high frequency components, as they are particularly designed for power frequency only [6].
- Dielectric heating that usually occurs because of high repetition rates and frequency components [6,7].
- Space charge injection/accumulation in the wire's enamel due to the high voltage wavefronts, (dV/dt), and frequency components [8].
- PD activity due to overshoots in the voltage waveform [9,10].

Overall, the progress in insulation technology has been slow and the few improvements are implemented only after a long and extensive evaluation. The introduction of new materials with higher thermal and electrical properties is essential for long-term reliability to avoid the above recognized problems. So far, with the conventional ac, the designs are optimized, so as to minimize the insulation degradation. However, problems of premature failure of medium voltage rotating machines, when fed by inverters must be addressed immediately, as it can affect the motor manufacturers standing. Although, different topics, related to the use of such power supplies have been investigated, the time has come to explore the physical mechanisms that are involved in the aging of insulating materials.

Therefore, the main objective of this thesis is to provide a comprehensive understanding of the degradation processes of medium voltage form-wound stator coils, in particular, within mica-based groundwall and turn-to-turn insulation, when they are exposed to various types of voltage waveforms [11,12,13]. More in depth knowledge of degradation mechanisms in form-wound stator coils will provide a better understanding of the phenomena responsible for accelerated aging and a better direction in the design and manufacturing of new materials and insulation systems.

1.2 Stator Winding Insulation Systems

To understand the design of a form-wound stator coil, various insulation systems are briefly described. The stator winding insulation system contains several components and features, which combined ensure that the required electrical isolation exists. The basic stator insulation systems that will be discussed in the following three subsections are composed of:

- Strand (or sub conductor) insulation
- Turn insulation
- Groundwall insulation

- Stress grading system

Figure 1.1 shows the cross-section of coils identifying different insulations in both random-wound and form-wound stator. Normally, the stator has two coils per slot in both medium and high voltage applications.

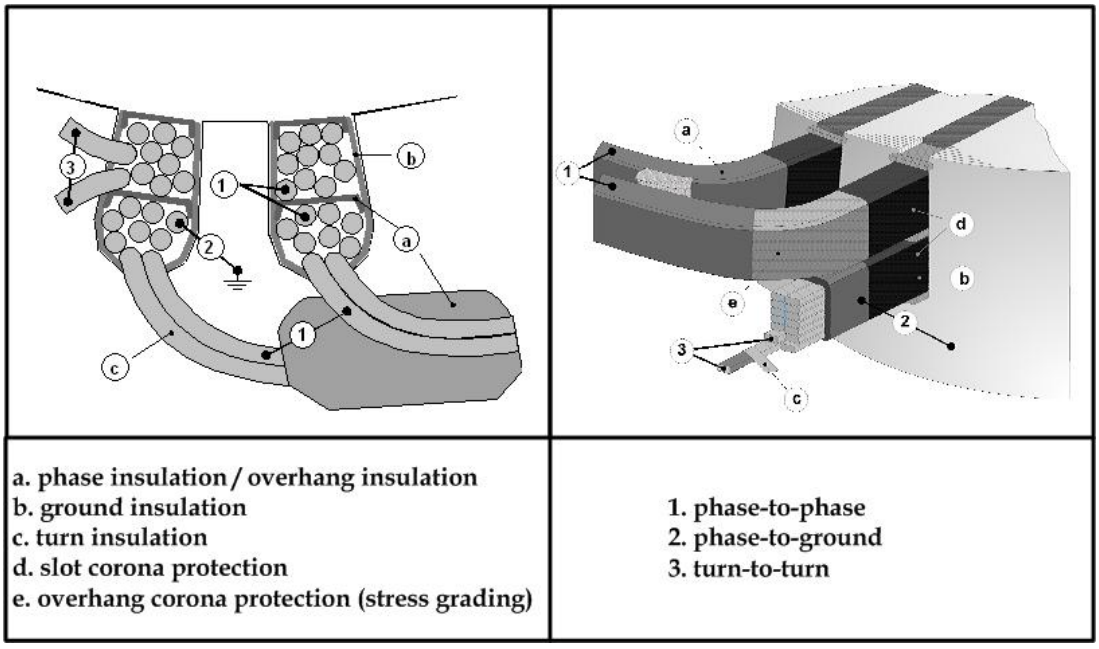

Figure 1.1: Cross-section of coils, identifying different insulation systems [14].

1.2.1 Strand and Turn Insulation

Typically, low-voltage motors are random-wound with round wire, insulated with polyamide-imide insulation or polyester with a polyamide-imide overcoat, having thermal class of 220 ^{o}C. Medium to high voltage motor are form-wound by rectangular shaped wire or strands. Such coils are divided into a number of turns that must be well insulated from each other. The cross-section of a typical form-wound stator coil showing strand insulation is depicted in Figure 1.2.

In multi-turn coils, the strand insulation can also be the turn insulation, a demand that, in the past, was met by separately wrapping resin rich mica tape. Often, this step can be

avoided by upgrading the strand insulation through machine tapping individual strands with a thin mica flake tape, supported with a polyethylene terephthalate (PET) or imide polymer film.

The magnet wire coatings in the form of enamel or polymer film may also contain additives such as alumina or special materials with a natural resistance to discharges, to protect it from PD [4]. Such corona-resistant enamels have been used since 1985 as turn insulation. The advantages are enhanced voltage endurance life, allowing reductions in the groundwall insulation thickness, and higher turn-to-turn surge withstand capability. However, the behavior of corona-resistant enamels is critical in today's variable speed drive applications [15]. In long-term, the continuous PD and overheating can cause shorts between the two strands, compromising the integrity of inter-turn and groundwall insulation systems.

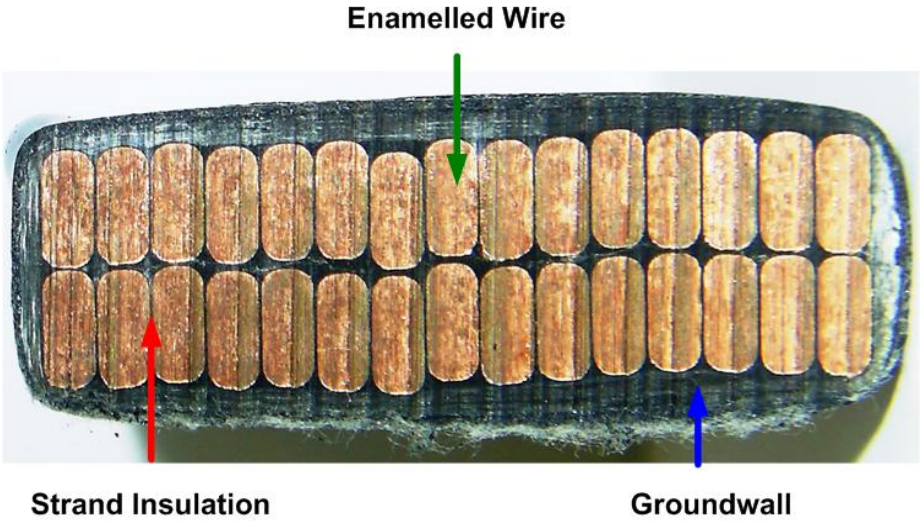

Figure 1.2: Cross section of a multi-turn form-wound motor coil.

1.2.2 Groundwall Insulation System

In the motor industry, the mica-based groundwall insulation system still predominates, where high voltage discharge effects and thermal stressing exist. The predominant mica species used in insulation systems are muscovite mica and phlogopite mica [16]. Mica, combined with different carriers, is considered the foundation of insulation systems.

These carriers are a mechanical support for the mica paper. Without them, the mica flakes cannot be applied to the conductors due to its own inherent low tensile strength. Currently, the commonly used carriers include films, fleece or mats, and glass fabrics [17].

The main purpose of the groundwall insulation system is to separate the copper conductors from the stator core. Usually, groundwall insulation failure triggers a ground fault relay. For a long service life, the groundwall must meet the rigors of the electrical, thermal, and mechanical stresses that it is subjected to. This class of insulation has additional stress relief coatings, which are important components in stator windings that operate at 4.16 kV or above [4]. These coatings are necessary to prevent PD from occurring on the surface of the stator bars or coils, and are described in the Section 1.2.3.

Common Groundwall Insulation Systems

Varnish Cambric (Class A 105 ^{o}C): In this class of insulation, the material is fully processed and no further impregnation or cure is needed when used for form-wound coil and bar insulation. It can be applied as half-lapped tapes or as a combination of tape and sheet. Slot pressing may be done to squeeze out the air between layers of the material and when heat is applied, the varnish softens and becomes tacky and on cooling, a weak bond develops between the layers of tape. This method, developed in Europe, was named the Haefley process. Due to the absence of mica, this insulation system was usually restricted to 2300 V and below [4,18].

Synthetic Resin Bonded Mica Tape (Class F 155 ^{o}C): This class of insulation system consists of small mica flakes that are deposited on a glass fibre backing tape. Once the tape has been wrapped around on the conductors, the synthetic resin is cured at an elevated temperature and pressure. This technique offers the possibility of manufacturing nearly void-free insulation that can withstand high dielectric stress. This insulation system has been in use since the sixties [15,18,19,20].

Silicone Rubber (Class H 180 ^{o}C): Silicone rubber is preferred in applications that need to withstand high temperatures. Although, there is no mica in this system, it can

withstand PD well. Silicone rubber is susceptible to mechanical damage and therefore restricts the voltage level to 6.0 kV. Silicone rubber can be used together with mica to increase the voltage level; however, the costs for such an insulating system are higher than for an epoxy system [18]. Later on, it was found by the motor manufacturers that silicone tended to creep with time and pressure. Therefore, the intended use in the slot section of machines was changed to end connections, where there is little or no compressive stress applied to the outside insulation [15].

In addition to the above groundwall insulation systems, shellac micafolium and asphalt-bonded mica tape (Class B 130 ^{o}C) were also used from the early 1900s to the 1970s. The use of these systems was discontinued due to heavy PD erosion and poor heat transfer.

1.2.3 Stress Grading System

In form-wound coils, it is not unusual to include semi-conducting tape and filler materials in the slot portion. Such tape provides a good electrical contact to the slot wall due to its low resistance. The filler materials protect the groundwall insulation from physical damage, and fill the gap between the coil surface and the slot. To avoid shorting the stator core laminations, a material with constant conductivity (10^{-2} to 10^{-5} S/m), which shows little or no field dependence, is typically used [21]. Silicon carbide (SiC) has been commonly used while zinc oxide varistor material (ZnO-VM) is under study as a replacement for SiC. This provides voltage stress grading system to limit the erosion from PD [18]. These materials exhibit electric field dependency, such that, high conductivity exists only where the electric stress is high, and a low conductivity, where the field is low [22].

Although semi-conducting tapes, slot fillers, black armour materials and stress grading coatings for stator coil insulation systems have performed well under normal power frequency, their exposure to PWM voltage source converters (VSC) led to an early failure of these coatings. It is reported that the high-frequency voltage pulses, associated with non-sinusoidal power supplies, cause a more rapid deterioration of the surface of

black armour or at the coil ends. This is a crucial consideration in the design of machines intended for inverter drives employing fast switching devices [23,24,25,26].

In this thesis, the focus is on turn-to-turn and mica-based main groundwall insulation system. Stress grading systems are not part of any investigation, as considerable work has already been reported in reference [25], to understand the impact of fast repetitive voltage pulses.

1.3 PWM-VSCs Waveform Stresses

As mentioned in Section 1.1, to control the speed of the ac motor and the power flow, a conversion of dc to ac voltage is necessary. For a broad power range, the two main concepts for conversion are the voltage and current source converters. These two categories are distinguished by the dc-link energy storage technique, such as, the current source converter (CSC) needs a dc-link inductor; whereas, the VSC requires a dc-link capacitor. In the early stages of high power conversion, CSCs are attractive due to the tight control of the converter current. However, this type of topology has lost its prestige in the drives market, and VSCs have become the most popular converters due to their simple topology, high efficiency, ease of control, and fast dynamic response. The PWM method is the dominant technique used in VSCs to control the voltage output [25].

The design of the VSCs is quickly changing so as to provide higher voltages and faster switching devices with steeper wavefronts. The option of increasing the voltage rating is preferred over increasing the current rating because of the practical limitations of the power components: motors, cables, and transformers [27]. The rapid developments in power electronics have facilitated this trend [28]. At present, it is possible to produce a VSC from 2.4 to 13.8 kV for motor drives [29].

To produce medium voltage drives for motor control, two types of power electronic devices with increased capabilities are used: the insulated gate bipolar transistor (IGBT), and the integrated gate commutated thyristor (IGCT) [27,28,30]. Both devices are used in PWM-VSCs. With advantages such as a high switching frequency, low cost, and more

mature technology, the IGBT is more commonly used in high power high voltage VSCs [30,31]. To meet the demand of converter manufacturers, IGBTs rated at 3.3 kV and 6.5 kV and with currents of approximately 1000 A are now available, and devices at 10 kV are being tested [27]. For PWM-VSCs, different schemes or topologies for connecting the switches can be found; however, at low voltages, the two-level converter is the most common, because it is simple and cost effective and more reliable than the multilevel topologies [27,32]. At this time, there is no predominant topology in medium voltage drives. Multilevel topologies (more than two-level) are preferred. The simplicity of three-level topology makes it one of the most common systems. In the present state-of-the-art, a two-level topology could represent the best option, especially with the higher ratings of the currently available switches; the associate insulation problems discourage the motor manufacturers to adopt it [23].

The typical PWM voltage waveform from an IGBT-based VSC is shown in Figure 1.3. These pulses exhibit rise times of hundreds of nanoseconds. Even though, two or more IGBTs are usually connected in series (stacks), despite they can present a high *dV/dt*, typically 15 kV/μs in machines and much higher in power system applications [28].

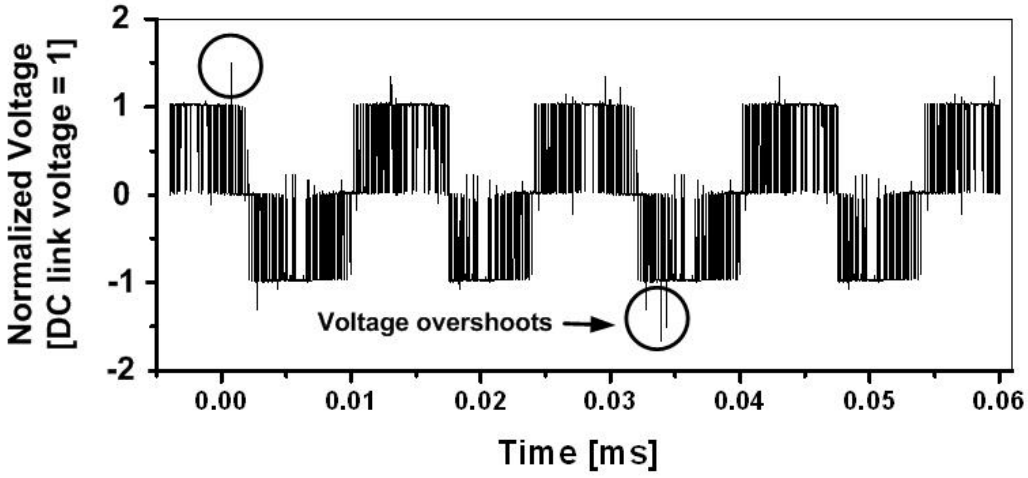

Figure 1.3: Measured voltage waveforms with overvoltage situation at the terminal of a star connection motor for a two-level converter.

A key point to make is that motors which were originally designed and manufactured to operate on sinewave 60 Hz power, are subjected to a significantly reduced dielectric life, when PWM voltage is applied: that is, a motor operating on sinewave power has a longer winding life expectancy than an identical motor operating on a PWM supply, if all the other stresses are constant.

1.3.1 Stresses due to Nonlinear Voltage Distribution

The increased use of PWM-VSCs has increased the stress on the winding insulation due to non-sinusoidal nature of the voltage waveform. Besides the amplitude, the steepness of the applied voltage is much higher than that of sinusoidal voltage. Consequently, the voltage distribution within the windings and coils is highly nonlinear and may cause voltage stresses between two consecutive turns [33].

According to Oyegoke [34] and Suresh *et al.* [35], the steep-front surges that strike a stator winding results in a large voltage across the inter-turn insulation in the motor coil, connected to the high voltage terminal. The distribution of the voltage across the high voltage motor coils is not uniform; that is, the high frequency content (in the megahertz range) of the surge voltage results in the capacitive division of the surge across the turn insulation, rather than controlled by the inductance. The shorter the rise time of the surge, the higher the frequency content and the voltage will be greater across the first few turns of the winding. The results of turn-to-turn voltage measurements for various coil ratings are summarized in Table 1.1 [34].

Figure 1.4 shows an example of nonlinear voltage distribution in 4.0 kV form-wound stator coil for a short rise time pulse (~100 ns). The voltage source is connected to the input end of the stator coil via cable. Detailed measurement of the voltage over each individual turn of coil is then performed. Each turn conductor of this eight-turn coil is exposed at appropriate positions to allow the measurement. The voltages are measured with respect to the stator core keeping it grounded throughout the measurements. The difference between the maximum voltages across individual turns represents the inter-turn stress. In such cases, if a motor winding is subjected to steep-front surges, the

breakdown strength of the turn insulation may be exceeded, causing a turn insulation breakdown, and eventually the groundwall insulation is affected [36].

Table 1.1: Voltage drop across the turns of the coil (% of the applied voltage) as a function of the cable length, L (m).

Coil Rating	# of Turns	Pulse Rise Time (ns)	Cable Length (m)	Voltage (% of the Applied Voltage)	
				Min	Max
4.0 kV[a]	8	100	1.5	5.5	16.8
			6.5	13.5	20.1
6.3 kV[b]	11	200	2.3	12.0	18.9
			4.0	14.2	19.2
			17.0	14.9	22.2
13.8 kV[c]	4	100	1.5	2.4	10.9
			6.5	2.1	14.3

[a,b]*Data obtained from reference [34].Both coils are non-turn tape and coil in (a) has no stress grading system.*

[c]*Data obtained from laboratory measurements. Test coil has resin rich mica turn tape and 3.5" stress grading system.*

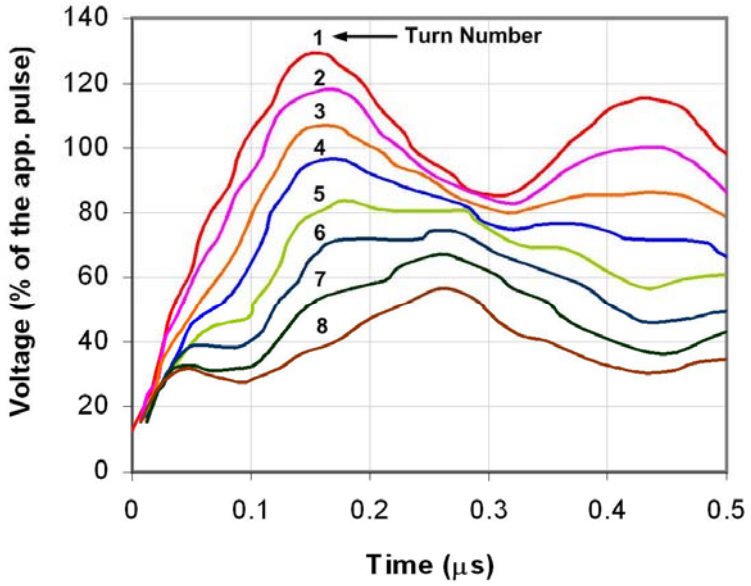

Figure 1.4: Measured pulse voltage for each turn in a single form-wound 4.0 kV stator coil having rise time of ~100 ns [34].

1.3.2 Impact of Cable Length

In many industrial applications, the inverter and the motor are at separate locations, requiring long motor leads. Although, the high switching speeds and zero switching loss schemes drastically improve the performance of the PWM drives, the high rate of the voltage rise (*dV/dt*) has an adverse effect on the motor insulation and bearings, and deteriorates the waveform quality where long cables are employed [37].

According to Bonnett [38], Wu *et al.* [39] and Lebey *et al.* [13], long cable lengths contribute to a damped high frequency ringing at the motor terminals, resulting in over voltages, further stressing the motor insulation. This ringing is due to the distributed nature of the cable leakage inductance and coupling capacitance (L-C). In addition, the voltage reflection is a function of the inverter output pulse rise time and the length of the motor cables, which behave as transmission lines for the inverter output pulses. It has been found that the pulses travel at approximately half the speed of light [40]. Moreover, if the pulse takes longer than half the rise time to travel from the inverter to the motor, a full reflection occurs at the motors, and the pulse amplitude is approximately double [12]. It is important that the insulation of the induction motor should be designed so that the insulation can withstand generated voltage stresses in the system. The stator winding overvoltages are based on the theory of voltage reflections. The motor cable behaves as a transmission line for the PWM pulses, and the voltage amplitude depends on the surge impedance of the motor [40].

In the mid 1990s, manufacturers introduced a combined motor inverter topology in which the inverter is integrally mounted within the motor enclosure, typically in the terminal box, or sometimes, as an extension to the motor casing. A very short cable length between the inverter output connections and the motor windings limits the reflection. As a result, the peak voltage problems do not exist. Due to the additional benefits of the simplified installation, reduced stress problems and lower costs, the topology is well suited for lower power applications, and is now rapidly gaining market acceptance [12]. However, problems still persist in large motor-drive systems due to space and cost issue during installations.

1.3.3 Partial Discharge (PD) Erosion

PD is a localized intermittent discharge, resulting from transient gaseous ionization in or on an insulation system, where the voltage stress levels exceed a critical value. Figure 1.5 illustrates some critical spots in the stator coil, which can cause PD activity.

Binder has provided some guidance for the acceptability of the discharge levels in machine insulation [41]. According to the author, machine insulation usually consists of mica, bonded with resin that has high discharge resistant. As a result, a discharge magnitude as high as 1000 pC is acceptable in the stator bars. However, if the discharge magnitude is within the range of 10-100 nC, the deteriorated bar should be located and replaced as soon as possible, since it can cause severe damage to the entire stator insulation system [41,42].

According to Shugg [43] and Stone *et al.* [36], the major factors that affect the PD or corona are voltage, frequency, temperature, voltage pulsation, humidity, geometry, dielectric thickness, and pulse rise time. The degradation of stator insulation that is exposed to a continuous voltage stress above the partial discharge inception level (PDIV) is a physical erosion of the insulation due to the PD attack. The aging process results from an erosion of the insulation material, reducing its thickness at the discharge sites, until its breakdown voltage capability is mitigated below the level of the applied voltage peak. However, if the voltage stress is below the PDIV, no premature degradation occurs [44]. Relatively little literature exists on insulation aging and PD development under fast repetitive voltage surges.

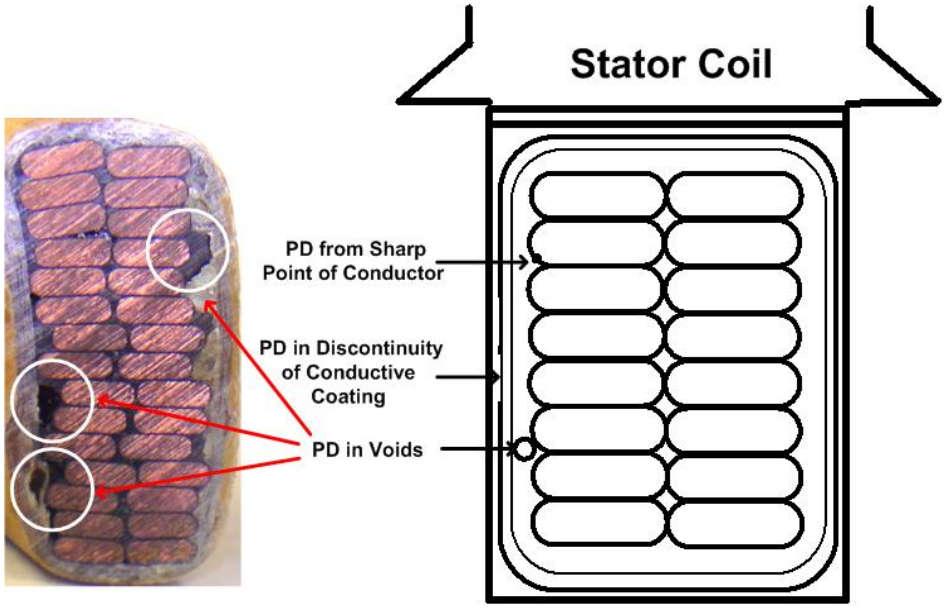

Figure 1.5: Origin of PD on stator winding insulation system.

1.3.4 Consequences of Space Charge

In PWM drive applications; the deterioration of magnet wire coatings can occur due to two detectable phenomena; namely, PD and charge trapping and injection. Furthermore, several investigators consider that the trapped charge carrier; establishing an electric space charge field, play an important part in the aging process [6,13].

The types of charge carriers in polymers and their role in conduction and breakdown have been presented by Idea [45] and Wintle [46]. There are four basic types of charge carriers possible in polymers: electrons, holes, positive ions, and negative ions. The principle charge carriers, which are important with reference to degradation, are believed to be electrons and holes. Polymers in terms of multi-layer arrangement provided considerable evidence for the existence of both these carriers from a large number of thermally stimulated current (TSC), pulsed electro-acoustic (PEA) method and photoconduction experiments [45,47]. However, the relative importance of electrons and holes is not so well established [48].

Carrier Injection

In polymers, the mobility of charge carriers has a significant effect on the conduction, tree initiation process, and degradation. At high values of electric fields (>1 MV/cm), where the electrons have sufficient energy to exist in the conduction band along polymers chains, much higher mobilities can occur. Before conduction can occur, there must be a source of charge carriers available. Some of these carriers could be liberated in the polymer bulk by radiation or extremely high electric fields, which are common in PWM-VSCs that are always acting on the trapped carriers. In practical situations, the most likely source of electrons and holes is injection from electrodes [48].

The three basic electrical mechanisms for injecting charge are Schottky-type emission, Fowler-Nordheim-type emission, and contact charging. The mechanism of contact charging will inject electrons or holes even when there is no external electric field [49,50]. Contact charging occurs because of the relative difference in the Fermi levels for the metal and polymer coating, and the existence of electron and hole traps between the valence band and the conduction band. Since the Fermi levels must be equal when the metal and polymer are brought in contact, charge is transferred to the polymer. This charge resides in relative deep traps, very close to the electrode. At moderate to high fields, electric field assisted thermionic emission, or Schottky emission, is one process. As, at higher stresses, adequate force is available from the field for the electron to be injected from the electrode; therefore, the injected current density (J) is given by the expression [49]:

$$J = AT^2 \exp\left[\frac{\alpha E^{\frac{1}{2}} - \Phi}{kT}\right] \tag{1.1}$$

where E, is electric stress, T, is temperature, Φ is metal work function and A, α, k are constants. According to Fowler-Nordheim, at higher fields, a greater number of electrons will gain sufficient energy to tunnel the barrier and J becomes [49]:

$$J = AE^2 \exp\left[\frac{-B\Phi^{\frac{3}{2}}}{E}\right] \tag{1.2}$$

The constants *A* and *B* in Equations (1.1) and (1.2) are conduction parameters, extracted from the experimental investigations [51].

Charge Trapping and Build-up of Space Charge

The trapping of electrons and holes plays a critical role in the build-up of space charges, conduction, and can probably cause slow degradation of magnet wire. Traps, by definition, are entities at a fixed location in the polymer, which attract either electrons or holes. In terms of energy, the traps have energy levels in the energy gap between the valence band and the conduction band. Hole traps are few tenth of an eV above the top of the valence band (shallow hole traps) or up to several eV above top of the valence band (deep hole traps). Similarly, shallow electron traps are just below the bottom of the conduction band; whereas, deep electron traps are several eV below the bottom of the conduction band. For clear description, a band model of a polymer containing electron and hole traps is depicted in Figure 1.6.

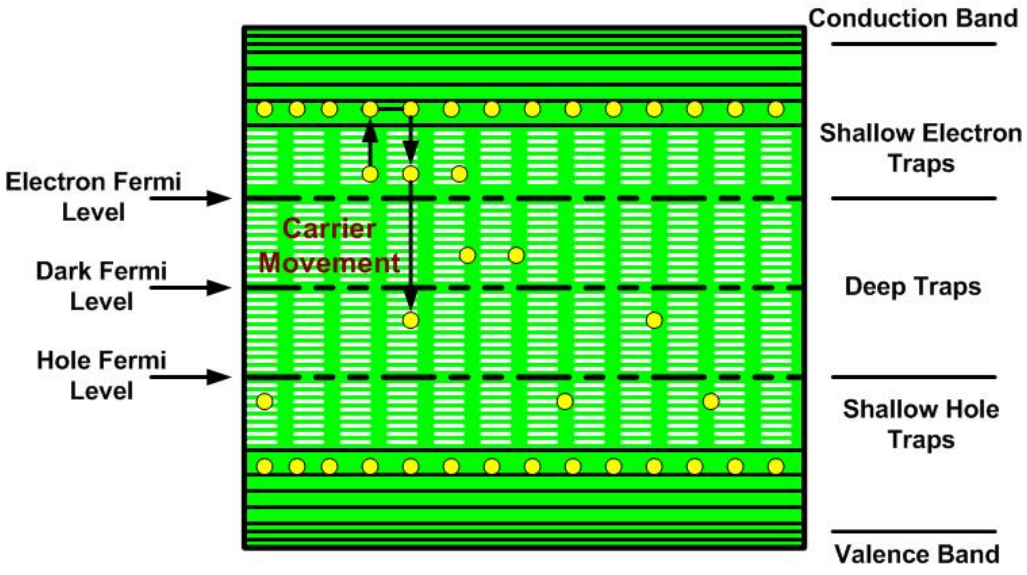

Figure 1.6: Energy band model in polymers containing electron and hole traps [52].

There are different causes of traps in practical polymers. The most probable types occur at the interfaces between crystalline and amorphous regions of the polymer, defects or dislocations in the polymer chain or side-chains, sharp bends or kinks in the polymer

chain, and at residual cross-linking agents. In such case, the TSC and thermally stimulated luminescence (TSL) studies are the most popular means of determining the trap energy levels.

Influence of PWM-VSCs Wavefront (*dV/dt*) on Space Charge

In PWM drive, the steepness of the wavefront (*dV/dt*) provides frequency components in the range of MHz. Thus, a possible relationship between the fronts and the dielectric response of the material exists. The presence of high frequency components, due to fast rise time voltage pulse produces maximum losses in the polymeric insulating materials, which are used in the motor stator coil.

The presence of such a component leads to a delay (out-of-step) polarization of some of the dipoles, and some of the charges might not disappear with voltage reversal. A sudden reversal of the voltage blocks the free charges of a particular sign, replacing them with free charges of the opposite sign. In fact, three types of charges are present on the surface of the insulation; that is, free charges, bound charges, resulting from a natural polarization; and blocked charges, which appear when the reversal of the voltage is too fast for certain types of dipoles. Once created, and independent of concentration, these charges, due to electrostatic forces, tend to move either perpendicularly or tangentially with respect to the surface. In the first case, the perpendicular movement creates a certain space charge in the bulk; whereas, in the second case, it corresponds to the charge flow on the surface. In the former, the electric field distortion ($\nabla.E \neq 0$), is biased to the injection of new charges and this cumulative process may cause the breakdown of the material [11,13]. In the later case, distribution of charges over the surface can lead to a high surface charge concentration at particular points, e.g., at the slot ends. During the unavoidable phenomenon of recombination, a local breakdown of the surface can occur, damaging the insulation system [53]. Several factors, including temperature, relative humidity, vibration, the nature of the insulation, and its geometry can mitigate or amplify this phenomenon.

1.4 Literature Review

This section offers a review of the previous research on various aspects of both groundwall and turn-to-turn insulation. The previous work has been classified into principal categories: namely; the evaluation of the groundwall insulation in inverter-fed stator coils, the effect of a high wavefront (*dV/dt*) and frequency components on magnet wire coatings in terms of the space charge accumulation, trapping, and charge injection, the performance of discharge resistant nanofilled magnet wires, designed for inverter-duty applications, and the modelling of the inter-turn field distribution under steep-front voltage pulses.

1.4.1 Space Charge Accumulation, Trapping and Charge Injection in Magnet Wire Coatings

The impact of space charge accumulation on aging processes of polymeric insulating materials, subjected to PWM-VSC stresses has been widely neglected. The main reason is that, in addition to the space charge detection problem, the cause of the breakdown is mainly attributed to manufacturing features such as the presence of contaminants, cavities, protrusions and, in general, the defects that are able to trigger localized degradation processes such as PD and electrical treeing [54]. Consequently, for many years, failure was associated with “macroscopic” causes, rather than to microstructure.

Recently, the contribution of space charge to the insulation damage in stator windings is considered more carefully [55]. The presence of space charges, in the insulation bulk and/or at the insulation-electrode interfaces, can significantly affect the electric field distribution, and, in turn, the field concentration, inducing accelerated damage that triggers early insulation breakdown [13].

To understand the failure of low-voltage winding insulation, Yin [56] has performed an extensive investigation by using a square wave with a varying voltage level, frequency, duty cycle, and rise time. They have concluded that the failure of magnet wires under repetitive pulses, as seen in inverted fed motors, is not the result of a single

factor but of the combined effects of PD, dielectric heating, and space charge formation. The voltage overshoots that are produced by PWM drives can be above the discharge inception voltage (DIV). PD may therefore be present in inverter-fed motors. In addition to PD, pulses with fast rise time and high frequencies enable the insulation to generate local dielectric heating, which increases the local temperature. The degradation rate of the insulation, is therefore, increased. Furthermore, the fast rise and fall of pulses make it possible for space charge to accumulate in the winding insulation and on its surface. However, the investigation focuses on problems in random-wound insulation only [56].

Bellomo *et al.* [13] and Lebey *et al.* [57] have also reported on low-voltage stator insulation with particular respect to intrinsic aging under the working conditions of a voltage *V*, *dV/dt*, and frequency, where an interaction between the voltage characteristics and the material properties exist, that is, for *V* lower than the DIV. In conclusion, the existence of a new type of phenomena, the building and trapping of charges associated with these new stresses that is responsible for the slow degradation of turn insulation has been proposed. However, the authors have suggested that it is now necessary to quantify, in more accurate manner, the consequences on the lifetime of real systems.

In response to the new phenomena [13,57], Hudon *et al.* [8] have conducted tests which confirm that PD might not be the only mechanism responsible for turn insulation failure. Other mechanisms can contribute to the degradation of insulation, when it is subjected to PWM pulses, even at voltages below the DIV. Since these phenomena are related to the interaction between the applied voltage characteristics (e.g., frequency, *dV/dt*, and duty cycle) and the materials, such aging is intrinsic. These inherent degradation mechanisms can be related to charge injection and charge movement within the insulation. However, one conclusion is that a further understanding of the degradation mechanisms involved is still required [8].

Degradation mechanisms occurring in low-voltage magnetic wires fed by PWM waveforms were recently investigated by Fabiani *et al.* [6] through PD and space charge measurements. Their experimental results of space charge measurements showed a relation between space charge features (e.g. trap depth and trap-controlled mobility) and PD quantities (e.g. PDIV, PD amplitude and repetition rate). It has been shown that

inorganic-filled corona resistance materials do not exhibit always life improvements. However, insulation systems with increased surface conductivity or smaller trap depth (increased mobility) can present smaller partial discharges and thus, a longer life.

From the previous discussion, it is clear that space charge accumulation and trapping influence the performance of stator winding insulation. However, most of the studies have targeted low voltage random-wound motors and such phenomena are not well understood for high voltage insulation systems with ASDs.

1.4.2 Performance of Nanofilled Magnet Wires

In insulation, the use of nanofillers is very attractive for upgrading and diversifying the properties of polymers. Researchers, scientists, and practitioners across almost the entire spectrum of disciplines are exploring and developing science and engineering at the nano-level. Among these disciplines, the progress in the field of polymer sciences has demonstrated that the addition of nanofillers represents a very attractive route to upgrade and diversify material properties. There is a broad range of nanofiller types, which has led to nanopowders with different morphologies (size and shape, cluster composition, and dispersion) that are currently being used in PD resistant magnet wire coatings [58,59,60]. When the size of fillers is reduced to nanometer scale, it has been observed that usually, less than 10 wt% is enough to significantly change the material properties [60].

Hudon *et al.* [61] have reported that the nanofillers in magnet wire enamel are essential for a variety of reasons, including discharge resistance, matching the coefficient of the thermal expansion, thermal conductivity enhancement, mechanical reinforcement, and abrasion resistance. Based on the experimental and field results, manufacturers of magnet wires with fillers that have a uniform coating has become popular due to the growing use of ASDs. In ASDs, the repetition rate of the IGBT pulses increases substantially, and can be as high as 20 kHz with a rate of rise of several kV/μs. Because of the inductive nature of the winding, large reflections can occur at the motor end, and a significant portion of this voltage can develop across the adjacent turns. If the DIV is exceeded, this will lead to discharge activity. Therefore, in the presence of PD, fillers in

the material then form a line of defense to limit the erosion process and prevent further degradation of the insulating material [61,62].

To prevent PD erosion, enamelled wires with a multi-layered insulation system containing dispersed metal oxides have been marketed. Such wires have a three-layer structure, in which a PD resistant coating film is placed in between the normal coatings to compensate for the electrical and thermal properties. This structure is also helpful in the improvement of the mechanical properties. However, according to Kikuchi *et al.* [63], even though the wires life is improved, they are vulnerable to the electrical degradation due to the weakening of the materials, caused by mechanical stresses such as elongation, bending, and stretching. Such defects are potential areas for electrical degradation due to PD activity. Recently, alumina (Al_2O_3) nanoparticles have been successfully applied to film-coated magnet wires. The outcome has resulted in excellent electrical, thermal, mechanical, and physical properties of wires available for medium voltage applications. However, experimental investigation has demonstrated some large scatter in the breakdown data, suggesting that the mechanism needs to be examined [64].

The use of nano-meter-level particle size of silica (SiO_2), if dispersed uniformly, has exhibited a high level of resistance to PD; however, the SiO_2 concentration has a strong correlation with the wire flexibility, compared with that of other types of fillers [63,64]. As a consequence, the control of material properties, such as uniformity in the organic coatings and concentration (wt%) of nanoparticles, are major issues in wire nanotechnology. Increasing the loading (wt%) of nanofillers can further increase the PD resistance, but weakens the mechanical strength, influencing the electrical degradation. In this regard, Kikuchi *et al.* [63] have developed, a state-of-the-art inverter surge resistance enamelled wire, which is based on silica-polyesterimide nanocomposite material. This wire is specifically designed for low voltage applications, and proves to be satisfactory for PD resistance, flexibility, and mechanical strength.

In addition, a reduction of the amount of accumulated charges common to materials with nanofillers has been reported [65]. The variation in the space charge is associated with the conduction current that increases for nanostructural materials. These materials release trapped charges more rapidly, and thus, the residual charge after long

depolarization periods is smaller than that of pure materials [65]. Also, Nielson has examined the effects of nanofillers on space charge accumulation, but the insulation integrity of the nanocomposites is still not understood [66,67].

Brütsch and Weyl [68] have reported some results for the filled enamelled wires that are available in the market. The authors have suggested the use of filled enamelled wire with the problem that it may have little effect or no effect on the PDIV, but does reduce the rate of erosion under corona conditions. Furthermore, filled enamelled wires have a limited mechanical strength due to the brittleness of the coating.

Overall, the literature review indicates that under most operating conditions that are relevant to inverter-fed motors, PD resistant insulation lasts longer. This is valid when the voltage surges are large enough or above the DIV. However, around the DIV, the materials behave differently and the use of PD resistant insulation can even reduce a motor's life [62]. This assumption does not apply in all operating conditions, or for all types of PD resistant and standard insulation. It is possible that testing the insulation at higher voltages is not adequate to evaluate the insulation intended for PWM operation. A more comprehensive set of quality control tests still needs to be conducted, along with the development of new techniques, to adequately compare different nanofilled insulating materials [62].

1.4.3 Modelling

It has been accepted that space charge is one of the parameters that influences the degradation of motor insulation significantly under pulse energization. Although PWM waveforms are bipolar due to the fast polarity reversal of the potentials, space charge accumulation is possible, and experimentally, its presence has been observed. However, there are no analytical procedures available to calculate the space charge influenced field that can cause localized discharges.

The dynamics of the electric field distribution, influenced by the charge accumulation between two adjacent enamelled wires and in the complex geometry of the coatings can be determined by two methods: the equivalent circuit method and the finite element

method (FEM) [69,70]. New methods such as the boundary element method [71] or improvements to the existing models [72] have been suggested. The validation of such methods has been difficult, but a good approximation of the influence of the various parameters can be obtained with the proper use of these models. However, most of these comparisons between the simulations and experimental measurements have been carried out at low frequencies (50 or 60 Hz). There is an interest in verifying the reliability of the models that are used to study the effect of fast pulses. The difficulties with the measurements under fast pulses make this task difficult if not impossible, as there are no measuring techniques to determine the voltage or electric field distribution under voltage pulses.

As a result, it is important to compute the space charge injected electric fields in the motor insulation interfaces under pulse applications by using FEM. Since, the applied voltage is a steep-front short voltage pulse, a transient finite element analysis seems be the best option for the computational studies. The effects of rise time and the accumulated charge with different concentrations on electric fields must be analyzed in simple geometries by using 2D software.

1.4.4 Evaluation of Groundwall Insulation

Several problems, relevant to reliable stator insulation system need to be considered and resolved, when medium voltage induction motors are fed from PWM-VSC. Due to some recent premature failures of motors fitted with adjustable speed drives (ASD), standards organizations such as the National Electrical Manufacturer's Association (NEMA) and International Electrotechnical Commission (IEC) are developing technical specifications to ensure that motors can withstand the increased stresses during their service life. In this regard, some of the initial standards are NEMA MG 1 Parts 30 and 31 [73], in which the inverter-duty motors undergo voltage impulses. However, it has been recognized that the short impulse test might not always ensure a satisfactory life. Similarly, the IEC TS 60034-25 [74], which provides a detailed discussion on motor insulation stresses and

methods for determining short-term withstand test limits, does not include the high-cycle fatigue conditions that motors undergo during their service life [75,76,77].

To complement the available test procedures, IEC TS 60034-18-42, which is under development, will propose a new test procedure for the qualification of groundwall insulation [78]. However, the inverter drive designers are employing higher voltages and faster switching devices with steeper wave fronts. There appears to be a lack of coordination between the motor manufacturers and the drive designers, which needs to be realized. Therefore, further experimental work is recommended for the establishment of a qualification scheme suitable for a variety of different inverter system designs [14,78].

Up to certain extent, the insulation performance of form-wound stator coils, rated at 4.16 kV for inverter-duty application, has also been investigated by Ramme *et al.* [44]. The parameters were the influence of voltage level, rise time, switching frequency, and temperature on the generation of PD for two different coil insulation systems. In their work, the authors did not study the insulation "life/aging" integrity test for longer duration. Accordingly, they have concluded that all the investigated factors influence PD inception, except the switching frequency. It has little effect on PD voltage inception levels but higher switching frequencies do generate a larger amount of external PD such that severe degradation occurs under inverter-fed conditions.

The literature review confirms that fewer investigations have been devoted to understand the fundamental problems associated with the dielectric breakdown of groundwall insulation under high frequency transients [79]. Although some work has been conducted in this area [26,44], experimental results are still lacking. So far, most of the investigations have been carried out in the random-wound motor stators (Type I insulation) [14]; whereas, the rapid aging in form-wound motor stators (Type II insulation) still requires clear understanding. Therefore, the proposed test method, along with the present results can be considered as a possible contribution for the further development of test standards and new techniques for the design of form-wound insulation of inverter fed motors.

1.5 Aim of the Present Work, and Thesis Organization

It has been demonstrated that the supply waveforms that are generated by the power converters play a major role in insulation degradation. Although, modern PWM converters have significantly reduced the harmonic distortions at low frequencies, the higher frequency harmonics has increased significantly. High frequency harmonics affect the voltage waveform with ringing and overshoots having amplitude, which depend on the supply-motor connection and commutation time of solid-state switches. In addition, the voltage drop is not uniform along the motor winding, being concentrated on the first few turns of a winding. Therefore, if PDIV is reached, even in a portion of the winding, PD activity that can be negligible under 60 Hz sinusoidal ac, can promote accelerated insulation degradation, especially in the presence of organic insulation (e.g., polyamide-imide based insulation).

The principal goal of this work is to promote a comprehensive understanding of the degradation processes of medium voltage form-wound stator coils that are exposed to various voltage waveforms. Medium voltage form-wound stator coils are selected since much of the previous work deals with low voltage (~1000V) random-wound motors fed by ASDs. A more in-depth knowledge of degradation mechanisms in form-wound stator coils provides a better understanding of the phenomena responsible for accelerated aging and a better direction in the design and manufacturing of new materials and insulation systems.

This research therefore focuses on a better understanding of the aging mechanism in form-wound coils under steep-front pulses. The main objectives of this thesis are listed below:

- A better understanding of the degradation phenomena in form-wound coils under steep-front voltage pulses.
- Contribution to the development of an accelerated aging test technique for form-wound insulation.
- A possible contribution to the development of new techniques for the designs of form-wound insulation for use on PWM-VSCs.

This thesis is organized as follows:

In Chapter 2, the preparation of the groundwall and turn insulation samples for this research is detailed. Also, the experimental setup and numerical analysis using FEM for the estimation of field distribution, due to space charge buildup, is described.

Chapter 3 presents the results of the long-term pulse aging test on groundwall insulation to determine its impact regarding the operating temperature range, pulse switching frequency, and voltages. In addition, the degradation mechanism of enamelled wires, subjected to different voltage waveforms, is examined. Since PWM drives exhibit significant harmonics and transients, the aging of test specimens, prepared by using enamelled wires, is accomplished by sinusoidal (60Hz), fast repetitive unipolar voltage pulses, and high frequency ac waveforms. The relation between the enamelled wire failure and the type of aging is also established by determining the residual dc strength. The thermally stimulated depolarization current (TSDC) technique is used to explain mechanisms such as charge injection and trapping, and to characterize the electrical behavior of the dielectrics under steep-front unipolar pulse voltage applications.

The analysis of results presented in Chapter 3, along with the examination of failed areas in the groundwall insulation, is discussed in Chapter 4. An empirical relationship between the relative release of the stored charge and aging time is additionally performed. Also, the performance of nanofillers for the suppression of PD in enamel wire coatings is included in the discussion.

Chapter 5 provides a summary and conclusions of the work on stator coil insulation systems studied. This last chapter also suggests some further work to improve the reliability of stator coil insulation system.

Chapter 2 Materials, Experimental Setup and Modelling

2.1 Introduction

In this chapter, the methods for preparing the samples for the turn and the groundwall insulation are described. For the turn insulation, in addition to the three commercial magnet wires, specially tailored nanofilled magnet wire specimens are also used. Both high frequency and steep-front pulses are adopted to age the specimens, and later, the residual life is determined by using the two-parameter Weibull distribution. To test the groundwall insulation, samples are prepared with a single layer of mica tape. To evaluate the performance of the groundwall insulation, the IEEE Std. 1043, 1553 [80,81], and IEC TS 60034-18-42, which is under development by IEC TC2 Working Group (WG) are followed [78]. To examine the space charge behaviour of the magnet wire coatings, the thermally stimulated depolarization current (TSDC) technique is employed. The experimental setup described in this chapter includes a high frequency ac and pulse aging circuit, thermovision system, PD measurement system, and imaging tool software. The software is applied to measure the surface roughness after capturing images using scanning electron microscopy (SEM).

2.2 Materials

2.2.1 Magnet Wire Base Material

The material used for the base coat for the magnet wires, relates to Pyre-ML® products, which belongs to the family of materials based on aromatic polyimides [82]. Pyre-ML® wire enamel RC-5019, which consists of polyamic acid; 13 wt% solution in NMP/aromatic hydrocarbon, is the most thermally stable organic material. It is essential

to note that RC-5019 does not contain any filler. The magnet wire base coat polyimide, after curing, can withstand high temperatures and is therefore used to protect motors, generators, transformers, and other apparatus, which operate continuously at temperatures up to 240 ºC [82]. Also, Pyre-ML® protects heavy-duty motors which, due to a temporary extreme overload, acceleration torques, or stalls, are subjected to even higher temperatures (up to 400 ºC) for limited periods of time. Some of the properties of Pyre-ML® RC-5019 are summarized in Table 2.1 [82,83]

Table 2.1: Polyimide **(**ML® RC-5019**)**, magnet wire base material properties.

Property	**Value**
Viscosity	5000-7000 cps
Glass Transition Temperature	285 ^{o}C
Thermal Conductivity	0.12 W/m·K
Dielectric Strength	345 kV/mm
Dielectric Constant @ 1 MHz	3.2
Dissipation Factor @ 1 MHz	0.008

2.2.2 Nanofillers for Magnet Wire Overcoat

The proposed magnet wire specimens are built following NEMA MW-1000 specifications [84]. The first three layers consist of Pyre-ML® polyimide, are the base, on which the nanofilled insulation layer is applied. Three different types of nanofillers are selected for the overcoat. Their desirable characteristics for application in magnet wire insulation are highlighted below.

- Rutile Titanium Oxide, TiO_2

  TiO_2 is useful as a filler to achieve a higher thermal conductivity and improved electrical properties. Since the heat stability improves significantly when it is used

with organic materials, nanoparticles of TiO_2 are promising candidates for the magnet wire coating. Table 2.2 lists typical values of some of the properties of interest [85].

Table 2.2: Properties of selected rutile titanium oxide, TiO_2.

Property	**Typical Value/Characteristic**
Particle Size (nm)	54
Density (gm/cm^3)	4.2
Particle Appearance	Crystal Structure
Applications	Semiconductor materials, capacitors, pigments and coatings
Disadvantage	Not cost effective
Advantages	1. Good dispersion 2. High resistance to PD 3. Improves dielectric withstand and voltage endurance characteristics 4. Mitigate space charge effects 5. Improves thermal properties

- Fumed Silica, SiO_2

  Fumed silica is man-made silica of nano-size. It has desirable properties in terms high purity, extremely large surface area, and a characteristic to prevent slumping in coatings. Fumed silica has good thermal properties and imparts excellent mechanical and electrical characteristics to dielectric coatings. It can also be successfully used in a Pyre-ML® polyimide solution, a typical enamel wire coating. Consequently, in this work, the silica is chosen to improve the PD

resistant property of an enamelled wire. Table 2.3 reflects the typical values of some of the properties of the selected fumed silica, SiO_2 [86].

- Alumina, Al_2O_3

  The nanoparticles of alumina (Al_2O_3) are selected due to its excellent dielectric and thermal properties. The reason for the selection of Al_2O_3 is to obtain a good comparison with the other two selected fillers by using the same concentration by wt% in the Pyre-ML® polyimide solution. The physical characteristics of alumina powder used in this work are given in Table 2.4 [87].

Table 2.3: Properties of selected fumed silica, SiO_2.

Property	**Typical Value/Characteristic**
Particle Size (nm)	32
Density (gm/cm^3)	2.2
Particle Appearance	Smoke-like
Applications	Rubbers and plastics, insulator coatings, batteries and abrasives, and sealants
Disadvantages	1. Difficult to get a good dispersion 2. Brittleness in coatings
Advantages	1. High resistance to PD 2. Prevents caking 3. Provide thickening 4. Improves dielectric strength

Table 2.4: Properties of selected alumina, Al_2O_3.

Property	Typical Value/Characteristic
Particle Size (nm)	62
Density (gm/cm^3)	3.2
Particle Appearance	Spherical
Applications	Outdoor insulation, HV insulator coatings, batteries and abrasives and thin film polymers
Disadvantages	1. Comparatively less resistant to PD 2. Destructed by acids 3. Brittleness in coatings
Advantages	1. Excellent dielectric and thermal properties 2. Good resistance to tracking and erosion

2.2.3 Turn-to-Turn Specimens for Insulation Test

Wire Specimen Preparation

The wire specimens are built following NEMA MW-1000 specifications [84]. Three layers of Pyre-ML® polyimide are the base on which the nanofilled insulation layer is applied. The addition of a small amount, 1 to 5 wt%, of inorganic nanofillers, is sufficient for performance improvement [88], and a higher concentration can cause the coating to become more brittle. Therefore, the nanofillers, ~1 % by weight, are used in standard polyimide enamel.

To prepare the nanofilled layers, the nanofillers and the polyimide base material are first weighed and then mixed in a blender. The material is degassed in a vacuum chamber, and applied to a magnet wire, having rectangular shape with smooth and continuous corner, bearing a width of 7.09 mm, and a thickness of 2.82 mm. After the material is cured in an oven for 2 hours at 90-100 ^oC, the uniformity of the filler

dispersion is checked by using a SEM with an energy dispersive x-ray (EDAX) attachment. The cross section of magnet wire specimen used for experimental investigations, is displayed in Figure 2.1.

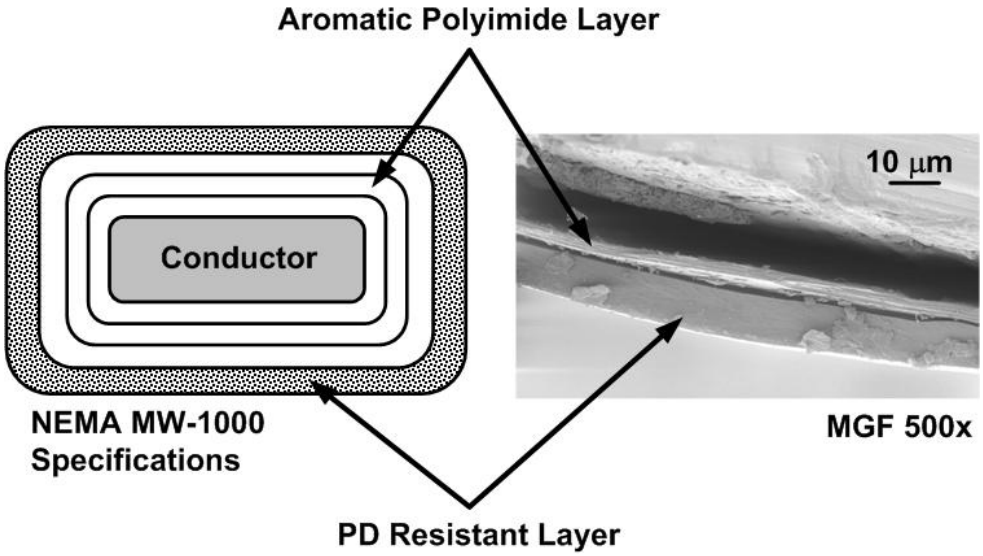

Figure 2.1: Cross section of magnet wire showing coating layer.

Table 2.5 summarizes the characteristics of the conventional (S_1, S_2, and S_3) and newly developed enamelled wires (S_4, S_5 and S_6). The coating on S_1 is achieved by a Pyre-ML® solution that is aromatic polyimide-based; whereas, S_2 and S_3 are PD resistant. Enamelled wires S_4, S_5, and S_6, developed in the laboratory, also belong to the family of PD resistant wires and have an additional coating of filled fumed silica (SiO_2), TiO_2, and Al_2O_3, respectively.

Table 2.5: Parameter related to magnet wire.

Magnet Wire	Coating Type on Magnet Wire	Coating Thickness (μm)	DC Dielectric Strength (V/m)x10^7	$PDIV_p$ (kV)
S_1	Pyre-ML® Polyimide	38	29.0	0.92
S_2	Corona Resistant MGF	25	31.0	1.28
S_3	Kapton FCR	41	29.0	1.70
S_4	Pyre-ML® Solution + SiO_2	28	27.0	1.15
S_5	Pyre-ML® Solution + TiO_2	24	29.0	1.05
S_6	Pyre-ML® Solution + Al_2O_3	27	25.0	0.98

Sample for Inter-Turn Evaluation

The type of testing necessary to evaluate the inter-turn insulation for inverter duty motors is not standardized; as a result, based on form-wound coil geometry, the turn-to-turn samples are prepared, as shown in Figure 2.2. These geometries (both type A & B), which are similar in configuration, based on the stator coil design. Here, the square or rectangular magnet wires are arranged in a parallel fashion to achieve a single turn. As shown in Figure 2.2, plastic sheets are used instead of metallic ones to avoid external damage to the magnet wire coating and to keep the stress uniform between the two turns.

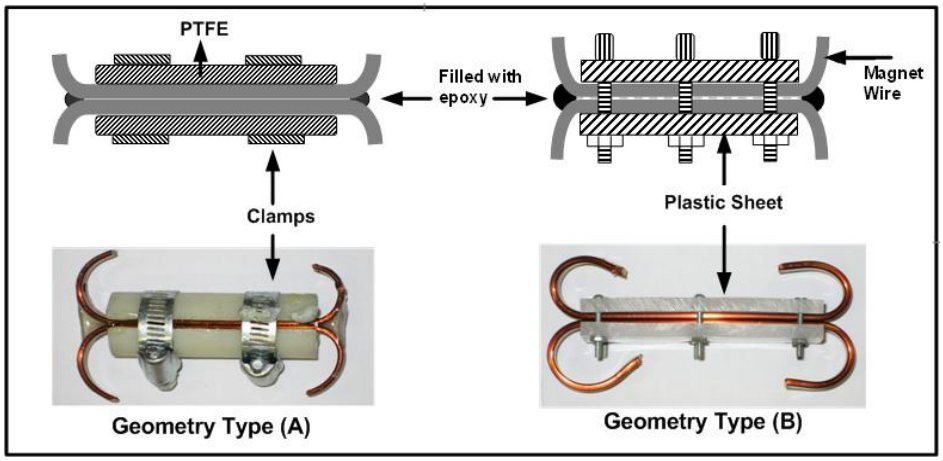

Figure 2.2: Turn-to-turn samples geometry.

2.2.4 Preparation of the Samples for the Groundwall Testing

The VPI stator bar samples received from the manufacturer rated at ~1.5 kV_{L-L} are wound with only one layer of the groundwall mica-paper tape. The samples are used for different types of accelerated aging tests. In this research, 42 stator bar samples are used. As a reference, the samples are serially marked. To reduce the capacitive load on the test supply, a reduced sample size of ~51 cm in length is chosen. Figure 2.3 depicts these VPI stator bars along with their specifications.

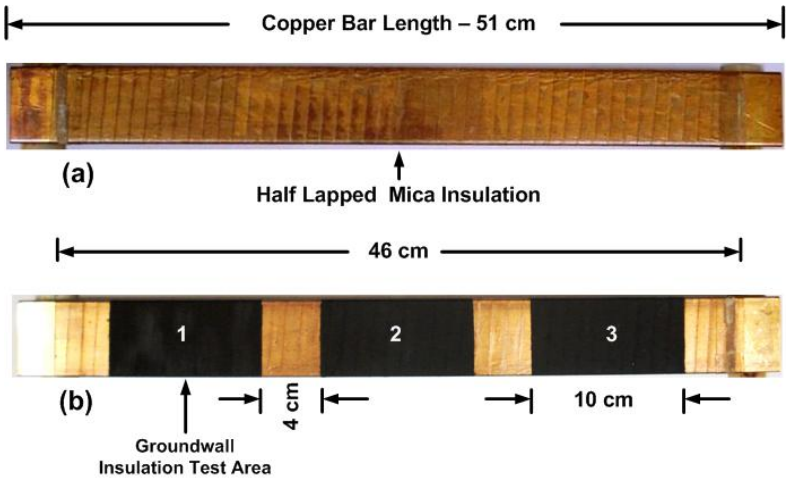

Figure 2.3: VPI stator bars with single layer of mica flakes tape (a) bars received from manufacturer, (b) divided into three test areas.

In Figure 2.3, each test area marked as 1 to 3 has further six-layer geometry. The six-layer geometry has several advantages and is depicted in Figure 2.4. A graphite loaded conductive coating in the form of paint is applied as layer 2 to the stator bar specimens, along with a stress grading layer 3, which prevents PD from occurring at the end of the conductive paint. Aluminum foil (layer 4) is used as a ground plate and for uniform heat distribution, when the heat is applied. The purpose of layer 5 is to fill the gaps at the edges of the foil and to precisely record the thermal profiles by using the infrared camera. In addition, the black conductive layer helps to correct the emissivity, which is adjusted to 0.92 in this experiment. Outer layer 6, like layer 3, consists of stress coating. This prevents any further PD from occurring at the end of aluminum foil and to avoid stresses that are concentrated near the ends during the high frequency pulse voltages.

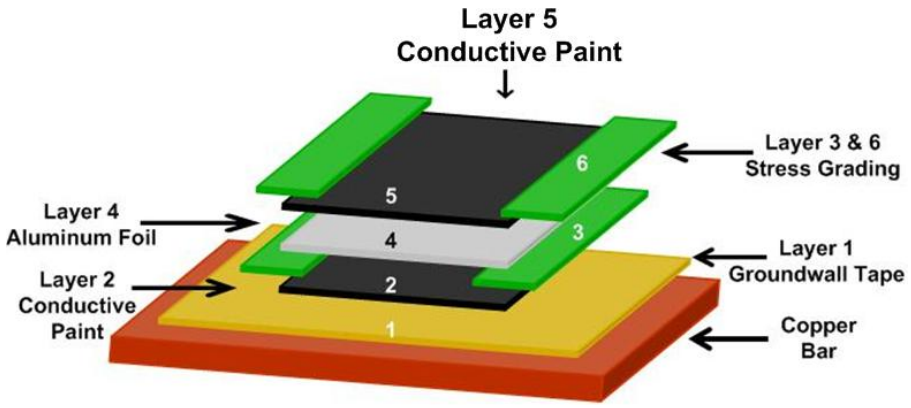

Figure 2.4: A six-layer system for evaluation of groundwall insulation.

2.3 Statistical Analysis

In the breakdown testing of the solid dielectric insulation and in reliability studies, scatter appears in the data, even within a fixed set of test conditions. Such variability is normal of life data. Moreover, substantial research has been done on how to analyze such data to extract the significant conclusion from the midst of the inherent variability. To summarize the data, statistical techniques are applied, such that, each set of recorded data is represented by a mean and standard deviation. The two most common statistical

distributions for analysis are the Weibull distribution and the Lognormal distribution [89].

In this thesis, a group of 15 enamelled wires that belong to the same class are aged. Therefore, the Weibull distribution, which is a version of the Extreme Value group of distributions, is applied for the measurement of dc breakdown strength. Considering the breakdown strength, E as the random variable, the cumulative Weibull distribution may be written, in its general form, as:

$$F(E) = 1 - \exp\left[-\left(\frac{E - E_{\min}}{\eta}\right)^{\beta}\right]; E_{\min} < E < \infty, \qquad (2.1)$$

$$\beta, \eta > 0$$

where E is the electric field in V/m. The parameter η represents the magnitude of E for failure of 63.2% tested units. Similarly, parameter β, which is also called the "shape parameter", is a measure of the dispersion of E. Parameter E_{min}, which is referred to as the threshold parameter (V/m), is that value of E, below which, breakdown is not possible. In order to plot the data on probability paper, it is necessary to rank them and assign cumulative probability failure, F, to each point. A calculation of F depends on the ranking scheme such as the median and mean ranking. The median ranking is given by:

$$F(i,n) = \frac{i - 0.3}{n + 0.4} \qquad (2.2)$$

where the mean rank approximation is:

$$F(i,n) = \frac{i}{n+1} \qquad (2.3)$$

In Equations (2.2) and (2.3), n is the recorded breakdown times or voltages in order from smallest to largest, which are ranked from i = 1 to n. Although, the mean rank function is recommended by IEEE Std. 930, the median rank is shown to be more appropriate [89,90,91].

2.3.1 Weibull Analysis

In predicting the equipment life, the Weibull analysis is well developed [48]. Usually, the shape and scale parameters are estimated by the method of Maximum Likelihood Estimation (MLE) [92]. Statistically, the MLE is considered to be robust and yields estimators with good statistical properties. By considering Equation (2.1), the likelihood function is defined by [93,94,95,96]:

$$L(E_1,E_2,...,E_N \mid \overline{\eta},\overline{\beta}) = L = \prod_{i=1}^{N} f(E_i;\overline{\eta},\overline{\beta}) = \prod_{i=1}^{N} \frac{\overline{\beta}}{\overline{\eta}}\left(\frac{E_i}{\overline{\eta}}\right)^{\overline{\beta}-1} \exp\left[-\left(\frac{E_i}{\overline{\eta}}\right)^{\overline{\beta}}\right] \quad (2.4)$$

The logarithmic likelihood function is given by:

$$A = \ln L = \sum_{i=1}^{N} \ln f(E_i;\overline{\eta},\overline{\beta}) = \sum_{i=1}^{N} \ln\left[\frac{\overline{\beta}}{\overline{\eta}}\left(\frac{E_i}{\overline{\eta}}\right)^{\overline{\beta}-1} \exp\left[-\left(\frac{E_i}{\overline{\eta}}\right)^{\overline{\beta}}\right]\right] \quad (2.5)$$

The ML estimators ($\overline{\eta},\overline{\beta}$) are determined by taking the partial derivatives of *A*, with respect to $\overline{\eta}$ and $\overline{\beta}$, and setting them to zero; i.e., $\frac{\partial A}{\partial \overline{\eta}} = 0, \frac{\partial A}{\partial \overline{\beta}} = 0$. By solving Equation (2.5), best estimates $\overline{\beta}$ and $\overline{\eta}$ are:

$$\frac{1}{\overline{\beta}} = -\frac{1}{N}\sum_{i=1}^{N} \ln E_i + \frac{\sum_{i=1}^{N} \ln(E_i)^{\overline{\beta}} \ln E_i}{\sum_{i=1}^{N} \ln(E_i)^{\overline{\beta}}} \quad (2.6)$$

and

$$\overline{\eta} = \left[\frac{1}{N}\left(\sum_{i=1}^{N} (E_i)^{\overline{\beta}}\right)\right]^{\left(\frac{1}{\overline{\beta}}\right)} \quad (2.7)$$

Equation (2.6) is written in terms of $\overline{\beta}$ only, and is solved by an iterative technique such as the Newton-Raphson iterative technique. Once $\overline{\beta}$ is obtained, $\overline{\eta}$ can be determined by using Equation (2.7). Although the methodology for the MLE is simple, the implementation is mathematically complex [97]. In this work, a specialized package, WinSmith Weibull software, is used to find the ML estimates of the Weibull distribution parameters [98].

2.4 Modelling of Systems with Inter-turn Stress

The modelling of the inter-turn insulation to identify the stresses is an essential tool in the design and optimization of such systems. An accurate model can be applied to do the following [99,100]:

- To describe how the system is likely to behave under particular conditions,
- To modify the material characteristics to fit specific requirements;
- To predict the effects of aging and determine the material's lifetime in order to establish a maintenance policy.

Typically, problems with magnet wire coating systems can be represented with the subdomains of the conductors, subdomains of perfect dielectrics (air or another surrounding medium and main coating insulation). Conductors are considered to be perfect conducting regions of known potential.

For a region with the coating materials, the first Maxwell equation (Ampere's law) states that:

$$\nabla \times H = J + \frac{\partial D}{\partial t} \tag{2.8}$$

J is the conduction current density and $\frac{\partial \mathrm{D}}{\partial \mathrm{t}}$ is the displacement current density.

By applying the divergence to both sides of Equation (2.8),

$$\nabla \cdot \nabla \times H = \nabla \cdot [J + \frac{\partial D}{\partial t}\ ] = 0$$

or

$$\nabla \cdot [J + \frac{\partial D}{\partial t}\ ] = 0 \tag{2.9}$$

Equation (2.8) is known as the continuity equation, where

$$J = \sigma_{DC} E + D\,,$$

$$D = \varepsilon_o E + P\,,$$

where P is the remanent polarization, which is the displacement when no electric field is present, and E is:

$$E = -\nabla V$$

In the above equations, σ is the electrical conductivity and ε_0 is the vacuum permittivity [101]. In this thesis, the above equations are solved, by considering σ as a constant, because the main conduction mechanism in polyimide is the Ohmic, which remains stable in a wire range of electric field [102]. The surrounding media is assumed to be perfect, linear, and isotropic dielectrics. The equations for each subdomain are combined by boundary conditions [103], and solved analytically or numerically. FEM (finite element method) [104] Finite Differences [105], or an Equivalent Circuit Model [99] can be used for this purpose. In this research, FEM is used to model the field distribution in the intern-turn insulation due to some advantages it has, for example, over the equivalent circuits models. More details on the inter-turn model for verifying the electric field stress are found in Appendix A.

2.4.1 Finite Element Method (FEM)

The FEM approximates the solution to the partial differential equations in a domain, composed of a mesh of elements whose vertices are called nodes. FEM, applied to any problem, is defined in four steps [106] as follows:

Step 1: Discretize the solution region in a finite number of subregions named elements.

Step 2: Define the equations that describe a typical element.

Step 3: Combine all the elements in the solution region.

Step 4: Solve the system of equations obtained.

In the FEM, the potential distribution in a volume is defined by the principle of minimum energy [107]. In this case, the electrical energy over the domain $\boldsymbol{\Omega}$, is given by as follows [108,109]:

$$W = \int_{\Omega} \frac{1}{2} (\sigma + \varepsilon \frac{\partial}{\partial t}) \mathrm{E} \cdot \mathrm{E} \, d\Omega \tag{2.10}$$

or, in the frequency domain, as:

$$W = \int_{\Omega} \frac{1}{2} (\sigma + j\varpi \varepsilon) \mathrm{E} \cdot \mathrm{E} \, d\Omega \tag{2.11}$$

In the FEM, the functional, given by Equation (2.9), is discretized and formulated as a function of the nodal potentials, and then minimized to give the voltage distribution [109,110].

In the present work, FEMLAB® version 3.3, a finite element software, is used to compute the electric field between the polymer interfaces. FEMLAB® can directly solve the problems, described by Equation (2.10) and Equation (2.11).

2.5 Characterization of Stored Charge in Solid Dielectrics

Solid dielectric materials may store charges, when subjected to external electric field. In highly resistive materials, such as polyethylene and polyimide, space charges, usually, accumulate near the electrode. These stored charges move out of the sample under the short circuit conditions with the assistance of the thermal motions of the molecule, leading to a current in the external circuit. Various mathematical models and experimental techniques are now available to study charge trapping and its release in solid dielectrics [111,112].

Thermally stimulated depolarization current (TSDC) is one of the techniques that is available to investigate the electrical properties and charge storage mechanisms in dielectrics. Before initiating TSDC measurements, specimens of enamelled wire S_1 and S_2 were sent to TECHIMP in Bologna, Italy, to confirm the existence of space charge build up by using pulsed electroacoustic (PEA) technique. Excessive charge trapping was observed in both types of specimens, for which, the results are reported in appendix B.

Once the charge trapping is confirmed, TSDC method was adopted for different type

of magnet wire samples during the course of this investigation. In TSDC measurements, it is additionally possible to confirm the contribution of more than one factor that can contribute to the measured current. The magnitude of the current, which is affected by the disorientation of the dipoles [111], is determined by the charge liberated from the traps. The existence of this current is explained by the movement of the de-trapped charge in the field that is determined by the accumulated charges [112]. The motion of the molecules, which substantially increases with higher temperatures facilitates the movement of the charges and determines the increase in the current and is commonly known as the temperature-dependent component of the current. The experimental conditions are selected so that the time-dependent component can be neglected in certain cases, and the analysis can be carried out as a function of the temperature.

2.5.1 Thermally Stimulated Depolarization Current (TSDC) Method

The TSDC method is based on the depolarization of a sample by thermal activation. The depolarization current, when the temperature is increased at a constant rate, exhibits a series of maxima, which correspond to the different thermal transitions. In this technique, which is also known as the temperature-dependent TSDC method, the sample is polarized by externally applied electric field, E_P, at temperature, T_P. Polling time, t_P, which varies and is much longer than the relaxation time, models the aging period of the specimen. Subsequently, this polarization is frozen-in by cooling the sample in the presence of the applied electric field to room temperature such that the frozen-in polarization remains unchanged, even if the external field is switched off. By heating the sample at a constant rate, the depolarization current, as the polarizing specimens relax, is detected by a high sensitive electrometer. For dipoles with a single relaxation time, the decay of the polarization, due to the disorientation of the dipoles following the removal of the electric field at $t = 0$ and temperature T is given by Bucci *et al.* [113]. The authors developed a complete theory to account for the dipolar reorientation. During the TSDC measurements the dipoles reorient on reheating the dielectric and the rate at which the instantaneous

polarization P decays with time can be expressed in terms of the polarization and relaxation time τ by:

$$\frac{dP}{dt} = \frac{-P}{\tau(T)} \tag{2.12}$$

and the solution to Equation (2.12) is:

$$P(t) = P(0)\exp\left[\frac{-t}{\tau(T)}\right] \tag{2.13}$$

where $P(0)$ is the "frozen-in" steady state polarization at $t = 0$, and $\tau(T)$ is the relaxation time, which is characteristic of the frequency jumps of the dipole and is given by the Arrhenius relationship:

$$\tau(T) = \tau_o \exp\left(\frac{-\varepsilon_a}{kT}\right) \tag{2.14}$$

where τ_o^{-1} is the characteristic frequency factor, ε_a is the activation energy of dipolar orientation, and k is Boltzmann's constant. By assuming a linear increase in temperature, from low value T_o, at rate x (where $T = T_o + xt$), the non-isothermal equation for the polarization decay is:

$$P(t) = P(0)\exp\left(-\int_0^t \frac{dt}{\tau(T)}\right) \tag{2.15}$$

Therefore, the current density j, generated by the decay in polarization is simply the rate of change of polarization and expressed by:

$$j(T) = -\left(\frac{P(0)}{\tau}\right)\exp\left(-\int_0^t \frac{dt}{\tau(T)}\right) \tag{2.16}$$

Combining Equations (2.14), (2.15) and (2.16) corresponding to depolarization,

$$j(T) = -\left[\frac{P(0)}{\tau_0}\right]\exp\left(\frac{-\varepsilon_a}{kT}\right)\exp\left(-\frac{1}{x\tau_o}\int_{T_0}^{T}\exp\left(\frac{-\varepsilon_a}{kT'}\right)dT'\right) \tag{2.17}$$

As described, $P(0)$ is the level of polarization, which is 'frozen-in' at temperature T_o. In a TSDC experiment the initial polarization is performed at a high temperature T_P and the specimen is then cooled to T_o [114].

2.5.2 Stored Charge and Trapping Levels

The electron traps have various energy and density [115], especially for wire coatings. The charge storage in a dielectric and its release from different trap levels are estimated by utilizing the TSDC plots. By modifying equation (2.15), the charge remaining in the sample is computed as:

$$Q = \int_{t(T)}^{\infty} j(T)dt \tag{2.18}$$

and the relaxation time is

$$\tau = \left(\frac{Q}{j} \right) \tag{2.19}$$

From (2.13),

$$\ln \tau(T) = \ln \tau_o + \frac{\varepsilon_a}{kT} \tag{2.20}$$

The plot of ln $\tau(T)$ versus $1/T$ yields a straight line with slope ε_a, which determines the activation energy for the charge carriers [116]. Trap levels, which have discrete energy differences, can be identified by a distinct peak in the thermogram by using TSDC plots.

2.6 Experimental Setup

The following sections describe the setups used in the experimental work. The arrangements for the PD measurements under pulse, the temperature measurement system, and the setup for the measurement TSDC are described. In addition, the pulse and high frequency ac aging circuits are also described in the following sections.

2.6.1 PD Measurements

Electrical Detection Method

In the electrical detection method, to measure the PDIV, a device called the XTrac™ is adopted to identify the existence of PD from a surge pulse. The instrument is capable of measuring, on three channels; the PD activity of the PWM operated machinery [117]. The first two channels are rated for an input voltage as high as 5 kV_p; whereas, a third channel is rated for 10 kV_p. The unit contains PD detection along with noise filtering capabilities. The unit is installed between the pulse generator and the test bar for all the measurements. The overall electrical connection of the instrument for the PD detection is shown in Figure 2.5.

The detectable PD signal is accessible on the front panel as a low voltage signal that is displayed on an oscilloscope. For reference, the system output voltage, which is applied to the terminals of the test samples, is measured with a high voltage Tektronix probe. This probe is capable of measuring a peak voltage of 20 kV, and its output is also a low voltage signal that is displayed on the same oscilloscope. The digital oscilloscope has a 400 MHz bandwidth, four channels, and a storage capability.

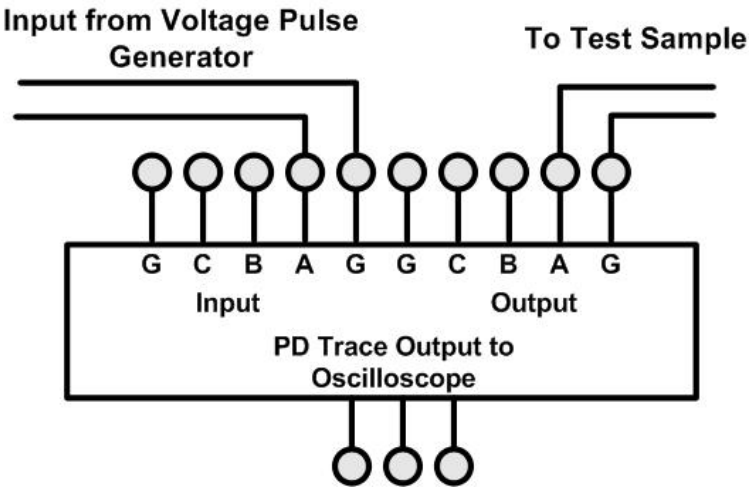

Figure 2.5: Electrical Connection for PD measurement using XTrac™ [117].

The measurement of PD under fast rise time voltage waveforms is difficult, since the frequency ranges of the rising voltage and PD signals almost overlap. In such cases, an

effective filtering is difficult and requires special tuning. But XTrac^{TM} has special features for the efficient filtering of noise with a predominant PD signal. To determine the PDIV in the VPI stator bar specimens, the test voltage is applied gradually, until PD is observed. A typical PD signal, detected by using the electrical detector, is shown in Figure 2.6 [117].

In all the waveforms recorded through XTrac^{TM}, the surge remnant, which can be easily distinguished from the PD pulses, is ignored which comes through the detector. The high frequency output from the detector indicates PD signals, which has a rise time between 5-10 ns.

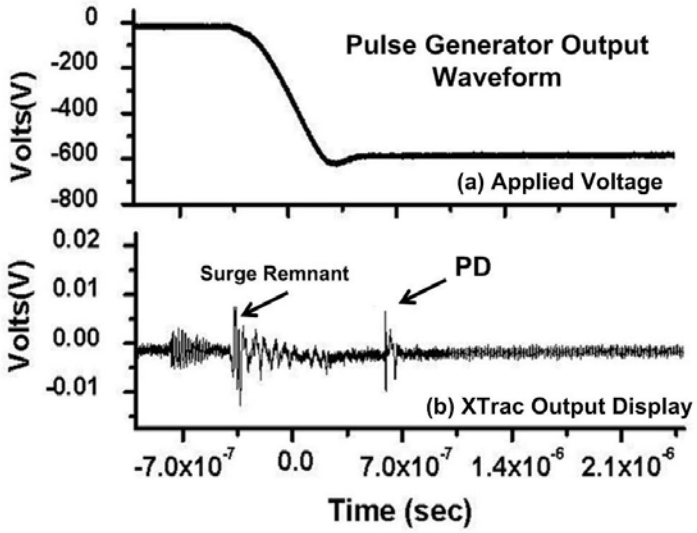

Figure 2.6: An example of the oscilloscope trace of a PD signal, along with the output voltage waveform from the detector.

Optical Detection Method

The daylight CoroSMART camera that belongs to CoroCAM's family of ultraviolet and bi-spectral cameras is used to visually locate the source of the electrical corona or arcing. The camera is low-light, UV filtered, very portable, battery powered, and rugged has an ultraviolet viewer to observe the electrical corona on switchgears, electric motor windings, low-light levels, and for outdoor substations between dusk and daybreak, and

many other applications. The camera is chosen for the test because of the need to reference and calibrate the electrical PD detection.

Figure 2.7 shows the images of twisted pairs recorded by using CoroSMART camera. The PDIV level, recorded with the electrical PD detector, demonstrate a value of 1.9 kV_p; whereas, the discharge activity, observed with an optical detector is approximately 2.05 kV_p. The XTrac™ is calibrated for ±7% error, accordingly, for all the measurements during this investigation.

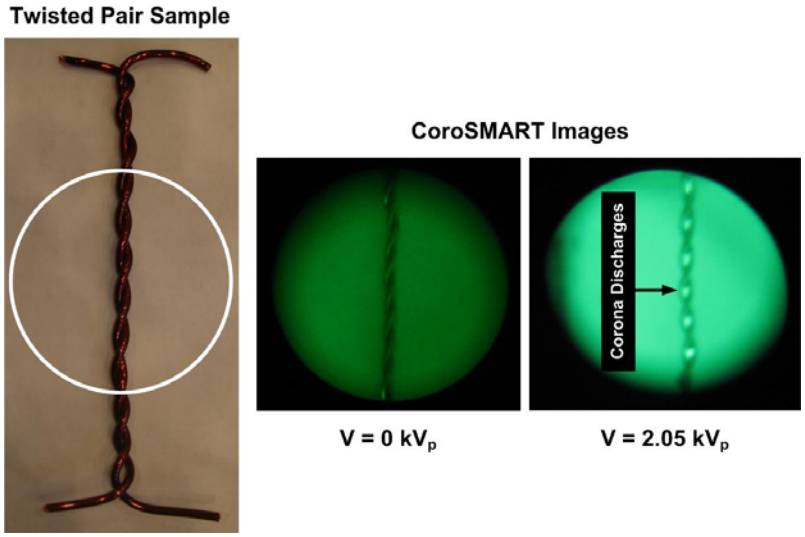

Figure 2.7: Image recorded using CoroSMART Camera (optical detector) with corona discharge activity.

2.6.2 Temperature Measurements using an Infrared Camera

The temperature measuring system consists of an infrared camera and thermovision acquisition software. The system consists of a FLIR-SC500 infrared camera with an emissivity spectrum between 7.5 and 13 μm that displays the temperature image in a 320 x 240 pixel array, Figure 2.8. The sensitivity of the detector is 0.07 K at a temperature of 303 K and with an accuracy of 2 K over the range 273 to 773 K. The acquisition software, ThermaCAM™ Researcher, allows different types of post-processing of the temperature distribution in the infrared image. The emissivity is adjusted to 0.92 for the

groundwall stator bar samples. The emissivity calibration is conducted on the samples, which are in an oven at 313 K (40 °C) using the temperature measured with a thermocouple as a reference. Figure 2.9 depicts the measured profile of temperature, T, on the surface of a 4 kV form-wound stator coil. The pulse voltage applied was 2.5 kV_p at a switching of 2000 pulses per second (pps).

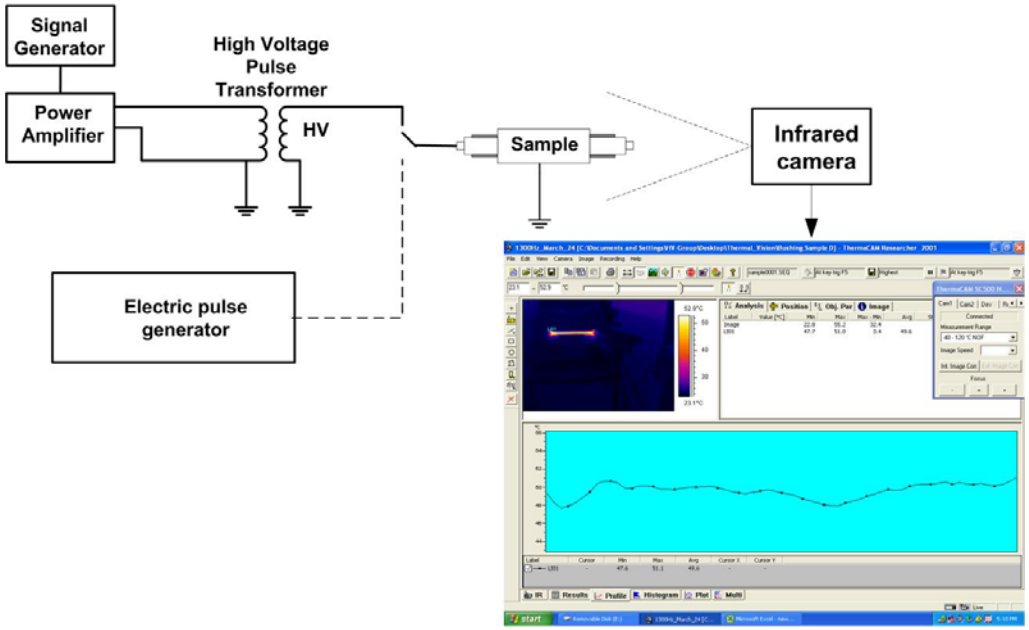

Figure 2.8: Temperature measurement system [118].

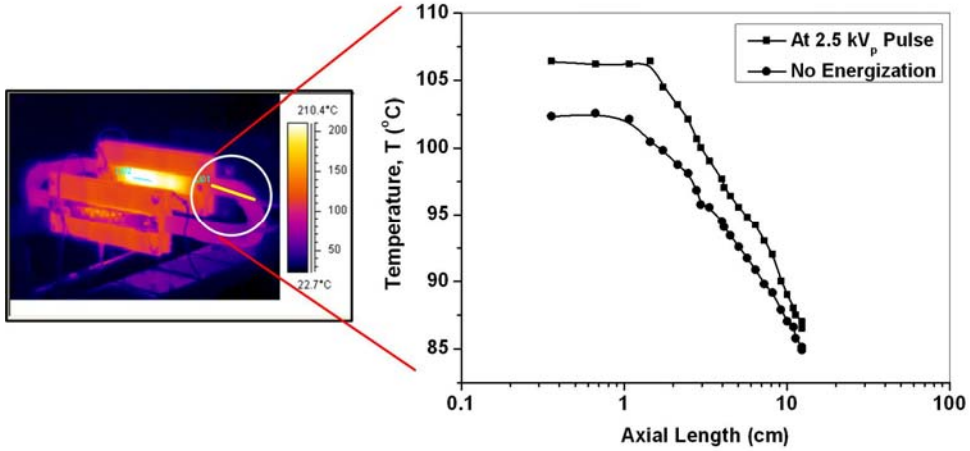

Figure 2.9: Measured temperature on the surface of the 4.0 kV_{L-L} form-wound stator coil energized at 2.5 kV peak (f_s = 2 kHz).

2.6.3 Measurement of the TSDC

Figure 2.10 shows the schematic of an experimental arrangement for the study of TSDC. The temperature of the specimen is controlled using an environmental chamber, which is controlled by a microprocessor unit designed to operate over a temperature range of –80 to 200 ^{o}C. The temperature control and measurement is accurate to 0.1 ^{o}C. The specimen under test is aged by different types of voltage waveforms for different durations and the current is later recorded.

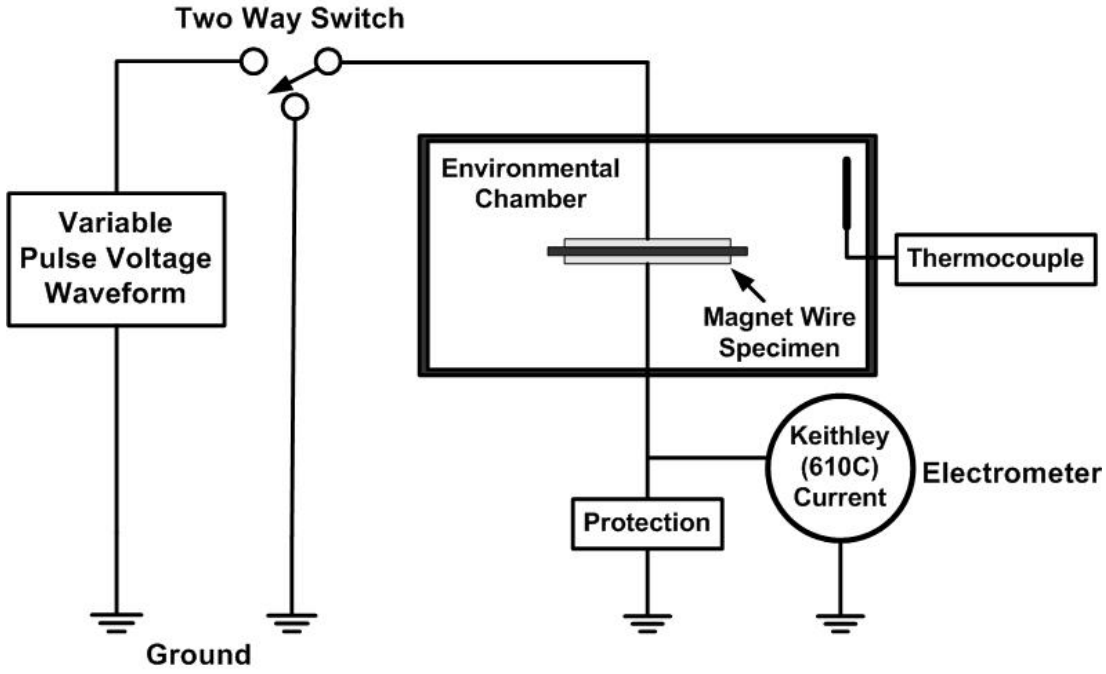

Figure 2.10: Schematic of an experimental arrangement for the study of TSDC.

Many small bar specimens, shown in Figure 2.2, prepared with enamelled wires, that belong to the insulation class F (155 ^{o}C), are adopted for all the TSDC experiments. Since the test specimens are partially dried and might contain moisture, the reproducibility of the currents is improved by adopting the thermal protocol in Figure 2.11. The environmental chamber, in which the test specimen is placed, is heated up to 200 ^{o}C (A-B), and the temperature is held constant for three hours (B-C). At the end of this period, the chamber temperature is lowered to the desired temperature of 155 ^{o}C (D-E), where the specimen is aged by different types of voltage waveforms for different

durations. After the aging, the temperature is decreased to 23 ^{o}C, and the sample is kept short-circuited for 30 min (F-G). Finally, the TSDC measurements (G-H) are carried out by using a Keithley 610C electrometer and a temperature controller [119]. Both the heating and polling of the test specimens are carried out under normal pressure.

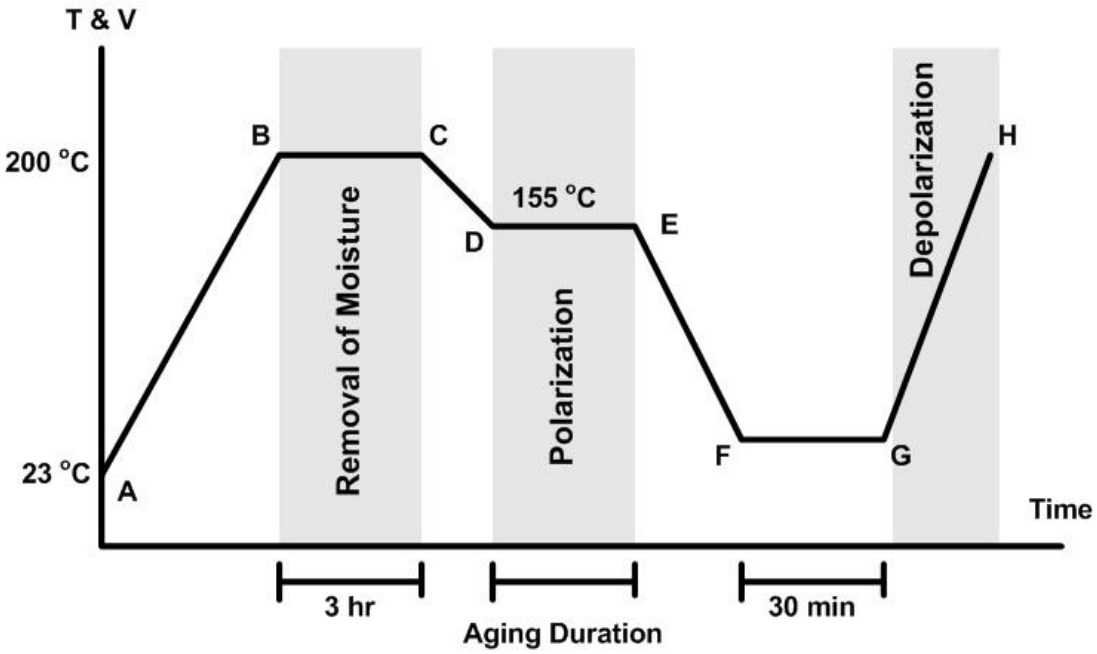

Figure 2.11: Thermal protocol and steps for the measurement of TSDC. [119].

The TSDC current, recorded as a function of the temperature, is easily converted to the function time for the measurement of the stored charge released, as the temperature is increased linearly. The conversion of the temperature to the time scale is achieved by following equation:

$$T = T_o + xt \tag{2.21}$$

where T is the temperature of the sample; T_o, the initial temperature; x, the heating rate; and t, the time. A typical TSDC plot for both low and high temperature polymers is shown in Figure 2.12. In low temperature polymers, the TSDC measurements could be extended up to a temperature at which the current vanishes. This is usually the glass transition temperature, T_g. At this temperature no more charge is released to the external circuit [116].

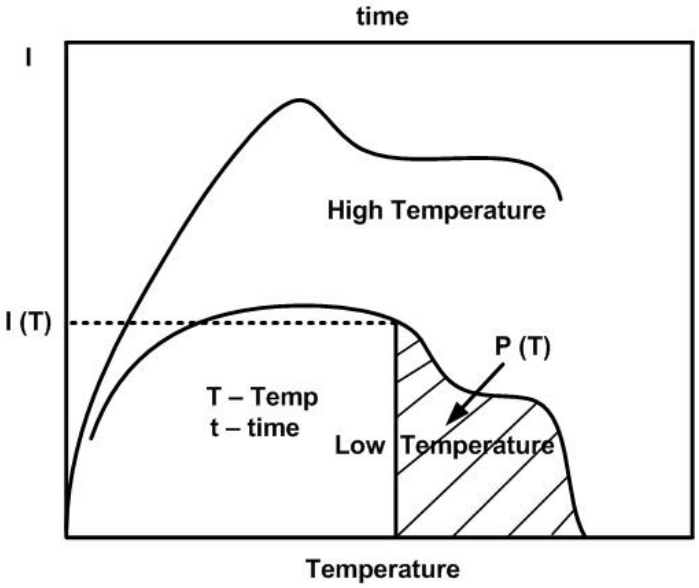

Figure 2.12: Schematic of TSDC in polymers.

2.6.4 Pulse Aging Test Circuit

Pulse Voltage Generator

To perform the long-term aging tests on both the magnet wire specimens and groundwall stator bar samples, a high voltage pulse modulator (HVPM), developed by DTI is used [120]. The HVPM, illustrated in Figure 2.13, is capable of providing the voltages that result from medium voltage (2.3-6.6 kV) PWM drives. The 30kV-30A voltage source modulator is built with solid-state switches in series, providing a high peak power and constant voltage during each pulse. Additionally, the modulator system contains a dc power supply, and a function generator. A variable voltage of 0 to 30 kV is provided by the dc power supply with a limit for the continuous operation of 540 mA. The voltage is varied by a dial indicator on the front panel. A standard function generator is used to generate the gate signals from the TTL output for the IGBT switch module. Switching frequency (f_s) of the output pulse voltage waveform can be varied up to 10 kHz by using the function generator.

According to IEC 62068 [121], simple voltage waveforms, either bipolar or unipolar, can be adopted for testing the insulation system objects and comparing their behaviour

with respect to reference assessed insulation systems [122]; therefore, a steep-front unipolar pulse is selected. Based on the latest developments and information available in the literature, most of the modern converter output voltage rise times fall in the 50–2000 ns range due to the power semiconductor switching characteristics [78,103,123]. In view of this information, a pulse rise time of 400 ns and a maximum switching frequency as high as 3 kHz are selected for the insulation aging.

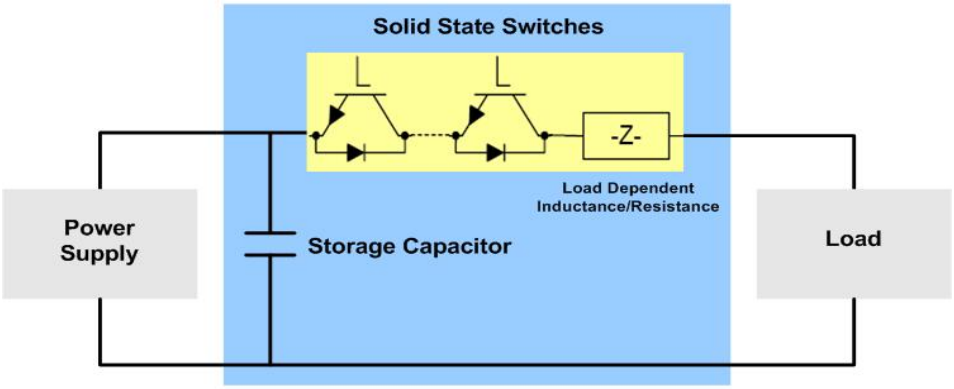

Figure 2.13: High voltage pulse modulator used for endurance test [120].

Test Procedure

The aging experiments are carried out under different pulse amplitudes and frequencies, and for different values of test temperatures using schematic shown in Figure 2.14 [124]. To determine the lifetime of an insulation sample, the time is measured until a puncture in the insulation occurs. Electrical and thermal aging deteriorates the insulation such that a hole is eroded through the insulation, and the copper in the bar shorts to the ground plate. Thus, the mean time-to-failure is a direct measure of the duration for which the test voltage is applied, before the power supply automatically turns off [4]. The accelerated aging conditions, to understand the degradation processes, are reported in Table 2.6.

The techniques for accelerated voltage aging are also described in IEC 62068-1 [121] and IEC 60034-18-32 [125]. They are based on a comparison of the life tests, performed on the candidate system and on the reference system, previously assessed for its service life, in which voltage endurance coefficient, n, is defined by the following lifetime equation:

$$D = kV^{-n} \tag{2.22}$$

Here, characteristic life, *D*, is related to the applied test voltage by using the inverse power law, and *k* is a constant that depends on the material and applied test voltage [78]. In particular, the values of constant, *n*, are likely to be different for the different breakdown mechanisms, operative at different applied voltages. Therefore, it might not be valid to estimate the aforementioned parameters in the test voltage range, which are very high, in order to estimate the expected lifetime. However, this technique requires further testing at three or more over-voltages and frequencies, summarized in Table 2.6. This allows the calculation of the voltage endurance coefficient from the regression line by the linear regression technique, applied to (log α, log V), the transformation, and any life at a generic percentile for a selected voltage [78].

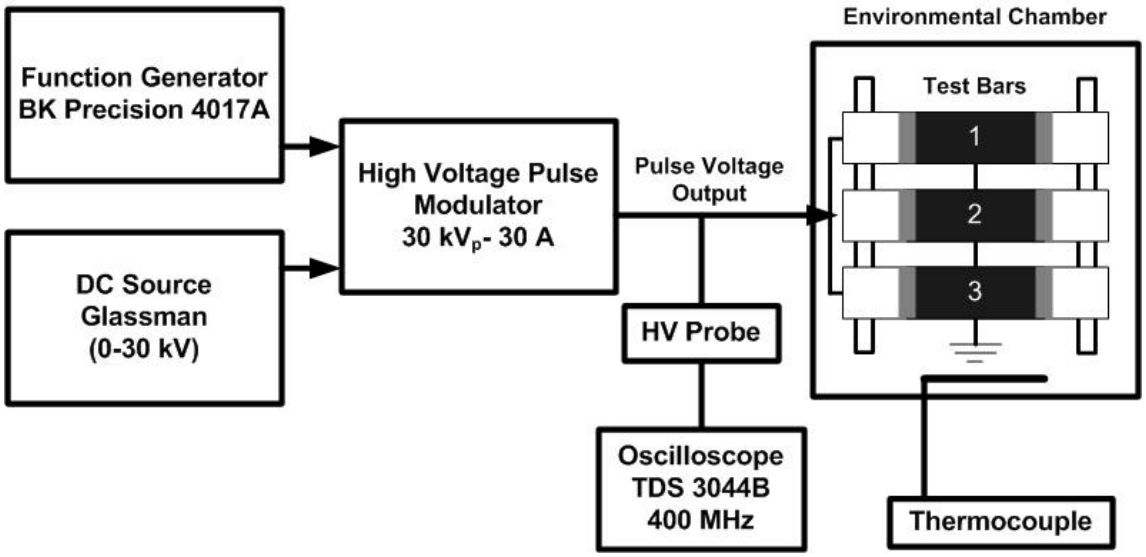

Figure 2.14: Schematic representation of circuit employed for pulse endurance test.

Table 2.6: Test conditions for groundwall aging.

Test Voltage Levels (V_p)	Voltage Waveform Frequency	Temperature (^oC)
4000, 5000, 6000	500, 1500, 3000 Hz pulses	20, 120, 155
4000, 5000, 6000	60 Hz ac waveform	20, 120, 155

As depicted in Figure 2.15, to acquire the temperature of 120 ^{o}C and 155 ^{o}C, a rope heater is wrapped over the aluminum foil for heating the groundwall insulation; whereas for the tests at room and below room temperatures, an environmental chamber is used, as shown previously in Figure 2.14.

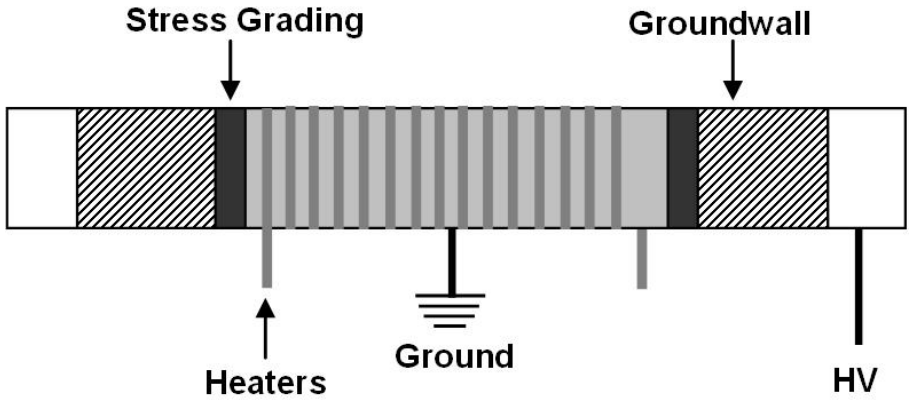

Figure 2.15: Stator bar specimens used for evaluation at high temperatures.

2.6.5 High Frequency AC Test Setup for the Aging of Magnet Wire Coatings

Choice of High Frequency AC Waveforms

The spectrum analysis of the PWM waveforms reflects a wide range of harmonic components. Although these high frequency harmonics exhibit a low-voltage amplitude and low-energy content, they can cause stress on the stator winding insulation due to high wavefronts (dV/dt). These harmonics can excite local resonance, causing voltage harmonics with a high amplitude. Often a filter is used in low voltage applications to absorb the standing waves, but at higher voltages, filters are not used.

The analysis of the spectra, obtained from a real drive with dominating harmonics between 3-4 kHz, is depicted in Figure 2.16. Modern IGBT-based ASDs have modulation frequencies in the range of 0.5 kHz to 20 kHz with rise times of 50–2000 ns. The spectrum of ASDs has an output frequency, close to the modulation frequency with a substantial power content as high as the sixth harmonic of the modulation frequency.

From this information and for accelerated aging, wide range of frequencies from 60 Hz to 10 kHz is selected for all the tests on the enamelled wires.

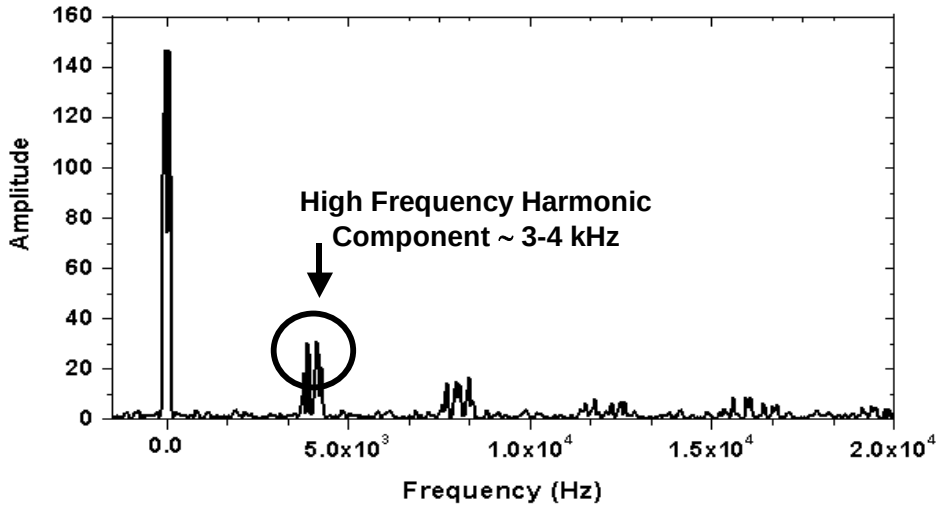

Figure 2.16: FFT spectrum of the PWM drive (Modulation frequency: 3-4 kHz).

High Frequency AC Endurance Test Circuit

For the magnet wire enamel evaluations, a voltage endurance test circuit with a high frequency voltage of a sine-wave power supply, is additionally adopted. In the test setup, as depicted in Figure 2.17, a high frequency generator produces a sinusoidal voltage signal that passes through an audio amplifier, and a high frequency step-up transformer (50V/20kV), which ages the samples. To identify the voltage across each test sample, a digital oscilloscope is used. Also, the same test circuit is employed for the PD erosion test to observe the surface roughness, which is described later in Section 2.6.5.

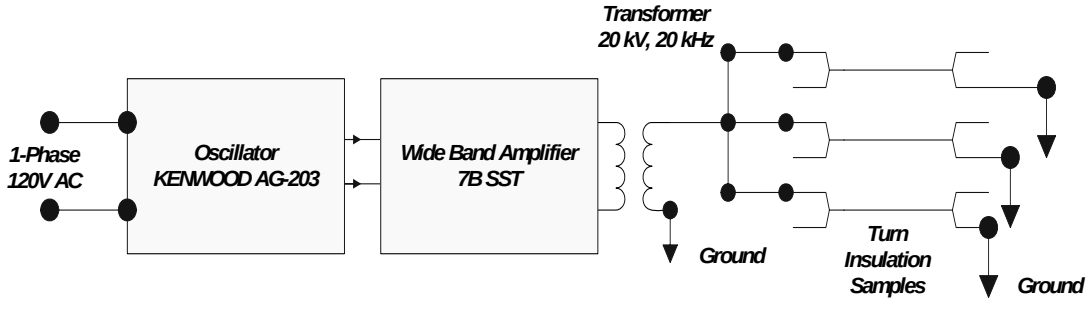

Figure 2.17: High frequency test voltage source.

Determination of Residual Insulation Strength

The most common and acceptable test for determining the breakdown strength of enamelled wire insulation is to use a dc test. The dc breakdown voltage experiment had shown that there is no significant difference between positive and negative polarity voltages, indicating that the field is nearly uniform between the two turns [126]. In both aged and un-aged specimens a group of 15 enamelled wires that belong to the same class are used. The experimental data, for both aged and un-aged samples, is then analyzed by using a two-parameter Weibull distribution to establish the scale and shape parameters, as described in Section 2.3.1. The scale parameter represents the time (or voltage) for which the failure probability is 63.2%. Similarly, the shape parameter, β, is a measure of the range of the failure times or voltages. The larger is the value of shape parameter, the smaller is the range of breakdown voltages or times [89]. It is comparable to the inverse of the standard deviation, σ, of the Normal distribution, Cochran and Snedecor [89,127].

2.6.5 SEM and Image Tool Software for Surface Roughness Measurements

For SEM analysis, the magnet wires, having rectangular shape with smooth and rounded corners, are coated with different types of multi-layer insulation. For assessing the surface condition after aging, the SEM images are for a region of ~13.3 x 13.3 μm.

The images are analyzed for the measurement of the erosion roughness by using an image tool software. To determine the surface roughness, after spatial calibration, the degraded areas are measured in nanometer scale. These measurements are then compared to the baseline values to report the relative surface roughness. The baseline values are determined before PD degradation of magnet wire enamel, which were selected randomly from their respective group.

In image tool software, measurements are displayed in a separate result window, with analysis features, like mean, and standard deviation. The software estimates the roughness by comparing the two surfaces before and after aging, as shown in Figure 2.18. The parameter used by the software is the dimensions of the detectable “dark areas”.

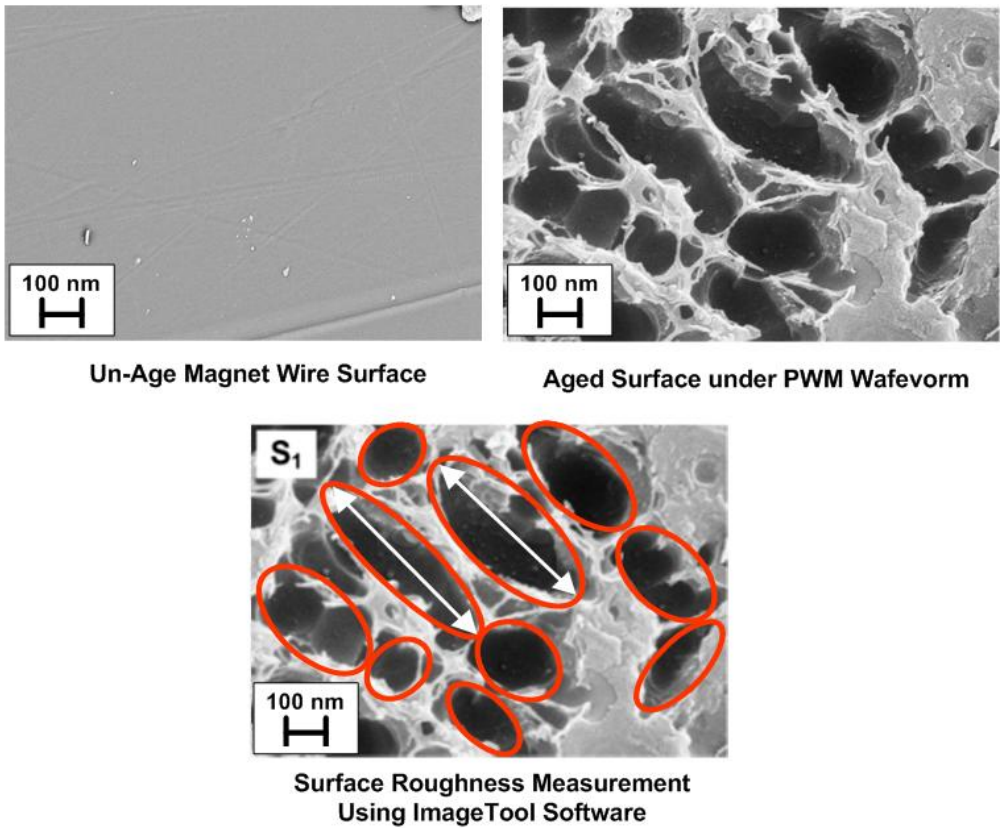

Figure 2.18 Comparison of SEM images for surface roughness measurements.

Chapter 3 Results

3.1 Introduction

In this chapter, using the test procedures described in Section 2.6, the test specimens prepared according to the procedures in Section 2.2 are evaluated for their performance under pulse applications. The aging results for the medium voltage induction motor inter-turn insulation, prepared with enamelled wires with polyimide and nanofilled coatings are done to understand the different mechanisms, in the insulation degradation. To assess the performance of the tested wire specimens, the residual strength is established by determining the dc breakdown voltages before and after aging. In addition, the TSDC results are given to provide information about the relaxation processes. TSDC results include the disorientation of the dipoles and the release of charges from the trapping sites in the enamelled wires. The principle objective is to establish a relationship between the space charge and the number of insulation layers of the magnet wire. Finally, the pulse aging results of the stator bar groundwall insulation with thermal analysis, and PD measurements are also presented.

3.2 Enamelled Wires Aging Test

Medium voltage induction motors are exposed to steep-front, non-sinusoidal voltages, when fed from PWM-VSC. Such steep-front voltage pulses propagate through the stator windings and impose stresses on the inter-turn insulation. This inter-turn stress is due to the fact that the distribution of the voltage across the motor coil is not uniform. The shorter the rise times of the pulse, the higher the frequency content and the greater the voltage across the turns of the winding. To understand the influence of such voltage stresses, the aging test results are discussed in two subsections: the results from testing the enamelled wire specimens subjected to steep-front pulse voltage waveforms and the results from testing under high frequency ac voltages. In each case, a group of 15

enamelled wire specimens from the same class are used [128]. To establish the residual strength of the wire specimens, dc breakdown voltages are recorded before and after the aging. As described in Section 2.3, the scatter of the breakdown voltage for both aged and un-aged samples, are analyzed by using a two-parameter Weibull distribution to determine the dc breakdown measurements.

3.2.1 Effect of Steep-Front Pulse Voltage Waveforms

In this section, the aging results of the conventional enamelled wire specimens, as well as the results of the laboratory developed wire specimens are described.

Conventional Enamelled Wires

The enamelled wires S_1 and S_2 are commercial materials. Enamelled wire, S_2 belongs to the family of corona resistant (CR) material, which has an additional coating of alumina filled THEIC (Tris-2-HydroxyEthyl IsoCyanurate) modified polyester resin. Before aging, the partial discharge inception voltage (PDIV) at 60 Hz ac of the enamelled wire specimens is determined by using the Haefely TE561 PD detector, (sensitivity level = 0.5 pC; bandwidth = 4-400 kHz). When the voltage is applied, a PDIV of approximately 900 V_p is usually observed for a 38 μm thick coating on a wire [63].

Each group of specimens is aged by unipolar steep-front pulses at different repetition rates (500 – 2000 Hz) for a voltage level of 1100 V_p for S_1, and 750 V_p for S_2, keeping the similar aging duration of 100 hours. It is commonly thought that during the manufacturing process of the wires, the coatings might have a number of defects that are distributed randomly [129]. These defects can additionally contribute to a weakness, which can result in lower values of the dielectric strength than those of theoretical values. Therefore, these premature failures are attributed to coating defects such as the improper thickness of the insulation, delamination, swelling, and cracks that occur during the manufacturing process. Figure 3.1 shows SEM images of some of the observed defects.

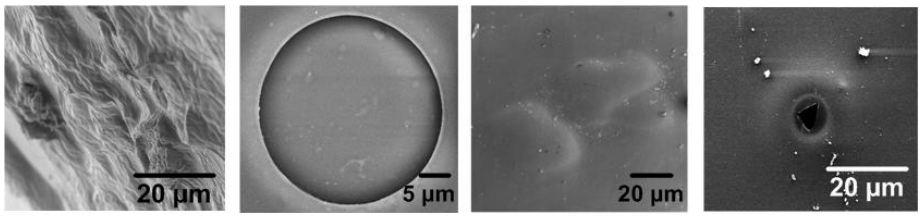

Figure 3.1: Defects found in magnet wire coatings.

As described in Sections 2.2.3 and 2.6.5, the dc breakdown voltages, η, along with the shape parameter, β, and standard deviation, σ, for S_1 and S_2 wires before and after the pulse voltage aging having duty cycle of up to 50%, are reported in Table 3.1.

Table 3.1: Parameters related to medium voltage conventional magnet wires S_1 and S_2, subjected to different pulse switching frequencies.

Magnet Wire	Switching Frequency, f_s (Hz)	Scale Parameter, η (kV)	Shape Parameter, β	Standard Deviation, σ
S_1 (No Filler)	Un-Aged	11.12	7.16	1.41
	100	11.01	7.20	1.53
	200	10.99	6.11	1.67
	400	10.95	5.10	1.92
	500	9.91	4.95	2.46
	1000	9.90	3.41	2.94
	1500	9.40	3.03	3.19
	2000	8.90	2.73	3.31
S_2 (Alumina)	Un-Aged	7.61	5.47	1.90
	100	7.40	3.17	1.89
	200	7.39	3.12	2.01
	400	7.38	3.11	2.05
	500	7.35	3.08	2.13
	1000	6.10	3.09	2.15
	1500	5.30	3.10	2.29
	2000	4.65	3.02	2.43

The Weibull plot for enamelled wire S_1 depicted in Figure 3.2, shows variation of dc breakdown voltage for un-aged, and at pulse switching frequencies of 1000 and 2000 Hz. According to the Weibull distribution, the value of the dc breakdown voltage corresponds to a 63.2% breakdown cumulative probability. To attain the best fit of the experimental data, the maximum likelihood estimation with a 90% confidence bound interval is used, as a 10% risk is reasonable from a statistical point of view [91,93]. In all cases, the fit of the experimental data, r^2, is observed to be in the range of 0.9 to 0.95. The dc breakdown voltage experiment proves that there is no significant difference between the positive and negative polarity voltages indicating that the field is nearly uniform between the two turns [126]. Therefore, for all the breakdown tests and to evaluate the insulation performance, a positive polarity is adopted.

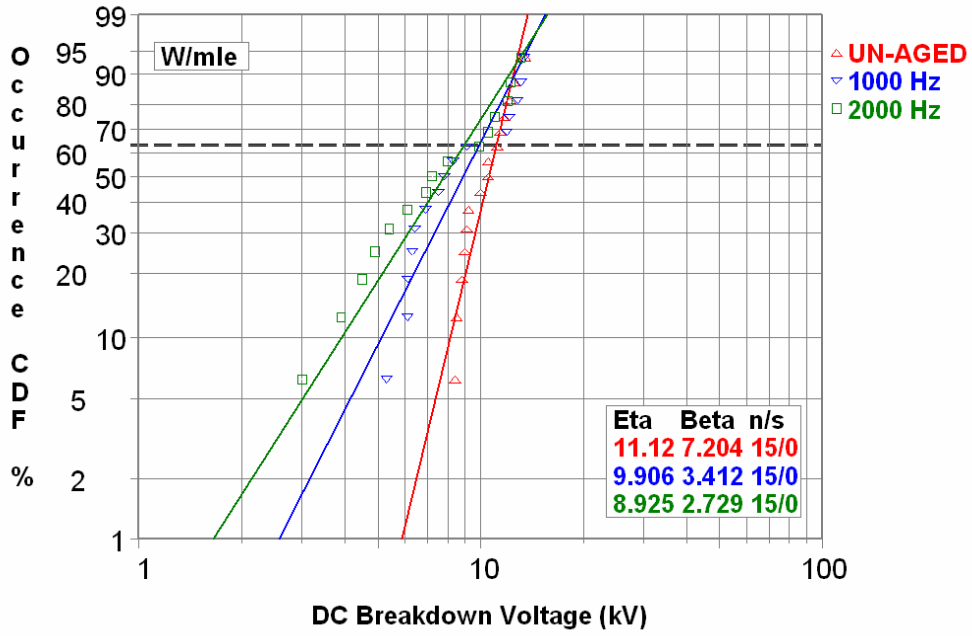

Figure 3.2: Weibull probability distribution plot of the dc breakdown voltages for wire S_1 at different pulse switching frequencies.

The test results listed in Table 3.1 are further depicted in Figure 3.3 to see the variation in breakdown strength as a function of frequency. The results reveal that more than one degradation process needs to be considered for both the S_1 and S_2 samples, as

suggested by the two distinct slopes. The two principal regions, based on the pulse repetition rate, correspond to the change in the aging mechanisms [13]. It is believed that the contribution of the charge accumulation, in addition to the PD activity, can result in two distinct slopes, as depicted in Figure 3.3.

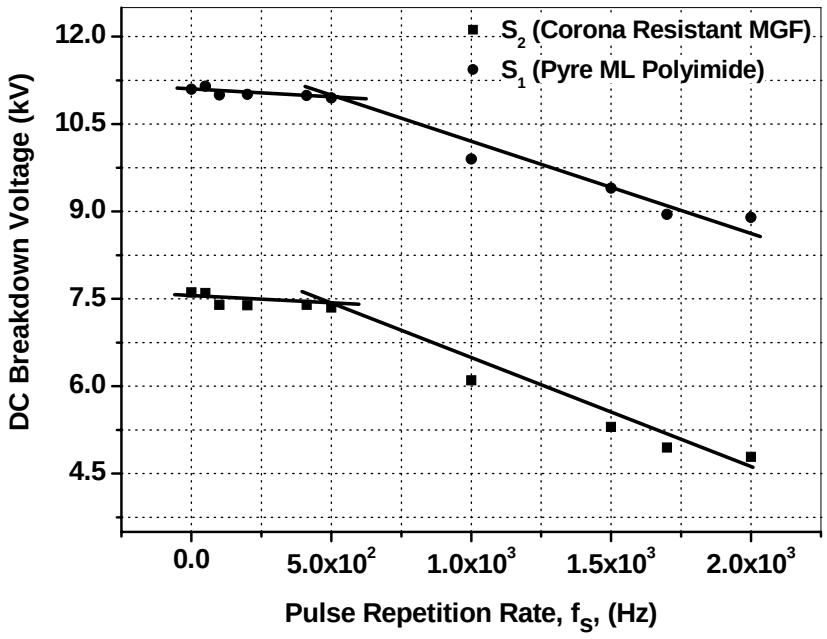

Figure 3.3: Residual life based on the dc breakdown voltage for conventional wires aged by unipolar steep-front pulses at different repetition rates (aging voltage S_1 = 1100 V_p; S_2 = 750 V_p for ~100 h duration).

The data listed in Table 3.1 for Weibull shape parameter β and standard deviation σ, for magnet wire S_1, is also included in Figure 3.4. The standard deviation depends on the number of samples in the test and appears to be most disturbing for β. The results demonstrate that an inverse relation, between the two parameters, exists. In Figure 3.4, the distance between these two parameters decreases as the pulse repetition rate increases. The higher scatter of data is observed at higher switching frequencies due to the increase of the randomly distributed defects. The inserted log-log plot in Figure 3.4 reflects a relation between relative standard deviation σ/β and the pulse repetition rate. The data

fits quite well and exhibit an almost exponential increase. It is evident that the higher pulse switching frequency leads to increased scatter, and thus, a higher deviation in the data. The domination of the standard deviation over the shape parameter is due to the response of the multi-layer coatings on the magnet wire. This can be attributed to the different aging mechanisms, which are causing the accelerated degradation. Almost, similar results are observed for magnet wire S_2.

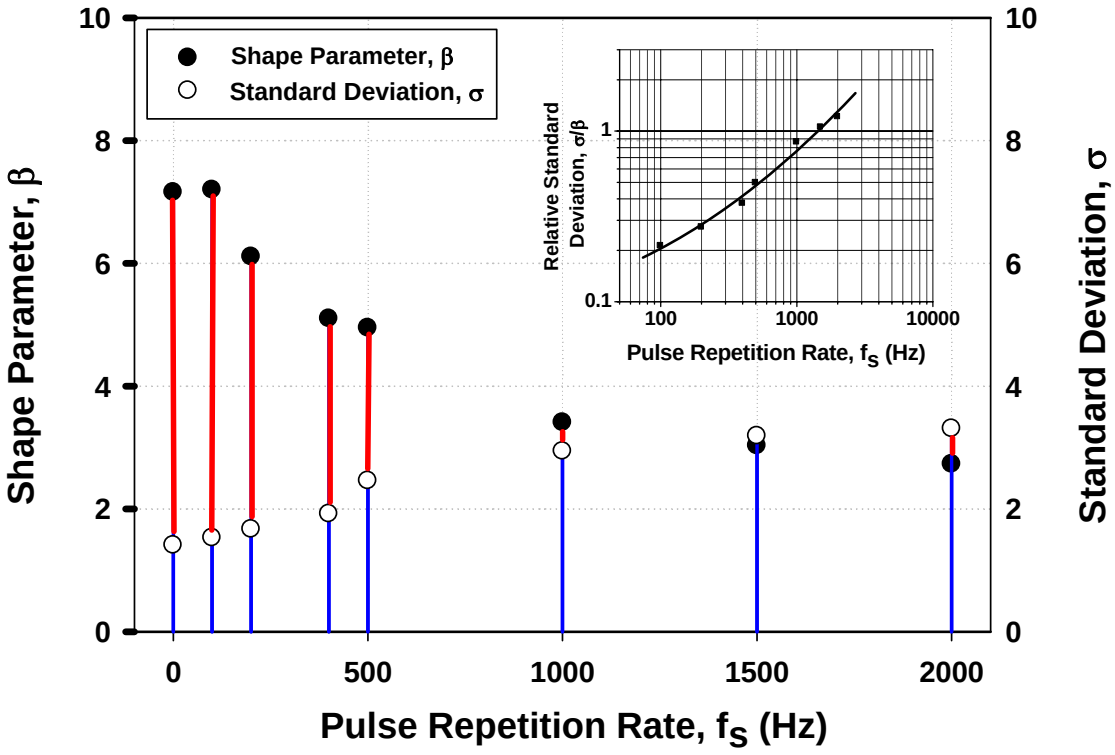

Figure 3.4: Variation in the shape parameter β and standard deviation σ for magnet wire S_1 under different pulse repetition rates. The log-log sub-plot shows the relation between the relative standard deviation σ/β and pulse repetition rate.

Laboratory Developed Enamelled Wires

The experimental results, as shown in Figures 3.3 and 3.4, suggest that the degradation process is due to both the PD and charge accumulation/trapping; thus, the analysis of the new enamelled wires, listed in Table 3.2, should be considered in detail [130]. The effect of the pulse aging on the newly prepared wires, which belong to the same class as of S_1,

is evaluated by measuring the dc breakdown voltages. The results, presented in Figure 3.5, indicate that in the new wires; S_{1A}, S_{1B}, S_{1C}, and S_{1D}, the residual life decreases with the increase of the insulation layers on the magnet wires. In addition, for the S_{1D} wire, two main regions, based on the pulse repetition rate, are observed. This corresponds to the change in the aging mechanisms, as shown in Section 3.2.1 for wires S_1 and S_2. The contribution, by the slow degradation process that is charge trapping and the accumulation in the bulk of multi-layer insulation systems of enamelled wires is presented in Section 3.4 by using the technique of TSDC.

Table 3.2: Dimensional and electrical parameters, related to magnet wires having coating type polyimide, Pyre-ML®, before aging (Reference Data).

Type	Number of Insulation Layers	Insulation Thickness [μm]	DC Breakdown Voltage [kV]
S_{1A}	1	7.2	0.615
S_{1B}	2	13.0	1.169
S_{1C}	3	19.0	1.620
S_{1D}	4	24.2	1.912

3.2.2 Effect of High Frequency AC Waveforms

For high frequency ac tests, the dc breakdown voltages of both conventional ($S_1$and S_2) and the custom designed enamelled wires (S_{1A}, S_{1B}, S_{1C}, and S_{1D}) are determined, after aging, by the various sinusoidal frequencies of 60 Hz, and 2-4 kHz for ~100 h. It is obvious from Figures 3.6 and 3.7 that the selected test frequency range plays a different role on the aging process. Further, the drop in the dc breakdown voltage is high for the magnet wires with the higher number of insulation layers, compared with the samples aged under pulse voltages. The dc breakdown voltage decreases almost linearly, as the frequency of test voltage is increased from 60 Hz to 4 kHz. This decrease is attributed to the degradation due to the enhanced PD activity between the gaps of the enamelled wires, and the heat build-up due to the dielectric loss.

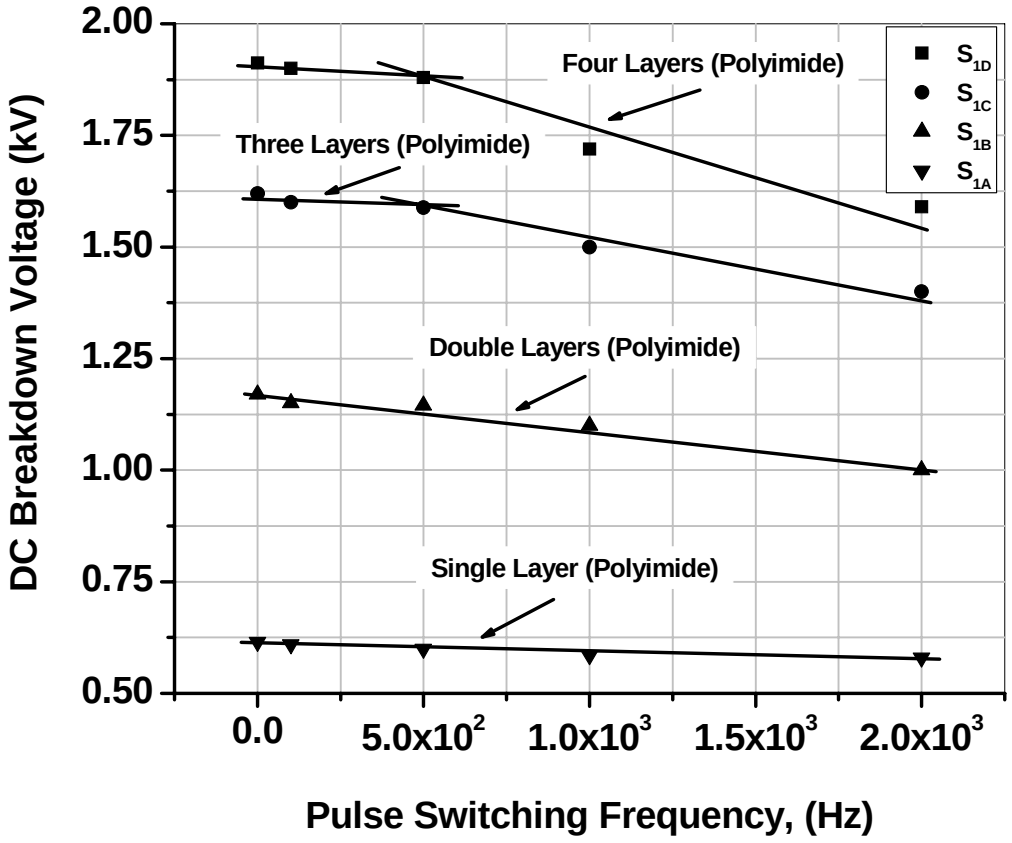

Figure 3.5: Residual life based on the dc breakdown voltage for laboratory developed wires, aged by unipolar steep-front pulses at different repetition rates (test voltages, S_{1A} = 215 V_p; S_{1B} = 390 V_p; S_{1C} = 570 V_p; S_{1D} = 720 V_p for ~100 h duration).

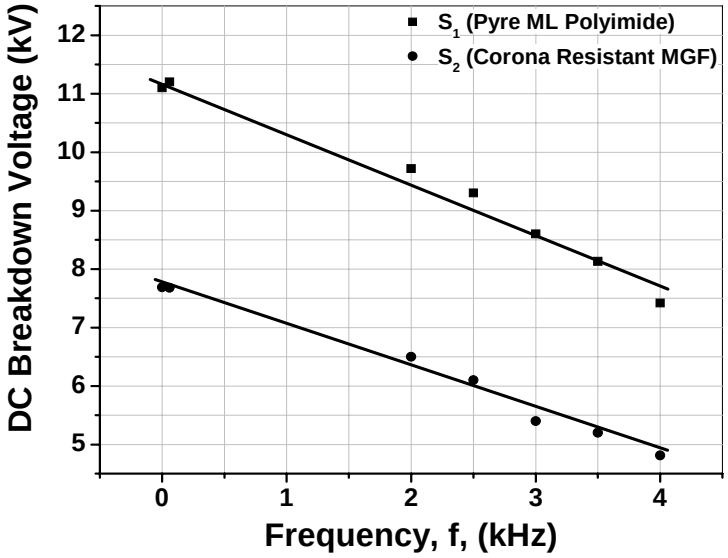

Figure 3.6: Residual life based on the dc breakdown voltage for conventional wires (S_1 and S_2) aged under high frequency ac waveforms at a constant electric stress of 30 kV/mm peak for ~100 h duration.

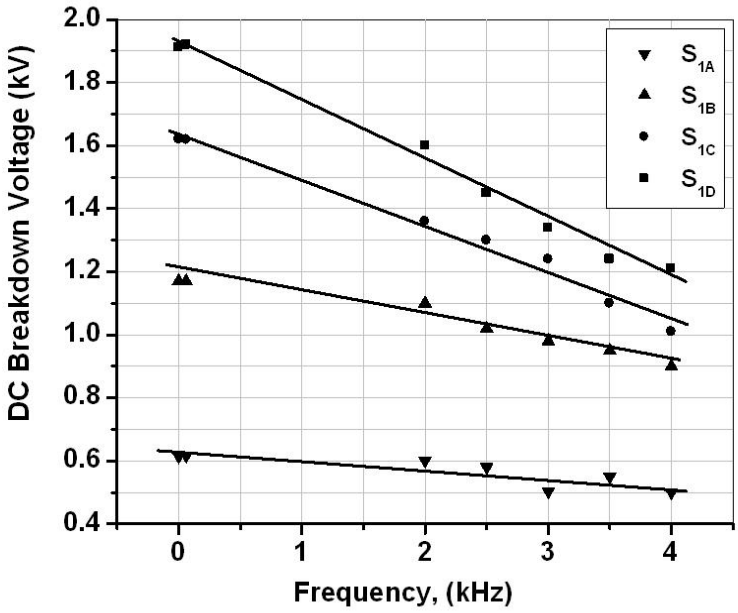

Figure 3.7: Residual life based on the dc breakdown voltage for laboratory developed wires aged under high frequency ac waveforms at a constant electric stress of 30 kV/mm peak for ~100 h duration.

3.3 Magnet Wires PD Erosion Tests

In this section, the results, relevant to the effectiveness of nanofillers on the erosion resistance of enamelled wires, are considered. The procedure, described in Section 2.6.5, is applied to the magnet wire specimens, as described in Section 2.2. The results in terms of the surface roughness for the aged samples are measured. For the PD erosion that results from the medium voltage (2.3-6.6 kV) PWM drives, a real PWM-VSC, 10 kV peak-to-peak, low power single-phase generator [131] is used to test the samples. Figure 3.8 signifies a PWM waveform, generated by the custom-built supply, with a fundamental frequency of 60 Hz and a switching frequency of 1.25 kHz.

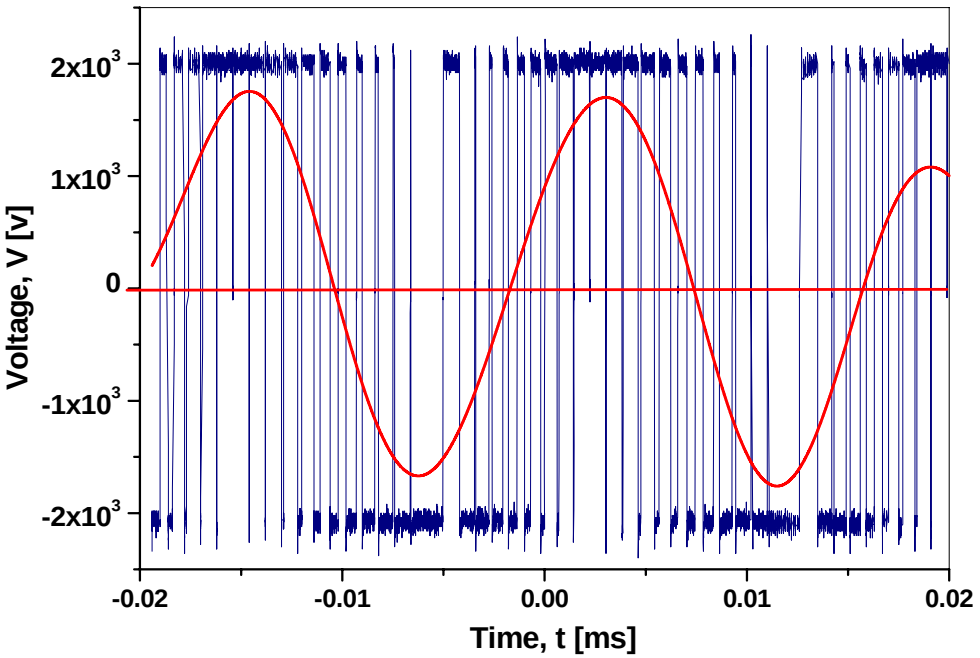

Figure 3.8: PWM waveform from a PWM generator used for testing of magnet wire specimens (S_1 to S_6).

3.3.1 PWM-VSC Aging

The magnet wire specimens (S_1 to S_6), examined for PD resistance, are exposed to a stress of 100 kV_p/mm for 1 h under PWM-VSC waveforms. Table 3.3 lists the average,

mean, and standard deviation of the results. From the results in Figure 3.9, the higher relative surface roughness of approximately 1195 with a standard deviation of 134.5 is observed for enamelled wire S_1 without nanofillers. Similarly, wires S_2 and S_3, which are commercially available PD resistant wires, reveal similar surface erosion, after comparing both un-aged and aged samples. The relative surface roughness is around 327 for S_2 and 313 for S_3, along with the piling up of nanoparticles, to reduce the PD attack [132]. Also, the standard deviation values are lower, compared with wire S_1, which are 63 and 45.5, respectively.

In magnet wires S_4, S_5, and S_6, filled with fumed silica (SiO_2), TiO_2, and Al_2O_3, respectively, the relative surface erosion, due to the PD, is comparatively lower. In magnet wires S_4 and S_5, the relative PD erosion seems to be around 240 and 280, respectively. In addition, in both cases, the scatter in the data is smaller; whereas, in comparison, S_6 shows surface erosion relatively higher in the range of 322 with a standard deviation of 52.5.

Table 3.3: Average, mean, and standard deviation of the relative surface roughness in magnet wire coatings subjected to PWM-VSC waveforms at 100 kV_p/mm.

Magnet Wire	**Nanofillers**	**Relative Surface Roughness**		
		Average	**Mean**	**Standard Deviation, σ**
S_1	-	1195	1166	134.5
S_2	Alumina	327	322	63.0
S_3	Alumina	313	320	45.5
S_4	Fumed silica	240	230	35.5
S_5	Titanium oxide	280	270	38.8
S_6	Alumina	322	313	52.5

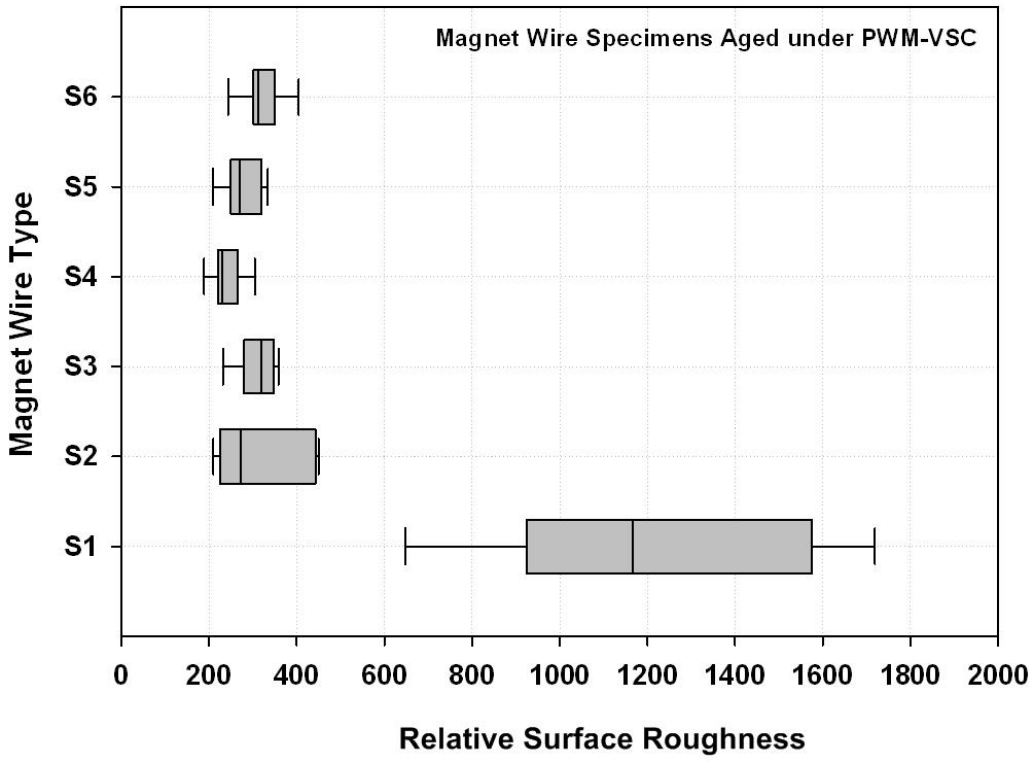

Figure 3.9: Summary of the PD erosion test results for magnet wires (S_1 to S_6) aged under PWM-VSC waveform at a constant stress of 100 kV_p/mm (f_s = 1.25 kHz). Bar mark the 5 and 95 percentiles; the extremities of the hatched box are 25 and 75 percentiles and the centre line represents the average of the data.

3.3.2 High Frequency AC Aging

The properties of magnet wires S_1 to S_6 are also examined at 10 kHz ac with a constant stress of 70 kV_p/mm for a one-hour duration. Table 3.4 lists the average, mean, and standard deviation of the results. From the results that are represented in Figure 3.10, severe surface erosion is observed in all of the commercial magnet wires, S_1, S_2, and S_3, after aging. A comparative investigation indicates an average relative roughness of approximately 701 in wire S_1; wires S_2 and S_3, commercially available PD resistant wires, portray relative surface erosion as high as 176 and 127, respectively. The surface

erosion in S_3 is comparatively lower in the case of high frequency ac waveforms because of the new polyimide film, which is specifically designed to withstand the damaging effect of PD activity [83]. In magnet wires S_4 and S_5, filled with fumed silica (SiO_2) and TiO_2, the surface erosion due to PD, is almost negligible under high frequency ac waveforms. In both cases, the relative surface erosion is observed to be in the close range of 12. For wire S_6, with Al_2O_3 nanofillers, the relative surface erosion is comparatively higher and observed to be approximately 37.

Table 3.4: Average, mean, and standard deviation of the relative surface roughness in magnet wire coatings subjected to high frequency ac waveform at 70 kV_p/mm.

Magnet Wire	**Nanofillers**	**Relative Surface Roughness**		
		Average	**Mean**	**Standard Deviation, σ**
S_1	-	701	720	88.8
S_2	Alumina	176	187	56.2
S_3	Alumina	127	119	41.2
S_4	Fumed silica	12	13	4.5
S_5	Titanium oxide	12	12	5.2
S_6	Alumina	37	36	8.1

The experimental results demonstrate that nanofillers are more resistant to PD, when they are used in the polymers. Also, the results confirm that the addition of a small amount of nanofillers is sufficient to improve the PD resistance. The comparative results indicate that under PWM-VSC aging conditions, the surface degradation in magnet wire coatings is much greater. This can be attributed to the stresses, due to the high *dV/dt* of the PWM waveforms. In the case of the high frequency ac aging, standard deviation σ of surface roughness is measured for wires S_1 to S_6. The higher value of 88.8 is measured for wires without nanofillers. For wire specimens with nanofillers, the standard deviation is very small; the scatter in the data, recorded for S_4, is only 4.5.

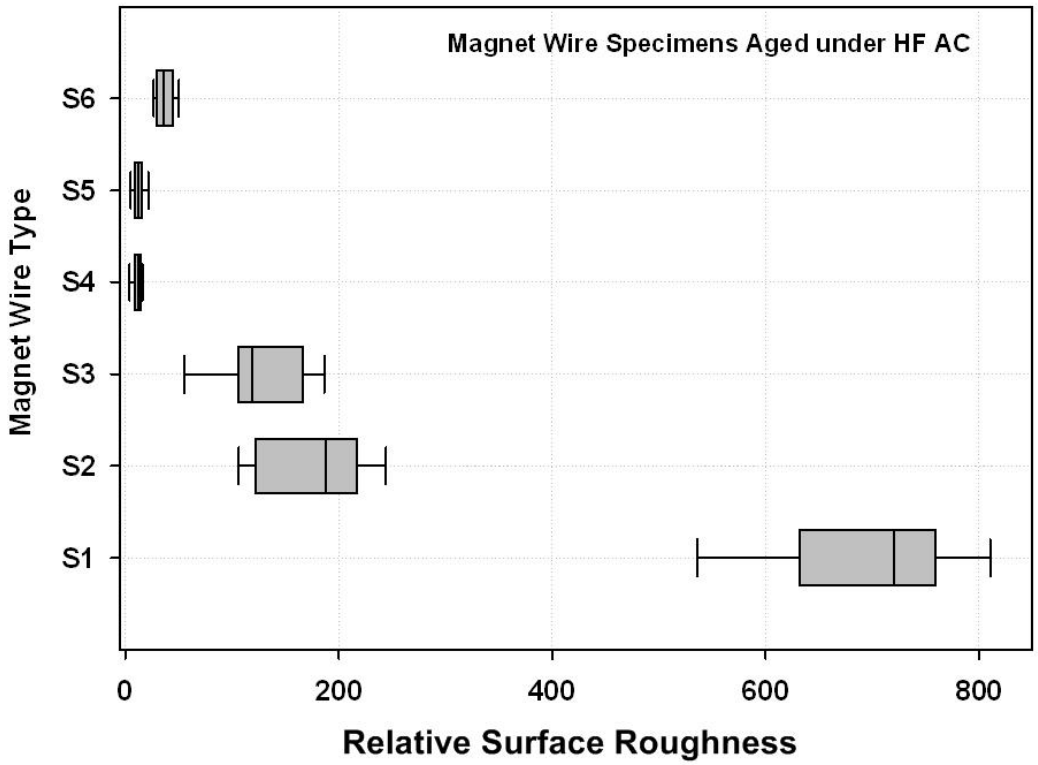

Figure 3.10: Summary of the PD erosion test results for magnet wires (S_1 to S_6) aged under high frequency ac waveform at a constant stress of 70 kV_p/mm (f = 10 kHz). Bar mark the 5 and 95 percentiles; the extremities of the hatched box are 25 and 75 percentiles and the centre line represents the average of the data.

3.3.3 Residual Insulation Strength

The specimens described in Section 2.2, are also tested for a comparative evaluation of the wire's residual life under a high frequency ac. The residual life is established by measuring the dc breakdown strength before and after aging, by following the procedure described in Section 2.3. Figure 3.11 displays a comparison of the changes in the dc breakdown strength for the wires with and without nanofillers. Since all the tests involve different test voltage amplitudes, a constant electric stress must be maintained across the insulation for the different wires and different frequencies.

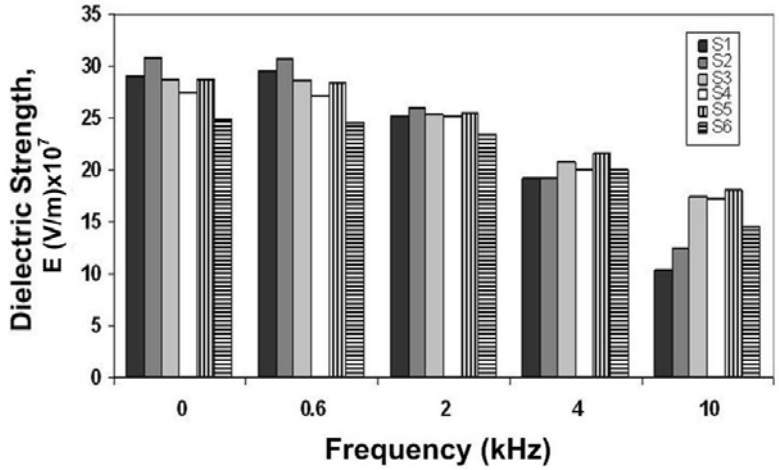

Figure 3.11: Variations in the dielectric strength of magnet wires (S_1 to S_6) by increasing the ac frequency.

The dispersion of the dielectric strength data is found to be smaller, and the values are closely clustered in a frequency range up to 4 kHz with a standard deviation of 2.24. However, at a higher frequency, 10 kHz, the dispersion in the data is larger for commercial wires S_1, S_2, and S_3 with the standard deviation values in the range of 6.9 to 7.5. For the laboratory-developed wires, due to the small scatter in the data, the standard deviation at 10 kHz is lower, in the range of 3.2 to 4.9. Although the results are difficult to compare, such high frequency tests lead to quick results that indicate the quality and characteristics of the coating material. For the PD resistant wires, the maximum variations in the dielectric strength are in magnet wire S_2, 65%; whereas, S_4 and S_5 exhibit a similar change in the breakdown voltage, 37%. For the commercially filled wires, S_3 exhibits the best resistance to PD, and its breakdown voltage changes as much as 40%.

3.4 Thermally Stimulated Depolarizing Currents (TSDC) in Magnet Wires

The procedure, described in Section 2.6.3, is applied to magnet wire specimens S_1 with Polyimide (Pyre-ML® RC-5019) coatings. Before the specimens are used, they are heat-

treated for 3 hrs at 200 ^{o}C to remove any moisture and to improve the reproducibility of the results. TSDC measurements are carried out to study the mechanisms, charge storage and the subsequent release from the bulk of the magnet wire coatings. The currents reveal a number of peaks, reflecting the processes which are related to molecular relaxation and the delocalization of the charges injected into the polymer bulk during polling [133].

Table 3.5 lists different conditions for which the TSDC spectra are obtained for magnet wire specimens S_1. Later, these spectra are utilized for the estimation of the parameters such as activation energy ε_a characteristic relaxation time τ, and charge released Q, during the relaxation process.

Table 3.5: Test conditions for TSDC measurements.

Type of Investigation	Thickness [μm]	T_P (^{o}C)	Charging Time t_p (min)
Long-Term Aging Effect @ 1 kV peak, for 6 to 100 h	38.4	155	360-6000
Effect of Unipolar Polling Voltage from 1.0 to 3.5 kV peak	38.4	120	60
Effect of PWM-VSC @ Polling Voltage 1.0 to 2.25 kV peak	38.4	120	60
Effect of Multiple Layers @ E = 5 kV/mm peak (1-9 Layer)	7.2–54.1	100	60

3.4.1 Long-Term Aging Effect (t_P)

The TSDC curves, for the commercially available type ML enamelled wire S_1, are shown in Figure 3.12. As seen, increasing the polling time (t_P) from 6 to 100 h results in higher peaks. The eight-hour unipolar pulse-aging curve offers two peaks: one at 70 ^{o}C and the other at 95 ^{o}C. Similar behaviour is observed for the specimens, aged by longer durations. As the polling time increases, more charges are accumulated in the distributed traps, causing an increase in the amplitude of these peaks.

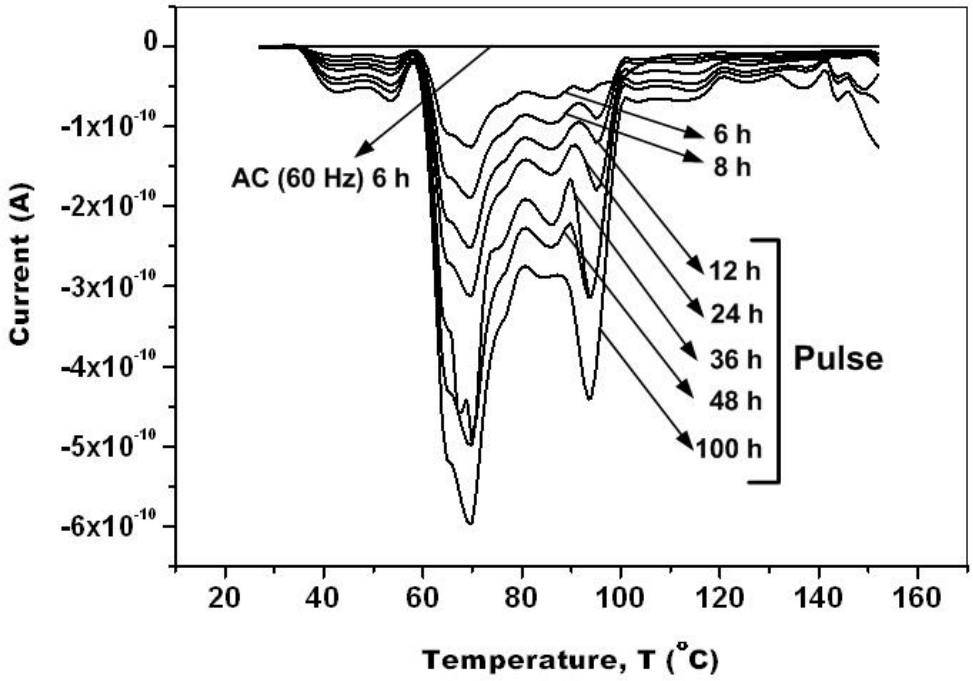

Figure 3.12: TSDC results for time dependence pulses aged at 1 kV peak (pulse repetition rate – 2 kHz).

Furthermore, by increasing the polling time to 100 h, the low temperature current peak at 70 ^{o}C becomes more pronounced than that at a higher temperature. Figure 3.12 also confirms that the origin of this peak is obviously related to free or shallow trapped charges, which are injected from the electrodes and accumulate in the boundaries of the magnet wire coating. Neagu *et al.* [134] and Sussi *et al.* [116] report similar behaviour for TEFZEL® and in KAPTON®, suggesting that the shallow trap density is probably greater than that of deeper traps [135].

Also, the elevated temperature and fast repetitive voltage pulses can lead to microscopic structural modification of the wire insulation. Such detectable changes and structural modification of the wire insulation may lead to trap formation that increases slowly with the length of the aging time. In Figure 3.13, the released charge (the area under the peaks) from the trap sites increases linearly with the increased aging time and slows down after 48 hrs. This is attributed to the permanent structural modification of the

wire insulation, which creates predetermined localized trap sites. It is believed that further aging might cause an increase in the concentration of the accumulated charges; however, similar behaviour as shown in Figure 3.15, is also reported by Fu *et al.* [136] for low-density polyethylene (LDPE) under ac aging.

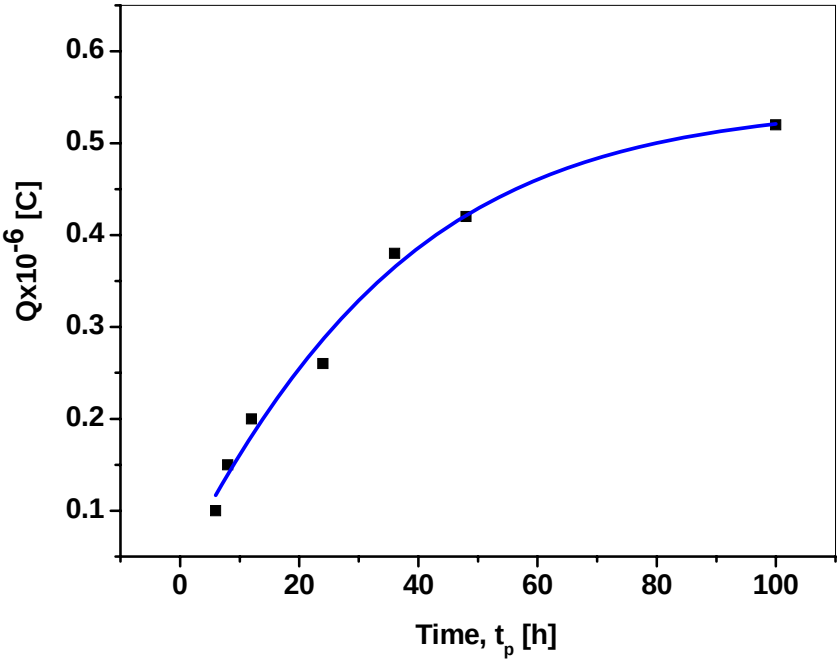

Figure 3.13: Total charge vs. polling time for magnet wire S_1.

3.4.2 Influence of Polling Field (E_P)

Figure 3.14 illustrates the TSDC curves for the multi-layered commercial magnet wire S_1 with a polyimide type ML coating with a thickness of 38.4 μm. The specimens are polarized at 120 ^oC for the different steep-front pulse voltages ranging from 1 to 3.5 kV peak with a duty cycle as high as 0.5 and by a pulse repetition rate of 2 kHz. The TSDC measurements are obtained with a heating rate of 2-3 $^oC.min^{-1}$. All the TSDC peaks occur in the temperature range of 70 to 170 ^oC. In Figure 3.14, curves 1 and 2 represent the current release from a specimen, polarized for one hour at 1 kV and 1.5 kV peak, respectively. In both cases, the observed peaks are relatively small. However, the specimens polled at 120 ^oC and 2.5 to 3.5 kV peak reflects four distinct peaks (curves 3-

6) in the TSDC spectra. These are not apparent for 1 to 1.5 kV peak pulses. Although the specimens are polarized at different voltages, the positions of all four peaks remain unaltered. Furthermore, it is obvious, from the TSDC curves, that the magnitude of the 70 ^{o}C peak increases more rapidly with the increase in the pulse voltage, compared with the increase in the 85 ^{o}C, 150 ^{o}C, and 170 ^{o}C peaks.

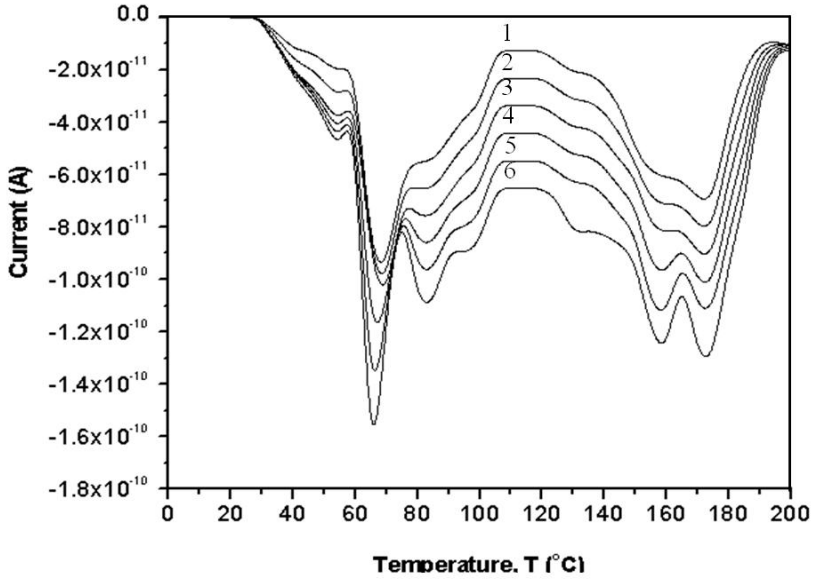

Figure 3.14: Effect of the polling field on the TSDC spectra of wire specimens for T_p = 120 ^{o}C, t_p = ~1 hr: steep-front unipolar pulse (1) 1 kV_p, (2) 1.5 kV_p (3) 2 kV_p, (4) 2.5 kV_p, (5) 3 kV_p, (6) 3.5 kV_p.

Figure 3.13 suggests that the 70 ^{o}C peak might be due to the release of the shallow trapped space charges; the other three peaks correspond to the release of the charges trapped at different depth levels in the wire insulation [137]. Also, the presence of several peaks signifies that the polarization mechanism is not the result of one relaxation, but of the distribution of several relaxation processes. The increase of the TSDC peaks at such high temperatures suggests that the change in the mechanism might be from the dipolar polarization to the conduction current mechanism that occurs at 170 ^{o}C.

The discharge values, with reference to the pulse magnitude, are shown in Figure 3.15, which provides another way of understanding the mechanism involved. The amount

of the total charge release shows a linear increase for the range of a 1 to 3 kV peak, which abruptly increases for 3.5 kV peak. This can be attributed to the injection and the accumulation of the higher charge concentration into the deeper trap sites of the wire insulation. The causes of the deep trap carriers in multi-layer insulation are associated to the presence of higher field stresses.

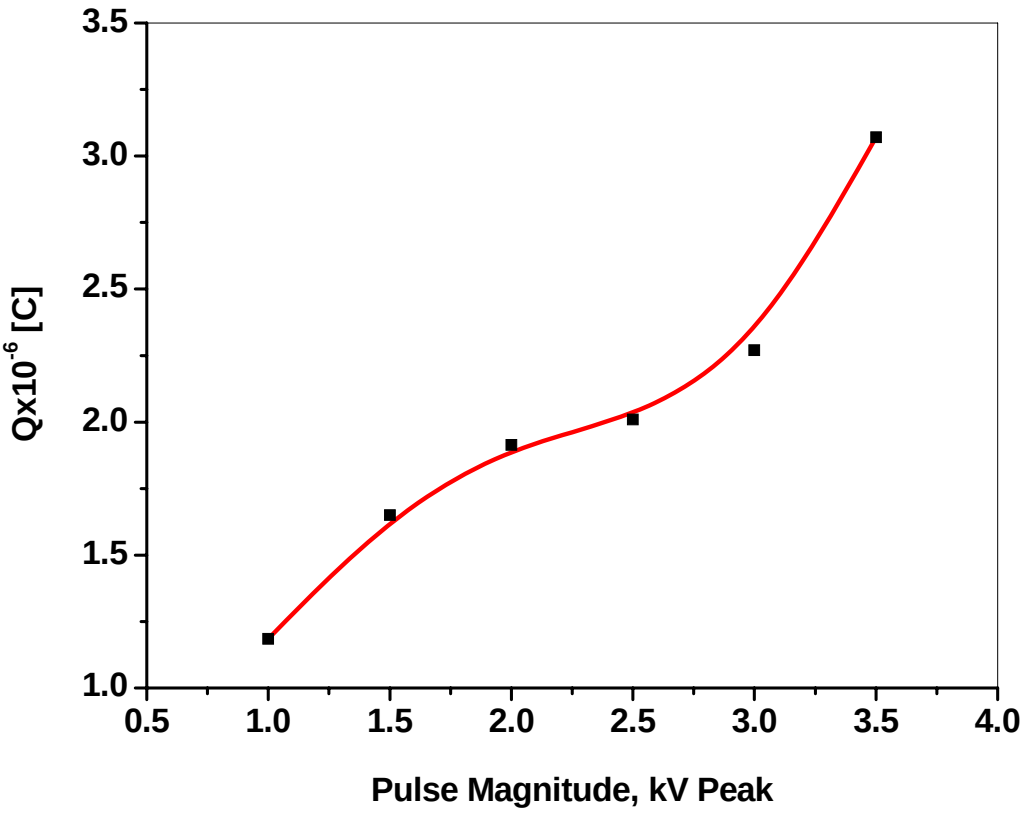

Figure 3.15: Total charge versus polling field for magnet wire S_1.

3.4.3 TSDC Measurements under PWM-VSC Waveforms

The TSDC measurements on enamelled wire specimens, depicted in Figure 3.16, confirmed that the charges can be trapped in the insulation after aging at elevated temperature under fast PWM-VSC waveforms. The TSDC spectrums obtained under bipolar waveforms are complex to interpret due to low ion mobilities in a solid polymer.

Since the spectrum recorded is clean, this suggests that the ion processes are secondary to electronic processes. Therefore, both positive and negative peaks are observed under all of the polling conditions. At 70 ^{o}C, a well-defined negative peak occurs with different potentials. A second positive peak appears in the higher temperature region at 140-180 ^{o}C with both change in the amplitude and position with different aging voltages. In polyimide coated type ML wires, the existence of shallow and deep trap levels has already been discussed in previous sections. The origin of shallow traps, although not fully established; include chemical impurities, oxidation products, broken chains and absorbed molecules have been held responsible for producing these traps.

The PWM-VSC with high frequency components and *dV/dt*, create additional surface traps during the aging process. Therefore, the appeared maxima at 70 ^{o}C can be associated with the de-trapping of the charge carriers from the shallow trap levels. It is believed that the peak at higher temperatures can result from the deeper traps in the multi-layer coatings. During heating, this positive current is attributed to the hetrocharge, which gains enough energy and is transported by the internal field to the shorted electrodes, giving rise to current maxima. However, the evidence of positive and negative TSDC peaks demonstrate significant enhancement in the bulk trapping centers. Thus, the currents detected with the electrically and thermally aged specimens is not effect of single factor generated by deep trap but combined action with shallow trap that may be responsible for slow degradation of enamel wire coatings.

Figure 3.17 shows the results of the total charge released to the external circuit as a function of the polarizing field dependence, which can be obtained by integrating the TSDC spectrum in terms of time from t = 0 to t = ∞. The results are similar to those previous conditions, reported in Section 3.4.2. The total charge released shows a linear dependency on the applied voltage. A strong increase in the charge concentration is observed at lower field, which increases slowly. Therefore, the total released charge at higher fields can thus be attributed to the cumulative effects of shallow and deep-traps.

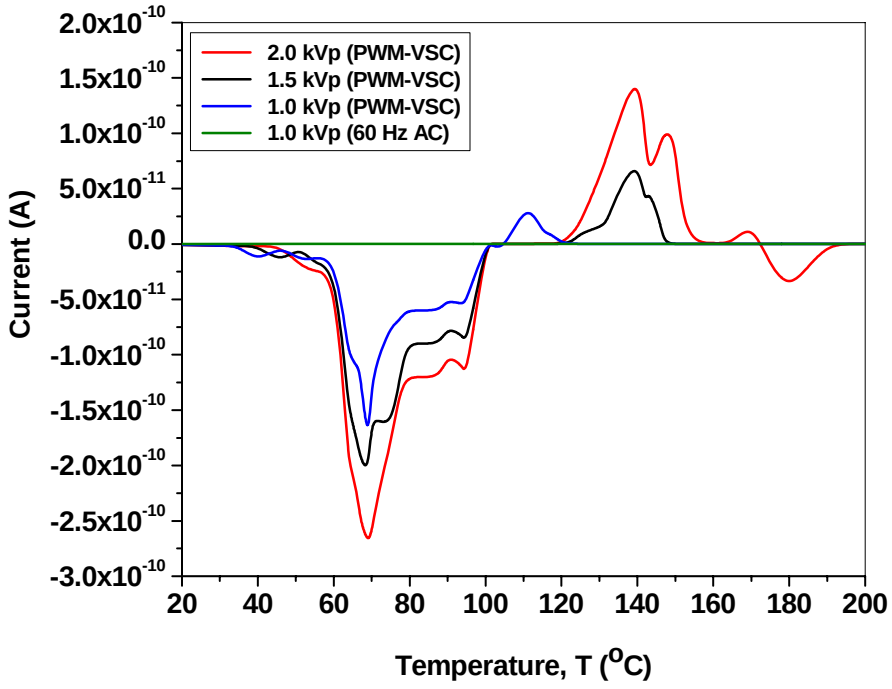

Figure 3.16: Effect of PWM-VSC waveforms on TSDC spectra of small bar specimens.

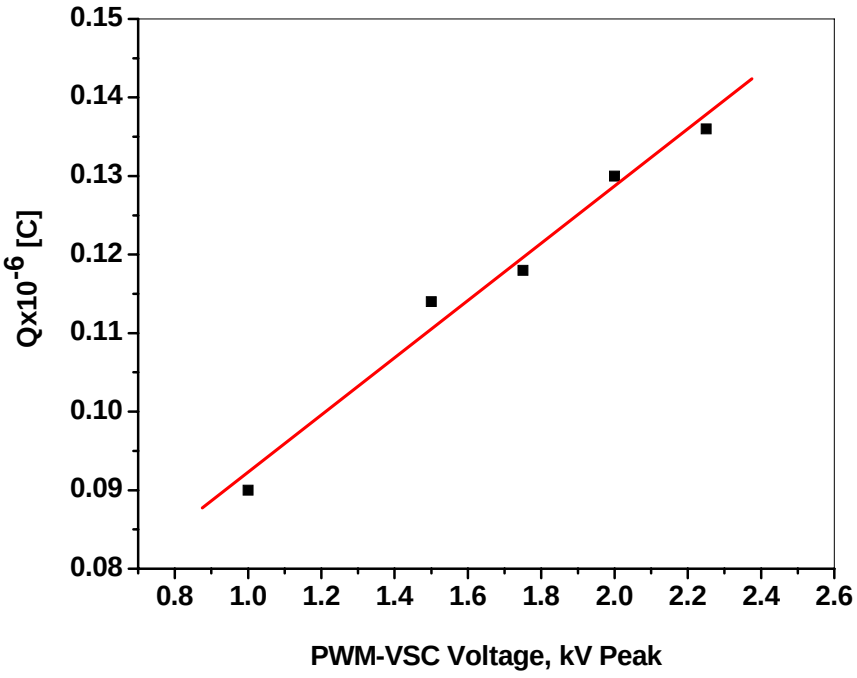

Figure 3.17: Total charge versus PWM-VSC output voltage, for magnet wire S_1.

3.4.4 Effect of Multiple Layers on the TSDC Measurements

Figure 3.18 exhibits a typical TSDC plot for the specimens listed in Table 3.2. These specimens belong to the class of S_1 enamelled wires. All specimens are aged for one hour at a polling field of 5 kV/mm peak.

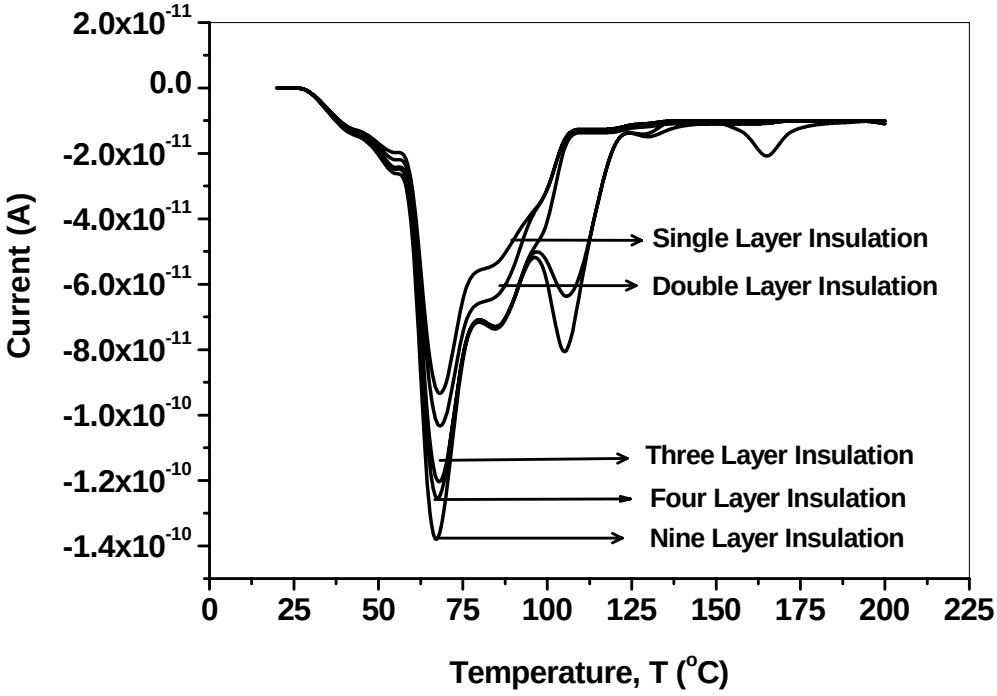

Figure 3.18: TSDC results for small bar specimens having enamelled wires with different insulation layers.

The TSDC, for the samples with coating layers as high as three, indicates no significant differences; in fact, the four to nine-layers produce a slightly higher current with four distinct peaks. Figure 3.19 summarizes the space charge measurements by plotting the total stored charge as a function of the insulation layers. It is evident that the total stored charge in the insulation bulk increases significantly as the insulation thickness increases. The magnet wires with four layers and the one with nine layers perform considerably different from the other wires. The concentration of the trapped charges is much higher which is likely due to the presence of broad distribution of the traps, occupied by the injected charges.

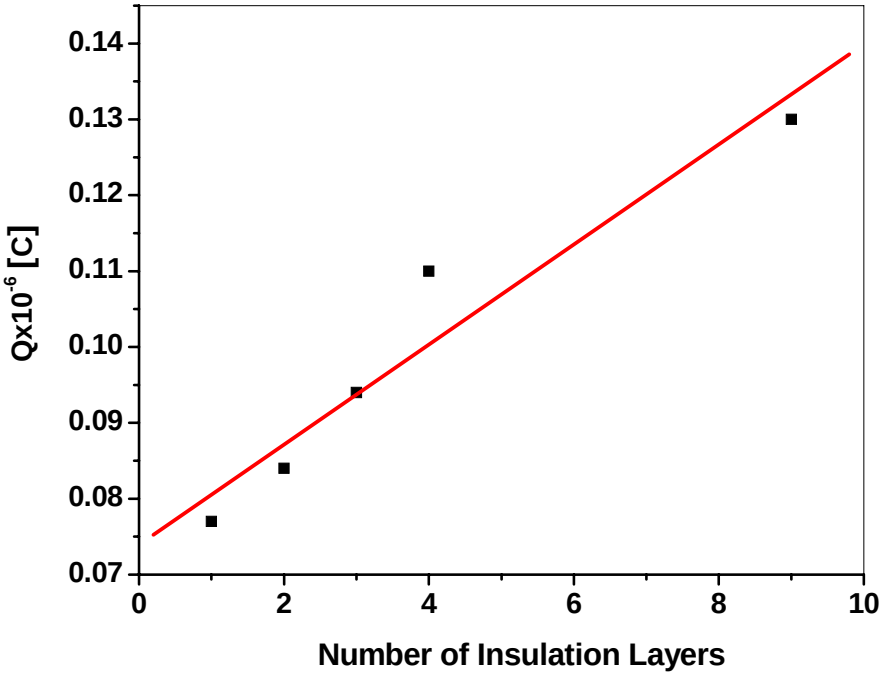

Figure 3.19: Total charge versus number of insulation layers.

3.4.5 Stored Charge in Nanofilled Magnet Wires

To render the motor magnet wires less susceptible to high *dV/dt* and more resistant to PD and space charge effects, nanofilled PD resistant wires are also tested. The use of nanofillers such as SiO_2 in standard enamel compositions presents an attractive means to upgrade the wires without changing either the enamel composition or the manufacturing process. The hybridization of the nanofiller compositions improves their life; however, due to the increased demand to further enhance the reliability and thermal performance, the development of such PD resistant insulation is crucial. In this context, an investigation into the comparison of stored charge, released using the TSDC measurements, is carried out. Figure 3.20 portrays the comparative results in wires with and without nanofillers that are subjected to 155 ^{o}C and at 1 kV peak unipolar steep-front pulse voltage waveforms. In this regard, the reduction of the amount of accumulated charges is observed, which is common to materials with nanofillers and has already been reported by Montanari *et al.* [65]. The reduction in the space charge is associated with the

conduction current which becomes larger for nanostructure materials. The trapped charges are released more rapidly by nanofilled materials, and thus, the residual charges after long depolarization times, is smaller than those of pure materials [65].

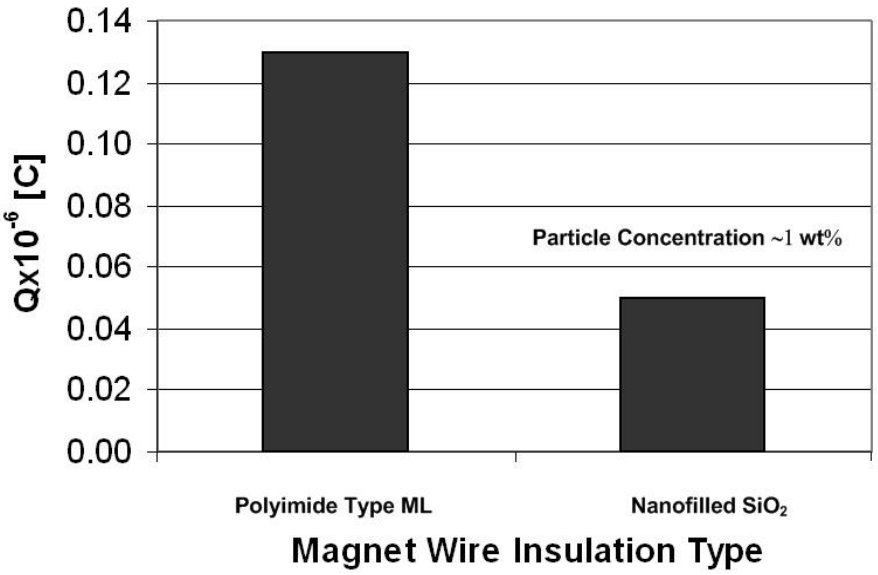

Figure 3.20: Comparison of stored charge released using TSDC measurements.

3.5 Groundwall Insulation Tests

The test methods described in Section 2.6 are considered for groundwall insulation evaluation. The methods considered in this work have little or no previous published data for medium voltage induction motor stator insulation systems, when exposed to steep-front pulses. It is therefore of interest to get some idea of whether and how these methods show changes in stator insulation systems after long-term aging.

3.5.1 Thermographic Results of Groundwall Insulation

In inverter-fed motors under high switching frequencies, hot-spots develop on the surface of the groundwall insulation system. In laboratory tests, the effects can be reproduced on

a VPI stator bar specimen, which has been prepared with a single-layer of normal mica-based insulation. With an infrared camera, the increase in temperature is measured after the application of a sinusoidal voltage of 60 Hz and pulse voltage waveforms (1 to 6 kHz) with a rise time of 400 ns. Figures 3.21 and 3.22 displays two infrared images, energized by a 5 kV peak 60 Hz sinusoidal and 3.5 kV peak at 3 kHz pulse voltage. From the images, no significant surface temperature increase is observed under power frequency voltage. However, hot-spots are evident on the test bars under going the pulse voltage. The rise in the temperature gradient is very rapid in the first 20 minutes, and stabilizes after 40 minutes, leading to a further increase of only 1-2 ^{o}C [138]. From the location of the hot-spots in Figure 3.24, a temperature increase of ~22 ^{o}C is found on the groundwall insulation surface [23].

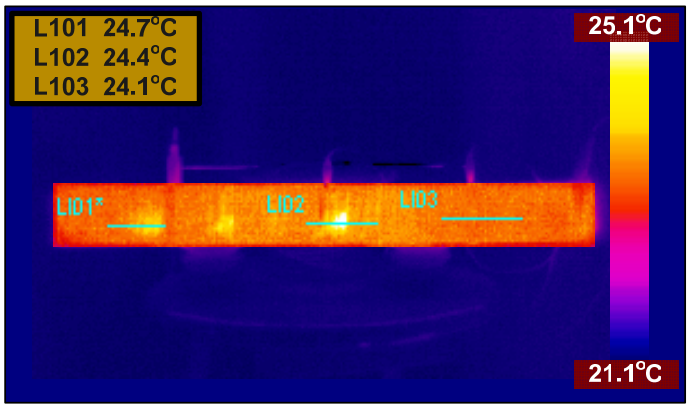

Figure 3.21: The identification of hotspots using infrared thermographic camera under 60 Hz ac, 5.0 kV peak.

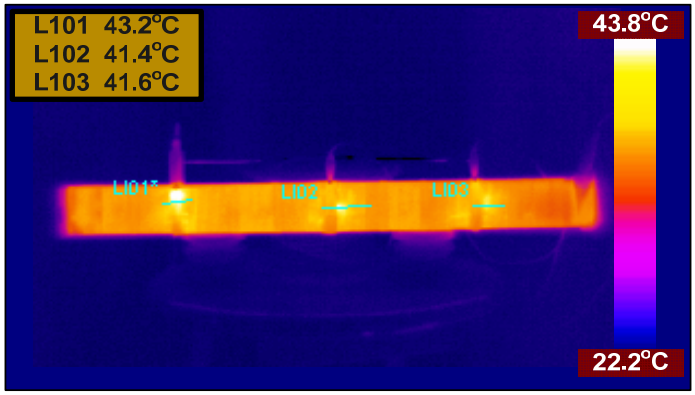

Figure 3.22: The identification of hotspots using infrared thermographic camera under 3.5 kV peak pulse, at 3 kHz.

A detailed investigation of the rise in the surface temperature in the actual stator coil is reflected in Figure 3.23 at a test voltage of 5 kV peak, in which a significant rise in the surface temperature is observed. In these coils, an average increase of ~10 ^{o}C is observed with a uniform increase in the switching frequency of ~1 kHz. Due to the increasing voltage frequency, the capacitive impedances are lower; therefore, the current passing through the conductive layer increases rapidly. In such cases, the temperature increase becomes more obvious with the increasing voltage frequency.

Thus thermal stresses, usually caused by a combination of losses generated in the motor and the ambient, are higher in the inverter-fed motors. When insulation materials are exposed to such elevated temperatures for prolonged periods, the chemical and physical breakdown is significantly accelerated, as described by the Arrhenius equation. This situation is further aggravated, if there is a mismatch in the thermal expansion rates of the various materials [139]. To confirm the influence of temperature effects on long-term aging results of groundwall stator bars specimens having single layer of mica are presented in Section 3.5.3, for the conditions, reported in Section 2.6.4.

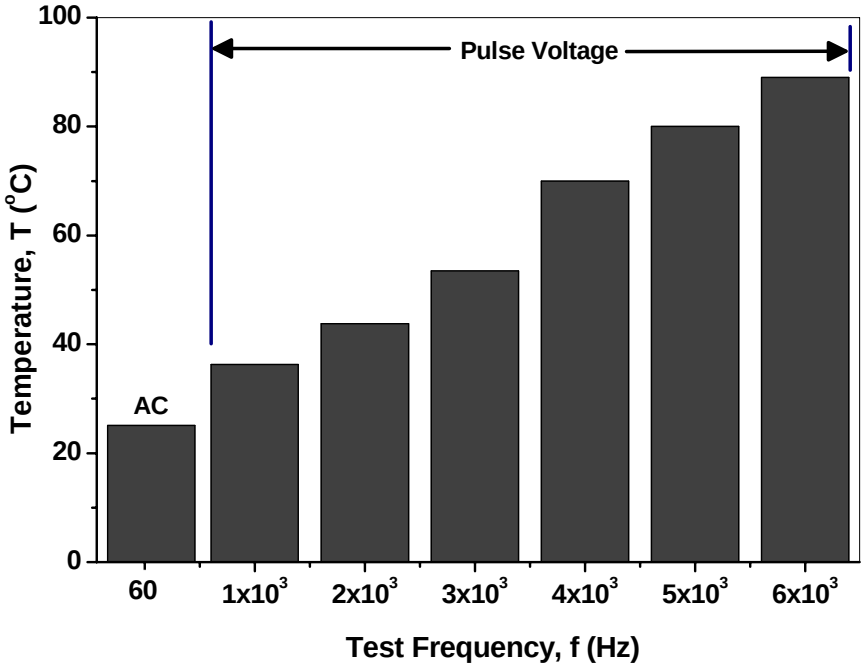

Figure 3.23: Temperature rise in groundwall insulation of stator with an increase in switching frequencies.

3.5.2 PD Measurement Results

As noted in ASTM Dl868 and IEC 60270, a PD pulse occurring within a stator winding can be changed profoundly by the time it is detected at the phase terminal. To observe such changes, the aging experiments are carried out under different pulse amplitudes and frequencies, and for different values of test temperatures for groundwall stator bars having single layer of groundwall mica tape. All PD detection up to breakdown of specimens is done with a device called Xtrac™ as described in Section 2.6.1. Figure 3.24 depicts the oscilloscope waveforms of PD pulses for specimens subjected to 5 kV peak and 3 kHz steep-front unipolar pulse voltage waveforms during aging. In all the waveforms, the surge remnant, which can be easily distinguished from the PD pulses, is ignored.

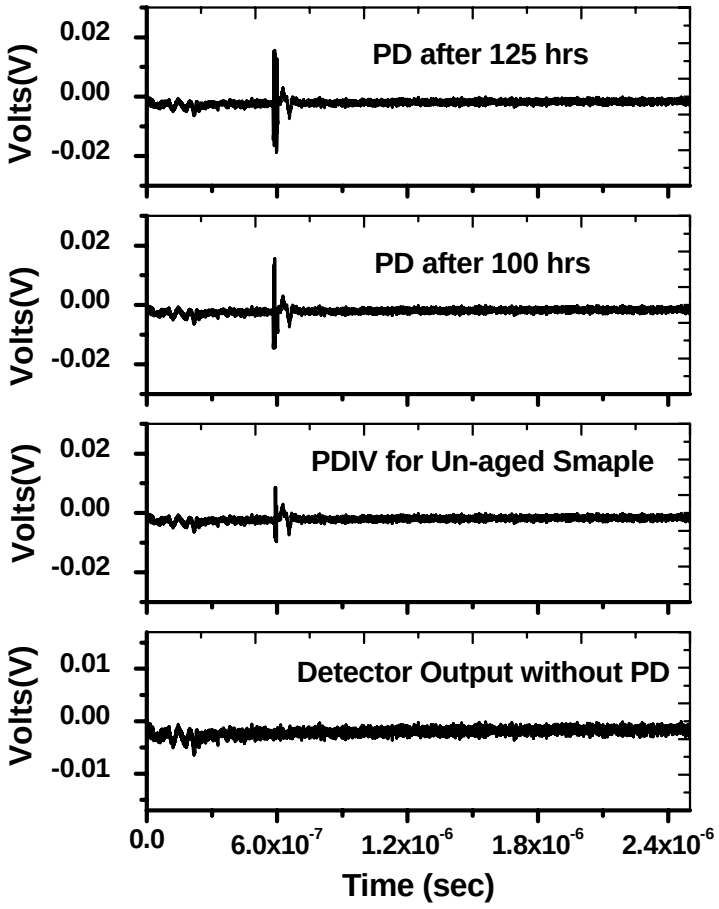

Figure 3.24: PD pulses from the stator bar groundwall insulation at room temperature before and after pulse aging subjected to 5 kV peak at 3 kHz.

The high frequency output from the detector indicates that the PD has a rise time between 5-10 ns. After 125 hours of pulse aging, the magnitude of the PD along with the repetition rate increases from ~50 mV to ~180 mV; whereas, the PDIV drops accordingly. It is noticed that the PD rarely occurs at each surge, but as the magnitude of surge increases above the discharge inception voltage, a stabilized PD pattern is seen to occur on every subsequent pulse.

The different PD inception levels for the two different stator bars indicates that pulse is severe compared to ac aging. The results prove a clear correlation between the PD activity and accelerated aging life. The transitions of the PD magnitude with time are higher in stator bar that were aged under steep-front pulses. Table 3.6 summarizes the test data of the PD inception levels obtained under different conditions.

Table 3.6: Comparison of PDIV (kV peak) levels for different test conditions.

60 Hz AC Aging, 5 kV_p at 23 ^oC		3 kHz Pulse Aging, 5 kV_p at 23 ^oC	
Time (h)	PDIV	Time (h)	PDIV
0	3.1	0	3.1
50	3.0	50	2.9
75	2.9	75	2.6
100	2.9	100	2.4
125	2.9	125	2.2
150	2.8	Specimen failed	
200	2.6	-	-
225	2.4	-	-
Specimen failed		-	-

3.5.3 Long-Term Aging Results

To predict the behavior of an insulation system under pulse voltage waveforms that are rated at 1000 V or more, long-term aging tests have been developed as described in Section 2.6.4. In this test, a voltage is applied to an insulation system that is higher than expected in operation, and the time to failure is measured. In addition, the degradation of the insulation can be further accelerated by increasing one or more aging parameters. Long-term aging tests under voltage surges for stator windings have yet to be

standardized. However, in this investigation, the aging parameters are the test temperature and the switching frequency of the applied test voltages. During the life testing, a scatter in the failure time is observed; therefore, a set of three data points for each aging condition employed [78].

To see the thermal and electrical effect on the insulation life, as reported in Section 2.6, the accelerated aging test is carried out at room temperature, 120 ^{o}C, and 155 ^{o}C, keeping mica-based groundwall insulation as a focus of attention. The results are reported in Table 3.9, in which, a drop in the service life of the groundwall insulation, with reference to the switching frequency characteristic of the power source at different temperatures, is observed.

Table 3.9: Summary of the results obtained from long-term accelerated aging of groundwall insulation rated at 1.5 kV_{L-L}.

Temperature (^{o}C)	Log (E) Stress in kV/mm	Time-to-failure Log (D) in hrs*			
		AC (Hz)	Pulse Switching Frequency (Hz)		
		60	500	1500	3000
20	1.12	2.66	2.56	2.45	2.28
	1.21	2.39	2.26	2.16	1.98
	1.29	1.98	1.85	1.76	1.65
120	1.12	2.46	2.31	2.22	2.05
	1.21	2.13	2.02	1.89	1.76
	1.29	1.83	1.76	1.51	1.45
155	1.12	2.42	2.29	2.16	2.03
	1.21	2.02	1.92	1.84	1.66
	1.29	1.72	1.59	1.49	1.38

*Average of three samples per test condition.

Figure 3.25 shows lifetime curves at different switching frequencies and voltages under normal ambient conditions. The maximum drop in the lifetime is observed to be ~58% when the pulse voltage waveform with switching frequency of 3 kHz is used instead of 60 Hz ac. The experimental data points are fitted by a linear regression technique. In all cases, the points seem to be well approximated by a straight line, and the linearity coefficient r^2 values are consistently found to be greater than 0.95.

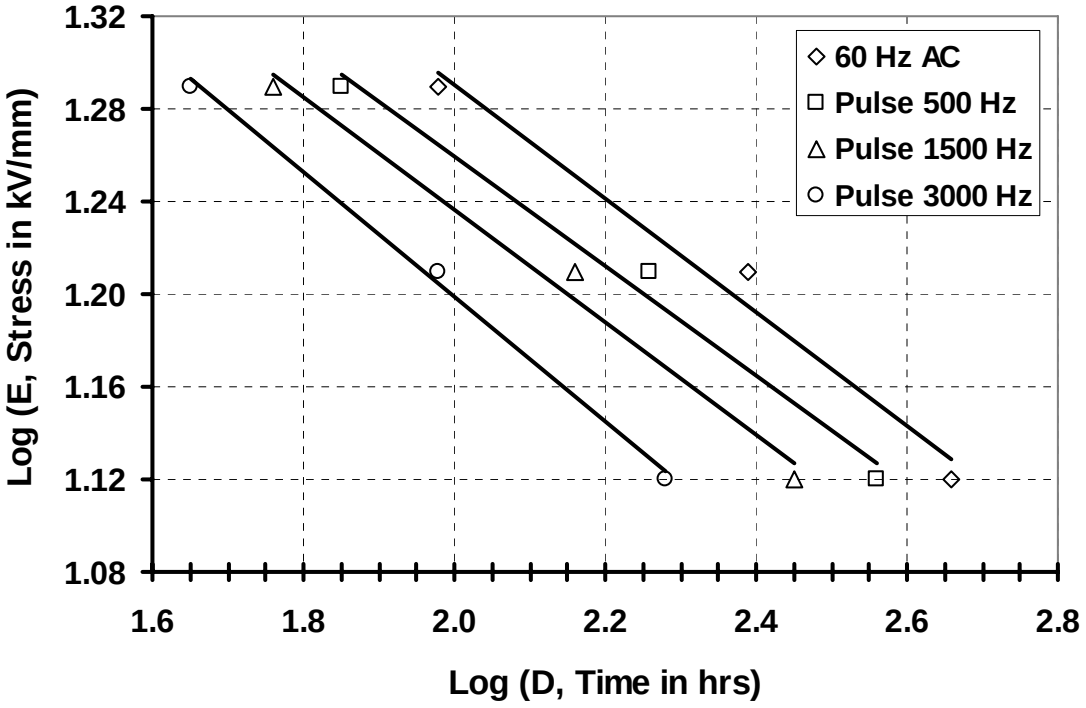

Figure 3.25: Log-log plot of the duration versus stress at different switching frequencies and at normal ambient temperature.

A change in the surface temperature is observed due to the development of hot-spots during the course of aging, which were between 60-70 ^{o}C at 5 kV peak 3 kHz. The test for pulse aging is repeated again with two different arrangements of cooling system; forced water cooling and by using environmental chamber, to keep the bar temperatures close to 23 ^{o}C. However, efficient cooling was better achieved with an environmental chamber as compared to water cooling system. It is evident from the results shown in Figure 3.26 that the insulation lifetimes improve and shift closer to power frequency lifeline. Also, the variation in lifetime is reduced to ~31%. The key cause of this variation in the life can be attributed to the aging phenomenon, which accelerates due to enhanced dielectric heating, especially under pulse application [140].

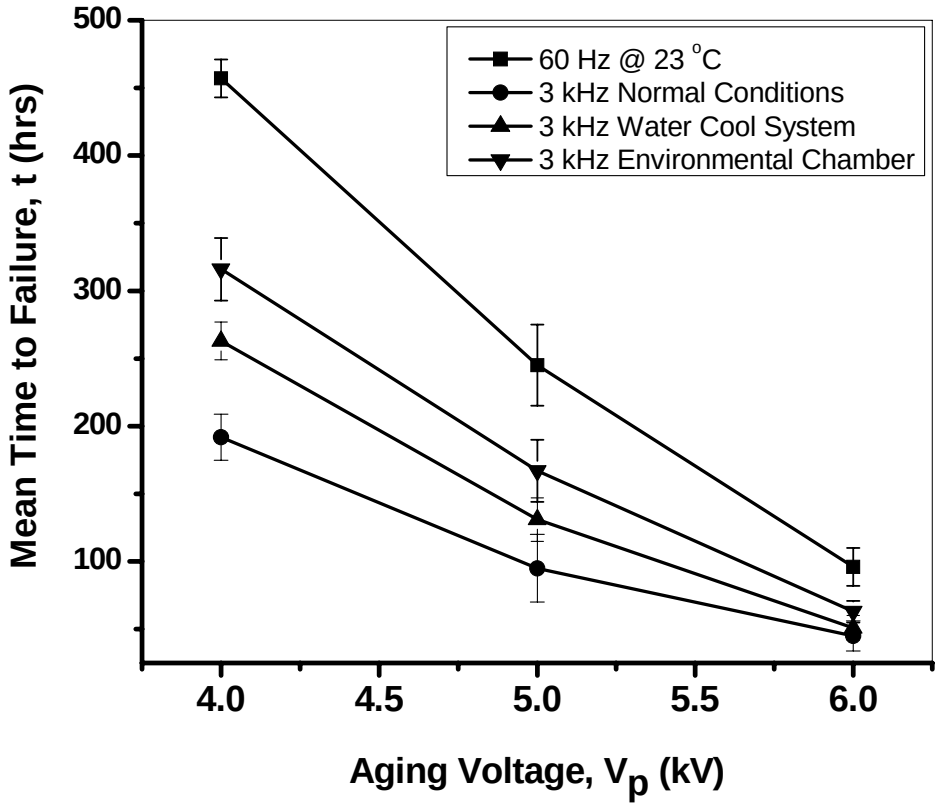

Figure 3.26: Comparison of life curves under ambient and forced cooling environments.

In addition to the stresses due to the high rise time of the pulse waveform, it is important to take into account the thermal effects upon the insulation system life. To accomplish this, a series of tests are conducted at 120 °C and 155 °C to confirm the contribution of temperature. Figure 3.27 reflects the impact of this variable, temperature, on the insulation life. Note that, in addition to pulse magnitude and frequency, the temperature has a drastic effect on the time to failure in the accelerated life tests. The results lead to the conclusion that as the operating temperatures increase the thermal aging accelerates, decreasing the insulation life. Moreover, this renders the material more vulnerable to other system stresses [28]. Therefore, the insulation life tests reveal that it is imperative to keep the motor operating temperature well within the intended design and operating limit to achieve the desire thermal life.

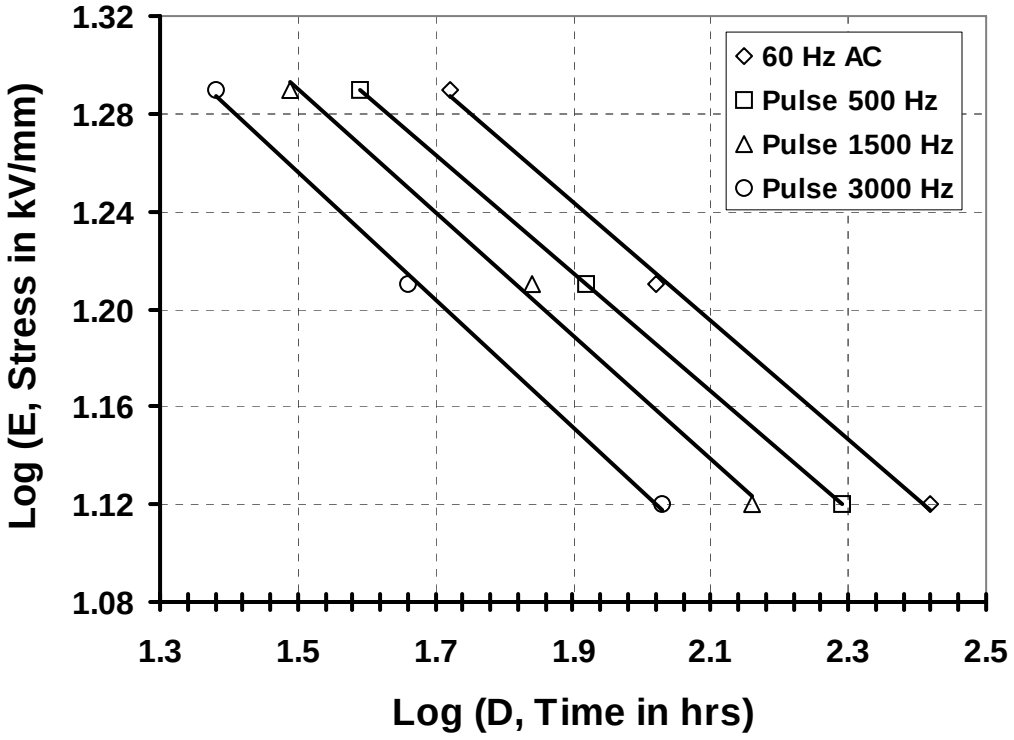

Figure 3.27: Log-log plot of the duration versus stress at different switching frequencies and at a test temperature of 155 ^{o}C.

Chapter 4 Discussion

4.1 Introduction

The introduction of medium voltage variable speed drives (VSD) using PWM-VSC has created concerns about the negative impact these drives have on the insulation system of a motor [121, 141]. Manufacturers need to improve the insulation systems of these machines in order to meet the requirements as specified in the upcoming technical guidelines [78]. As mentioned in Sections 3.2 to 3.5, both inter-turn and groundwall insulation systems are significantly affected by fast rise time pulses. In this chapter, the consequence of PD and the release of the stored charges from different traps levels in enamelled wires that are subjected to steep-front pulses are described. The results from the TSDC test indicate a consistent correlation between space charges and multi-layer insulation on magnet wires. Also, the enhancement of magnet wire enamel coatings by using nanofillers is introduced. In groundwall insulation, the information from long-term aging, described in Section 3.5, and the measurements of surface temperature profile along with the dc breakdown strength are used to identify the possible aging mechanisms. In addition, the visual examination of the failed stator bars, removed during the life testing, is discussed at the end of this chapter.

4.2 Enamelled Wire Degradation Mechanisms

Polymeric magnet wire coatings consist of polyimide, polyester with and without amide-imide, and polyimide-THEIC, are subjected to steep-front pulses under PWM-VSC applications. These coatings; thus degrade due to PD activity, formation of space charges in multi-layers and due to enhanced dielectric heating. This is evident in all of the tests carried out in this research. In the samples, a decrease in the dc breakdown strength is observed, as reported in Table 3.1 and Figures 3.2 to 3.7. The approach to study the

degradation of magnet wire coatings mentioned previously consists of the simultaneous measurement of the surface roughness, thermally stimulated depolarization currents, and the dc breakdown strength.

4.2.1 Influence of Voltage Waveforms

In the aging results, certain interactions among the stress factors are identified. The most significant interaction, observed is between the voltage *V*, *dV/dt*, and the pulse switching frequency. As seen from Figures 3.3 to 3.5 two distinct slopes between dc breakdown voltage and switching frequency under the pulse aging reveal that more than one degradation process affects the enamelled wire samples. Two principal regions based on the pulse repetition rate, indicates change in the aging mechanisms [35]. According to Kaufhold *et al.* [142], PDs are initiated in the air-filled gaps between the enamelled wires that are touching one another. These discharges transform a part of the capacitively stored energy in the insulation into heat and radiation, as well as mechanical and chemical energies, degrading the insulation materials. In addition to the PD activities, as discussed in Section 3.2, the space charge accumulation significantly contributes to insulation degradation.

The work of Bellomo *et al.* [13], with respect to intrinsic aging, which is the formation and trapping of charges is particularly relevant to explain the space charge influenced degradation. The voltage *V*, *dV/dt*, and pulse switching frequency suggest an interaction between the voltage characteristics and the material dielectric properties, where *V* is lower than the discharge inception voltage (DIV). In the samples, the presence of high frequency harmonics in the fast rise time of the applied voltage can lead to delayed (out-of-step) polarization, blocking of some of the charges. It is believed that the contribution of the charge accumulation, in addition to the PD activity results in the two distinct slopes in Figures 3.3 and 3.5 [13], where the injected charges relax at lower pulse repetition rates due to the longer time interval between the pulses. Once the pulse repetition rate is beyond a threshold value of 500 Hz, the time for relaxation is not

sufficient. As a result, the dipoles with the longer relaxation time can result in charge accumulation.

In addition, Bellomo *et al.* [13] have suggested that, once the charge concentration increases, it travels either perpendicularly or tangentially. In the perpendicular movement, it leads to a creation of space charges in the bulk; whereas, in the tangential movement it corresponds to a charge flow on the surface. However, the occurrence of discharges between coating interfaces due to recombination phenomenon will cause damage to the samples. Consequently, the building and trapping of charges, related to the new form of stresses due to the high *dV/dt* wavefronts, can be suggested as one of the reasons for insulation degradation in multi-layer enamelled wires. Furthermore, the creation and accumulation of space charges cause electric field distortion and favours the injection of new charges; initiating damage in the multiple layers [53,143,144].

On the other, for high frequency ac waveform aging, it is evident in Figures 3.6 and 3.7 that for the selected test frequency range, the mechanism is different. The dc breakdown voltage decreases almost linearly, as the frequency of the test voltage is increased from 60 Hz to 4 kHz. This decrease in the breakdown voltage is attributed to the degradation from the enhanced PD activity between the gaps in the enamelled wires and the heat build-up due to the dielectric loss. According to Khachen *et al.* [145], the corona inception level within voids or micro-cavities is also reduced by an increased frequency, causing extremely intense discharge at the same applied stress. The resultant degradation process causes the dielectric to breakdown much earlier, as the frequency is increased.

4.2.2 Consequence of Space Charges

In enamelled wires, PD represents one of the main factors for the accelerated insulation degradation in a high electric field, compared with the 60 Hz ac waveform; therefore, the lifetime of the insulation obviously decreases with the PWM-VSC [146]. This can be attributed to the increase of PD pulse quantities, which are much lower in the case of 60 Hz ac voltage. In addition to PD, it is now admitted that space charge accumulation can

also play a role in the accelerated aging of magnet wire coatings, affecting the mechanism of PD inception and repetition through an electric field modification, as well as giving rise to electrochemical energy storage and additional losses [6,147,148,149,150]. The extent of space charge accumulation depends on the supply voltage waveform and on the material itself, which performs in different way regarding space charge trapping features.

To understand the consequence of space charge behaviour in polyimide coated magnet wires, a detail investigation as a function of the insulation layers has been performed and the results are presented in Section 3.4, Figures 3.12 to 3.20. To measure the energy distribution of the free and trapped carriers, a TSDC technique is applied. A distinct change in the TSDC plots is observed for the various layers. The origin of this behaviour is discussed in terms of the release of the trap charges from their location that is interfacial and bulk, and for depth, shallow and deep. The TSDC spectra for polyimide coated magnet wires consist of several peaks under different test conditions, reported in Table 3.5. The trapped charges, released from the defect or localized states in the coating of enamelled wires, are related to the onset of dipolar motion. At the macroscopic level, the overlapping of several peaks indicates that the polarization is not due to only one relaxation, but from the distribution of several relative processes and charges trapped at different depths [151,152,153].

4.2.3 Relationship between the Stored Charge and the Aging Time

The time dependent aging, as explained in Section 3.4.1, results in the development of charge accumulation in the distributed traps. The results of the charge released after the TSDC measurements demonstrate logarithmic time dependence. A similar explanation has been given by Fu *et al.* [137] for low-density polyethylene (LDPE) after ac aging. The accumulation of space charges in the wire specimens can be directly attributed to the charge injection at the dielectric and electrode interface that reaches saturation with the polarization time due to possession of well defined trap carriers. Given the relationship between the release of the stored charge and aging time, verified in Figure 4.1, the following model, presented in Equation (4.1), indicates a good fit, and is simple.

$$\textit{Relative increase in stored charge, } Q_R \Rightarrow \left[\frac{Q_x}{Q_1}\right] = a\ln(t) + A \tag{4.1}$$

Constants a and A are 1.5 and -15, respectively, for magnet wire specimen S_1, when it is subjected to steep-front unipolar pulses and $Q_x \geq 1$. The value of Q_x increases with aging duration with reference to stored charge Q_1, which is determined after six-hour. It is noteworthy that relative charge Q_R and the time relation expressed by Equation (4.1) at a constant voltage of 1 kV_p, is convenient to estimate the change in the stored charge under similar test conditions.

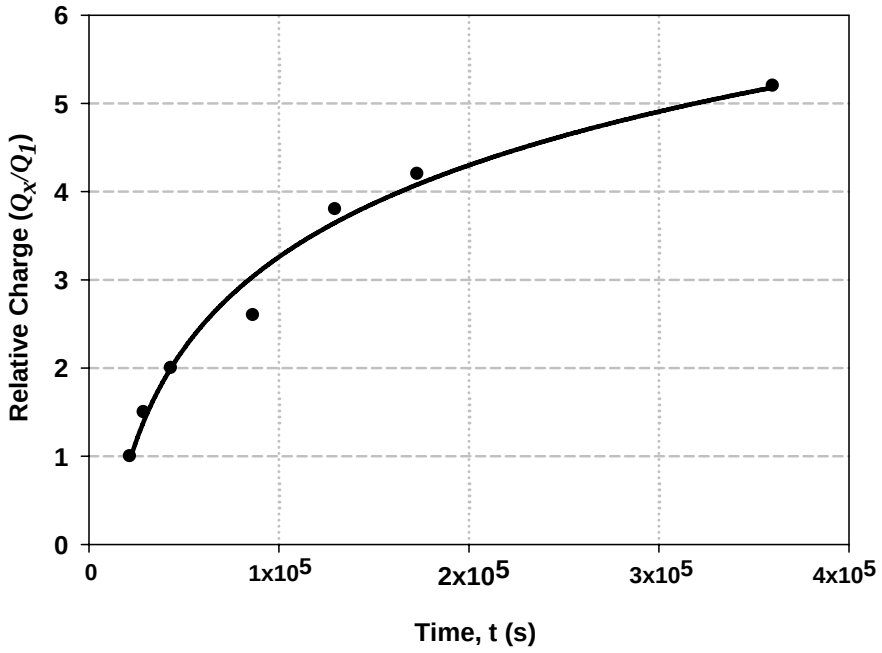

Figure 4.1: Relation of the relative charge and aging time under steep-front unipolar pulses evaluated at a constant stress.

The explanation in Section 3.4, based on the electric field and thickness dependence for charge trapping in the wire coating, is entirely different than the one for the long-term aging effects [154]. Under short-term tests, a linear increase in the charge concentration is observed with an increase in the stress and coating thickness. However, it is believed that similar behavior in charge concentration that fits well on Equation (4.1) could be

observed for both field and thickness dependence, if the polarization time becomes much longer, or close to long-term aging durations.

4.2.4 Trap Activation Energy

The quantification and analysis of the stored charge, based on the TSDC data, conveys the characteristic features of the trap distribution. These electron traps have various energies and densities [4], especially in the case of magnet wire coatings. As described in Section 2.5.1, activation energy (ε_a) is calculated by plotting ln(τ) vs. *1/T* employing the least square fit, as illustrated in Figure 4.2. The value of ε_a (the trapping depth) decrease from 0.48 to 0.22 eV with t_p tending to saturate, confirmed by the different slopes in Figure 4.2. This change in the activation energy during the aging of the magnet wire can be correlated to the joule heating of the samples, which occurs due to the increase in the carrier mobility, or because of the large tunnelling current [155].

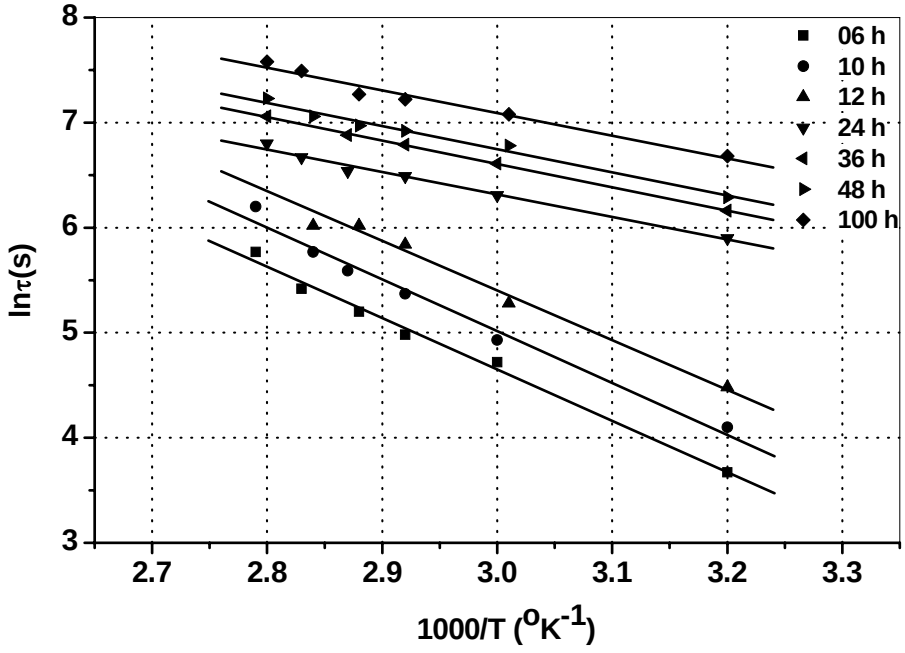

Figure 4.2: Relaxation time obtained from the TSDC studies as a function of *1000/T* in magnet wire S_1 specimens aged at different durations under constant stress.

Regarding the interaction between the polling field and space charge formation, entirely new behavior is observed compared to long-term aging effects. As the voltage increases, more of the electrons have a higher energy, such that they become deeply trapped. As a result, it will be harder to de-trap, since de-trapping depends on the electric field and the local temperature, as represented by the TSDC peaks in Figure 3.14. The results from Section 3.4.2 are reported in Figure 4.3, which denotes the Arrhenius plots as a function of the stress voltage. The trend demonstrates different energy levels which finally move towards saturation for voltages higher than 2.5 kV_p, as depicted in Figure 4.4. The observation of the various trapping levels proves that as the polarizing field increases, the barrier height of the traps in which the charges are found is decreased. This accounts for the saturation in the activation energy. Simply, the presence of a higher polarizing field within the sample will modify the potential barrier that moves the free charges from one site to another, leading to a lower rise in the apparent activation energy [156]. Almost similar results are observed, when the samples are aged under real PWM-VSC waveforms of different voltage levels.

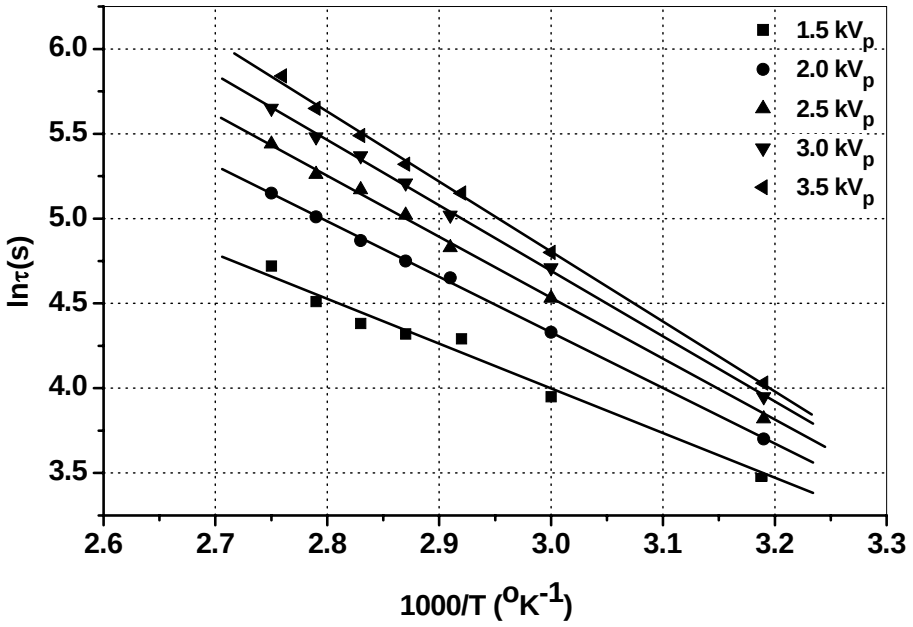

Figure 4.3: Relaxation time obtained from the TSDC studies as a function of 1000/T in magnet wire S_1 specimens aged under different polling voltages for a constant duration.

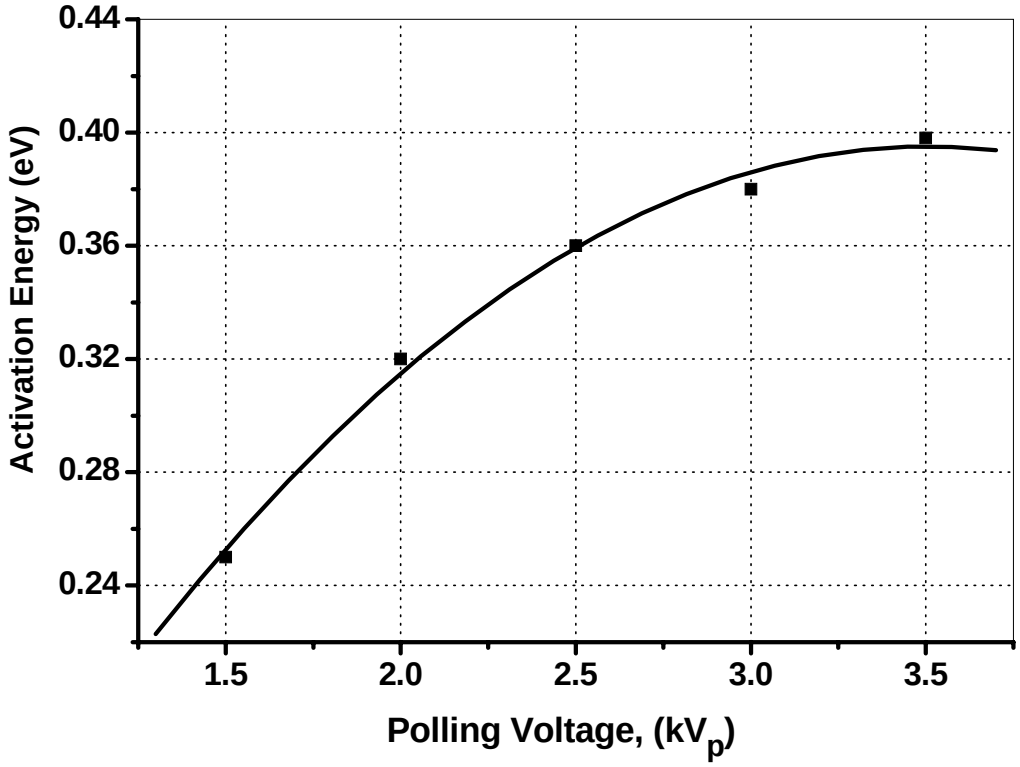

Figure 4.4: Relation between the polling voltages versus the activation energy.

In the thickness dependent investigation, in which the coating layers are increased from 1 to 9 in magnet wire S_1 activation energies, ε_a, are determined from the normal TSDC current peaks at lower temperatures. This is achieved by using the initial rise method of Garlick and Gibson [156]. The results are shown in Figure 4.5. So far, no data are available for this comparison. The activation energies have a constant value of 0.36 eV for magnet wires with as many as four layers. However, a different depth level is observed for the wire with nine layers with the corresponding activation energy of ~0.49 eV.

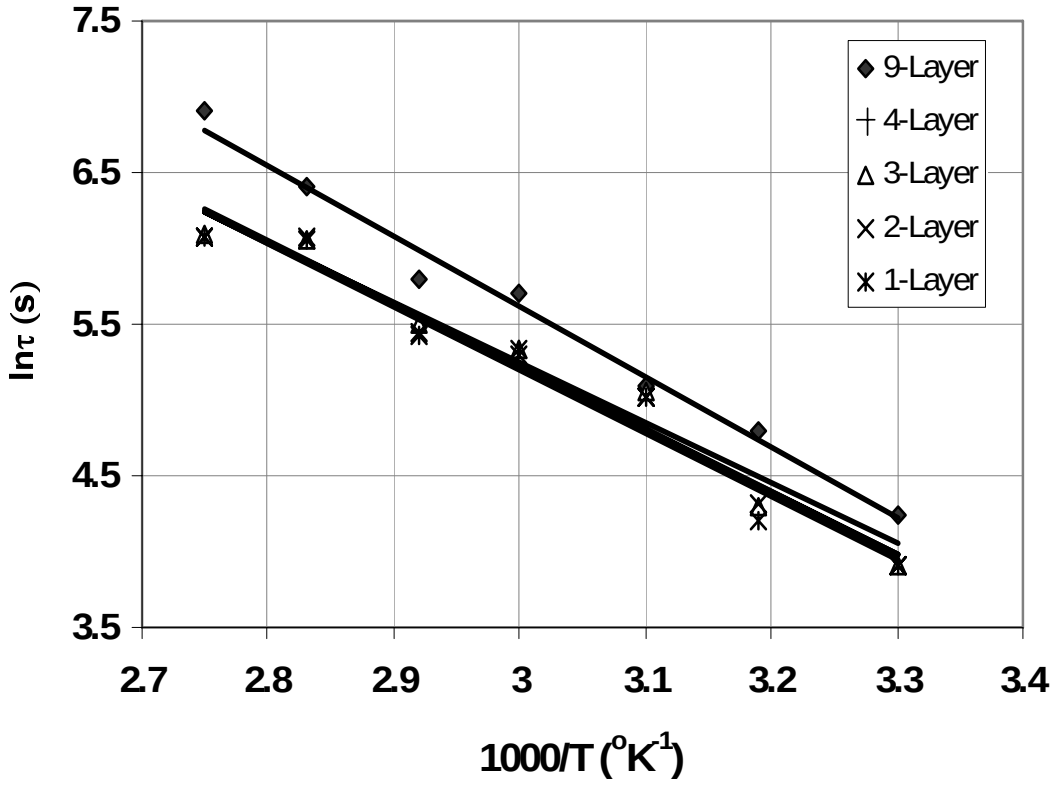

Figure 4.5: Effect of insulation layers on the activation energy.

4.3 Nanofiller Performance

The performance of filled coatings in magnet wire is studied in terms of surface roughness due to PD erosion. The control parameters during the investigation are filler type and its concentration. One of the motivating forces of the research in this thesis has been to find a correlation among the parameters, such as, filler with more resistance to PD with best concentration by wt%.

A material which has high discharge resistance, good matching of the coefficient of the thermal expansion, thermal conductivity enhancement, mechanical reinforcement, and abrasion resistance is able to conduct heat more efficiently. The use of nano-metre-level particle size, if dispersed uniformly, has exhibited a high level of resistance to PD; however, filler concentration has a strong correlation with the wire flexibility. As a result,

the control of material properties such as uniformity in the organic coatings and concentration (wt%) of nanoparticles are major issues in wire nanotechnology.

According to the results, presented in Section 3.3, it is revealed that the PD erosion process in nanofilled magnet wire coatings can be demonstrated in two subsequent stages. The first stage is referred to as the PD erosion stage, which is followed by the suppression erosion stage. In the first stage, electrical discharges generate charged and energetic species in the gaseous atmosphere around the material [16]. The interaction of these reactive species and insulation surfaces produce stresses, which contribute to the material degradation. The SEM analysis indicates that little degradation occurs on the surface of the filled enamelled wires, exposing the nanoparticles to the maximum surface of around 8-15 nm, as shown in Figure 4.6 [63,157].

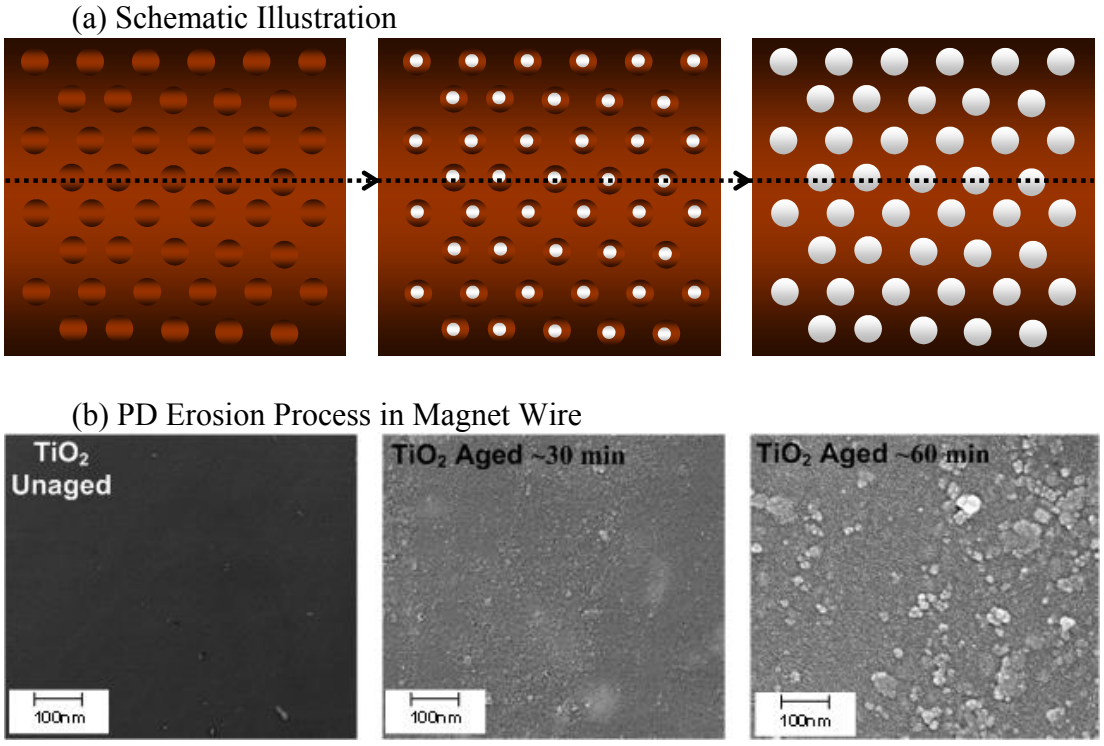

Figure 4.6: Comparison of schematic illustration of the erosion process on nanoparticles surface in magnet wire with a constant stress of 70 kV_p/mm.

During the erosion suppression stage, once the inorganic nanoparticles are exposed, the charged particles impinge on the filler particles thereby preventing further collisions with the organic material. In this way, the creeping distance is extended, and the collision energy of the charged particles is lowered considerably by the reflection and scattering so that the erosion is suppressed [88]. As mentioned earlier, the PD resistance can be further improved by increasing the loading of the inorganic material, but in doing so the mechanical properties of the enamel insulation is weakened. Thus, if the use of an inorganic material of a smaller particle size is feasible, it is possible to increase the surface area per unit weight, helping to increase the creeping distance significantly [63].

With reference to the surface degradation, Fuse *et al.* [157] also describes two possible mechanisms that are presumed to be dominant during PD activity. The first one is ozone oxidation on the surface that is produced by the discharge, and the second one is the impact of the electrons and ions that are accelerated by the sheath potential of the discharge. In addition, the authors have proposed that as the surfaces of organic polymers with nanofillers begin to volatize, the incombustible nanofillers pile up to form a thin-layered structure to avoid any further degradation [157,158]. According to Kozako *et al.* [158], the use of nanofillers reduces the PD degradation to a great extent. The regions between the nanofillers are eroded selectively, bringing up the fillers layer. As the surface erosion degradation proceeds further, the nanofillers eventually tend to pile up, and then form island-like structures over the eroded surfaces [159]. Figure 4.7 indicate such phenomena during the aging process.

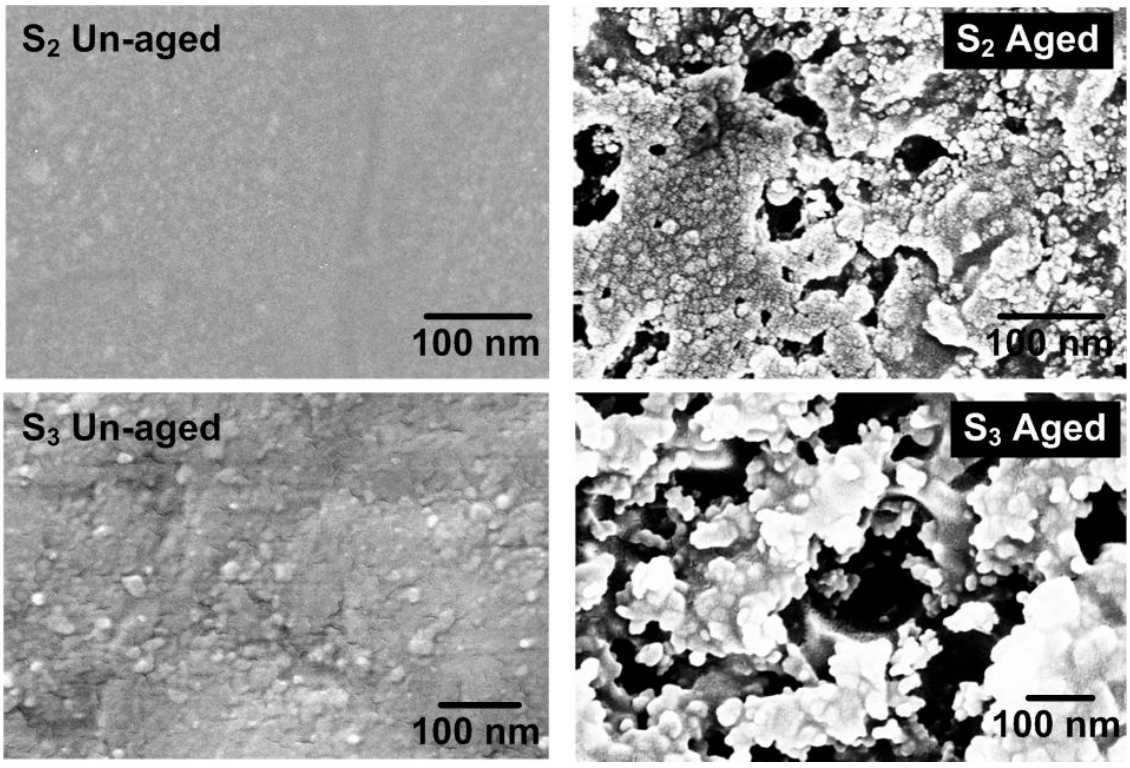

Figure 4.7: SEM images of commercially available magnet wire with PD resistant coating with alumina as the nanofiller (PWM aging); having average surface roughness of S_2 ~327 nm and S_3 ~313 nm.

4.3.1 Analysis of Weibull Distribution Parameters

To further explore the performance of nanofillers, a detailed investigation of Weibull distribution parameters; scale and shape, are performed. Most often, the breakdown strength also called scale parameter, corresponds to a 63.2% breakdown cumulative probability, is treated using the Weibull distribution. To attain the best fit of the experimental data, the maximum likelihood estimation (W/mle), with a 90% confidence bound interval is used, as described by Stone and Van Heeswijk [91]. The value of risk, which is 10%, is reasonable from a statistical point of view [91,160].

During the manufacturing process of wires, it is commonly thought that coatings contain defects, which are spread randomly. These defects contribute to a weakness, which can result in lower values of the dielectric strength than those of theoretical values.

As evident in Figure 4.8, the values of the Weibull shape parameter, β, is 2.16 for the wire specimen without fillers. From such a low value of β, it can be predicted that the aging frequency of 10 kHz ac can cause severe surface erosion, increasing the number of defects tremendously. However, the shape parameter value increases for the coatings with nanofillers, especially for magnet wire S_4. This indicates that the material becomes more homogeneous and consists of a smaller number of defects, generally present as a micro-void in a coating [65,160]. The inverse relation between Weibull shape parameter, β, and σ/σ_{min}, at 10 kHz ac waveform is also depicted in Figure 4.9.

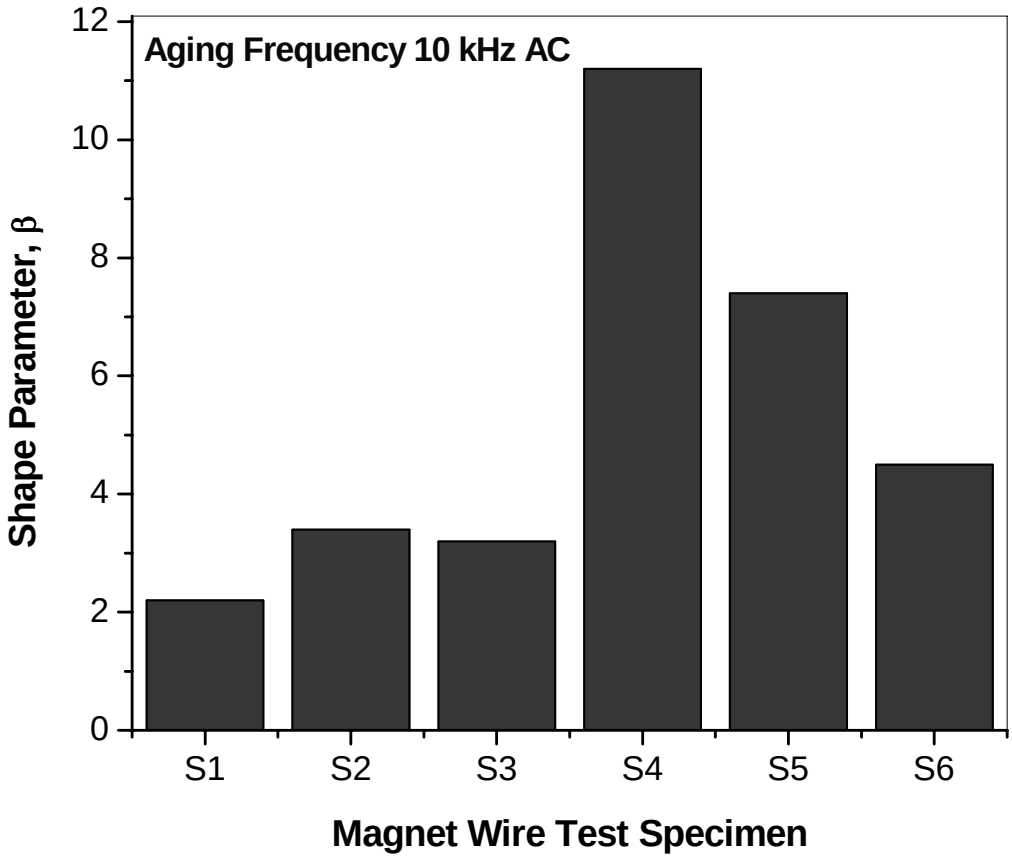

Figure 4.8: Shape parameter values obtained form the Weibull distribution for wire specimens aged at 10 kHz ac.

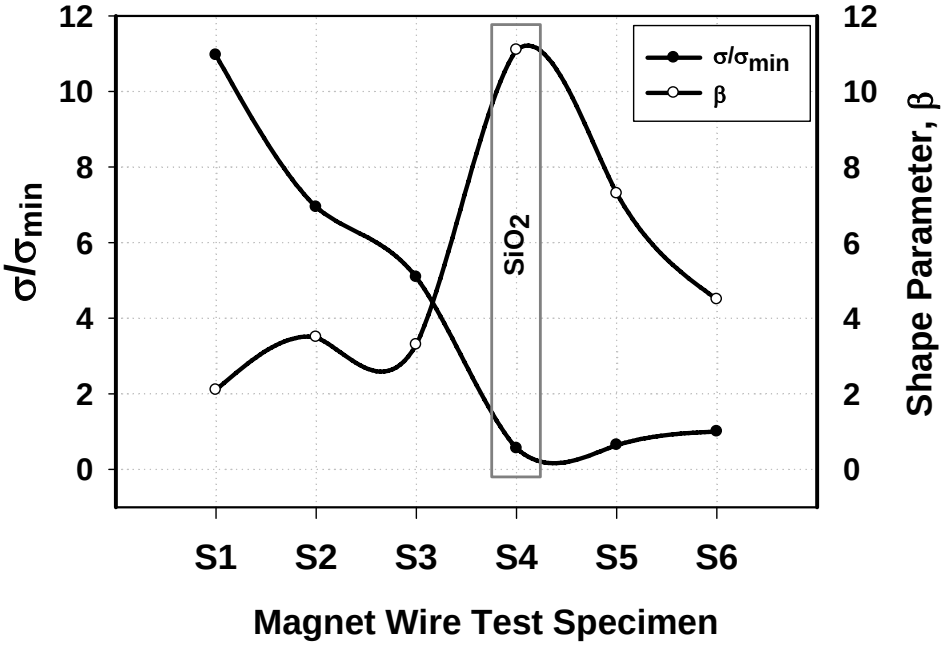

Figure 4.9: Relation between relative standard deviation (σ/σ_{min}) and Weibull shape parameter, β values obtained form the Weibull distribution for wire specimens aged at 10 kHz ac.

According to Tanaka *et al.* [60], nanofillers should have the effect of increasing the practical dielectric breakdown strength irrespective of the defects present in the material. To confirm the influence of nanofillers on the dielectric breakdown strength, four concentrations of SiO_2 (0.5, 1, 1.5, and 2 wt%) are used in a Pyre-ML®, polyimide solution. As denoted in Figure 4.10, an increase in the dielectric strength for the 0.5 to 1.0 wt% concentration is observed; but no further improvement in the dielectric strength is seen from 1.0 to 2.0 wt%. A saturation point in the dielectric strength is observed to be around ~1 wt%. Therefore, it is believed that a filler concentration in the range of 0.5 to 1 wt% has strong influence on dielectric strength. It is known that nanofillers will agglomerate, some types more than others, and this tends to develop a non-uniform dispersion. Obviously, a non-uniform dispersion of fillers will affect the breakdown

strength. Therefore, for further improvement in the breakdown strength a specialized mixing process is essential for the uniform dispersion of filler particles.

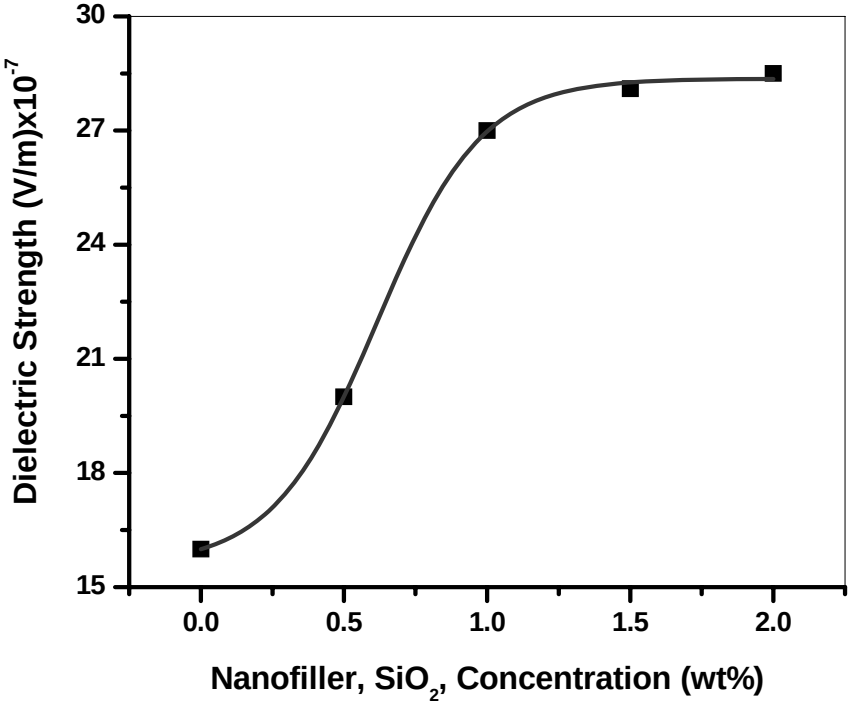

Figure 4.10: Effect of SiO_2 (fumed silica) nanofiller concentration on dc breakdown strength.

As discussed above, the main problem with increasing the concentration of nanofiller is the loss of mechanical strength. Materials that show a loss in mechanical strength due to increased filler concentration will also show a loss in electrical strength. There are a number of reasons for this and it depends on the type of filler used. One of the main reasons for this is a polymer has only a limited number of sites for bonding, which can be increased through the use of adhesion promoters. Without bonding, the material has nanosize cracks around particles that when flexed, will develop into larger cracks. Also, these cracks are weak spots dielectrically. Therefore, magnet wire coatings that have higher concentrations of nanofillers become more brittle, and thus, the number of surface cracks increases. Figure 4.11 shows such kind of problems in coatings for fumed silica (SiO_2). Finally, the breakdown investigation in Figure 4.10, and results in terms of

mechanical strength, suggest that the filler concentration of 1wt% seems to be more appropriate for the design of PD resistant magnet wires.

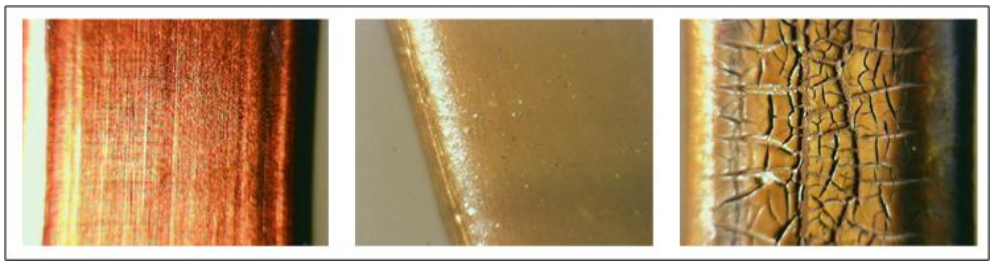

Figure 4.11: Images of wires having different filler concentration in wt%.

4.3.2 Relationship between Relative Surface Roughness and Frequency

In magnet wire specimens, the extent of surface degradation due to PD erosion is difficult to determine. In the literature, no reports were found which can predict the increase in the relative damages with the increase of test frequency. In this work, a constant stress approach is used to establish an empirical relationship between relative surface roughnesses, N_R ($=R_{f_x}/R_{f_1}$) and frequency. The value of f_1 corresponds to frequency of 60 Hz to predict the surface roughness; whereas, f_x corresponds to surface roughness for a particular frequency following $x \geq 60$. In this research work the frequency range between 60 Hz to 10 kHz is used; therefore, value of x lies between the same range. The N_R, which is the value of the relative increase in the surface roughness, is plotted in Figure 4.12 and the result data points are curve fitted by:

$$\textit{Relative surface roughness, } N_R \Rightarrow \left(\frac{R_{f_x}}{R_{f_1}}\right) = A.e^{B\times f} \tag{4.2}$$

The Equation (4.2) demonstrated that the surface roughness is strongly influenced by the test frequency, especially for magnet wire type S_1 having no filler. The constants A and B, which depends on magnet wire type with and without nanofillers, are given in Table 4.1.

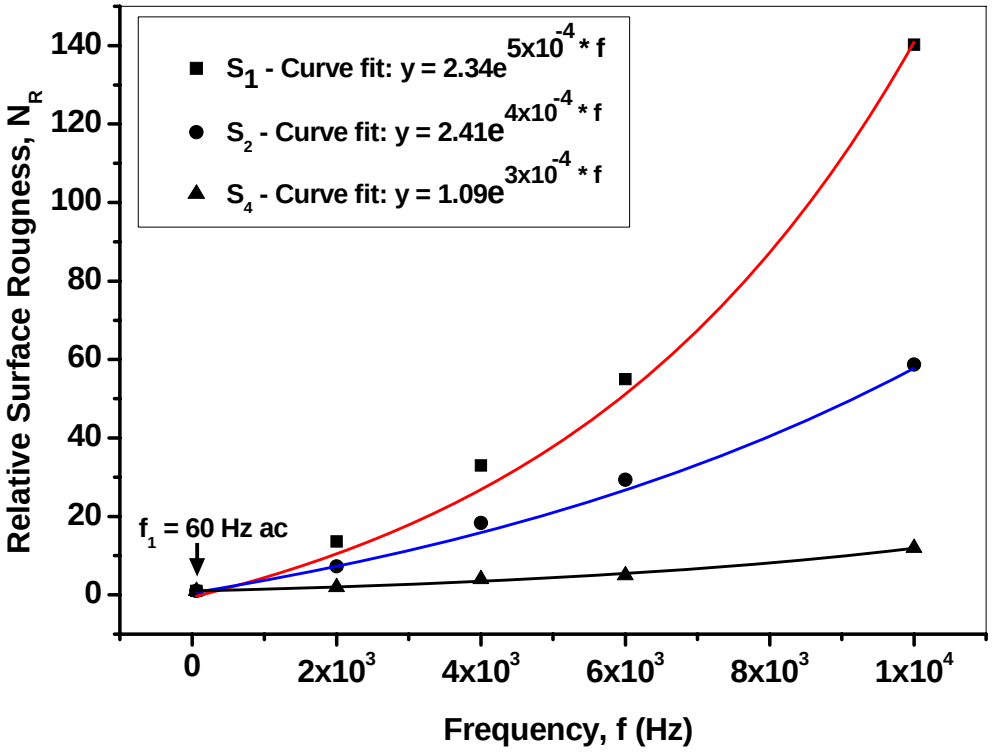

Figure 4.12: Relative surface roughness N_R, of magnet wire specimens exposed to voltages with different ac frequencies at constant stress of 70 kV_p/mm.

Table 4.1: Constants in Equation (4.2) obtained from the curve fitting procedure using the least square method, for relative surface roughness of specimens subjected to voltages of different ac frequencies at a constant electric stress.

Magnet Wire Type	Curve Fit Constants	
	A	B
Pyre-ML® Polyimide, S_1	2.34	$5x10^{-4}$
Corona Resistant MGF, S_2	2.41	$4x10^{-4}$
Pyre-ML® Solution + SiO_2, S_4	1.09	$3x10^{-4}$

The analysis of data points (N_R, f) show that the trend for the increase in the surface roughness is much higher for the specimens with no filler; whereas, the trend for the relative increase drops when nanofillers are introduced, especially for fumed silica. This is due to the increased thermal conductivity and higher resistance to erosion.

4.3.3 Effect of the Surface Roughness on the DC Breakdown Strength

The results on the surface roughness, reported in Table 3.3, indicate that the erosion process is much faster in commercial wire S_1 than commercial wire S_2. However, a comparison of the breakdown strength measurement in Table 3.1 suggests that the dc breakdown strength of S_1 is higher than that of S_2. This difference in the dc breakdown strength is because of the number of coating layers on S_1 and S_2. The SEM results indicate that the number of layers on wire S_1 is approximately 12; whereas, on wire S_2 consists of only four. Therefore, the damage due to PD erosion to the outer most layers of magnet wire S_2 causes considerable reduction in the overall thickness, compared with S_1. Thus, the overall dc breakdown strength reduces much faster in S_2.

4.4 Aging Mechanisms in Groundwall Insulation

It has been conclusively demonstrated that the epoxy insulation does age, when it is exposed to unipolar repetitive voltage pulses of either polarity [46]. In this regard, the long-term aging of mica-based groundwall insulation, described in Section 3.5, leads to a further understanding of the problems that arise due to the PWM-VSC. The effects of such voltage sources can become much rigorous, if manufacturing process defects are additionally present in the groundwall insulation. There are a number of reasons due to which defects can occur. One of the main reasons is if the viscosity of the resin is not proper for a good penetration in the lapped layers of mica paper tape. Also, the resin shrinkage during curing and inadequate bonding strength of the resin to the conductor, or between the insulation layers, also threatens the insulation system. Any of these

complexities can cause voids in the finished groundwall insulation. If, during service, the stresses are high enough to ionize the gases in the internal spaces, the discharges lead to the decomposition of the organic resin component. The net effect is a slow decline in the insulation condition and electrical strength, ultimately leading to premature failure. In addition, inappropriately cured resins can result in an increased conduction current during high voltage applications, resulting in insulation breakdown across the surface or through the groundwall [161].

4.4.1 Performance of the Groundwall Mica Tape

Glass fibre reinforced mica tape, as reported in Figure 4.13, is wound around the copper strands to the desired thickness. The winding of the tape creates a layered structure of insulation. Then, the layered insulation and the copper conductor are vacuum impregnated with epoxy resin. After the impregnation and cure, the mica tape layers and the epoxy resin are bonded, and a rigid and compact insulation is formed.

Before the application of mica-tape as stator coil groundwall insulation, the degradation mechanism in tapes own interface is analyzed. It is observed that the interface plays an import role in composite materials like mica. There are two kinds of interfaces in epoxy mica insulation, which are the interface between mica and epoxy resin as well as the interface between the glass fibre and epoxy resin. Figure 4.13 shows the SEM images from unstressed specimen and stressed specimens subjected to steep-front unipolar pulse voltage waveforms, up to their breakdown. It is obvious that the surface of the tape insulation changes drastically during the aging process. Mica and glass fibre are bonded by the epoxy, which diminishes and finally shrinks, precipitating the failure of the tape. The deterioration and shrinking of the mica layer due to PD erosion gives an indication that such physical changes can contribute to the development of gaps or defects in actual stator coils, which can affect the overall life of the insulation system.

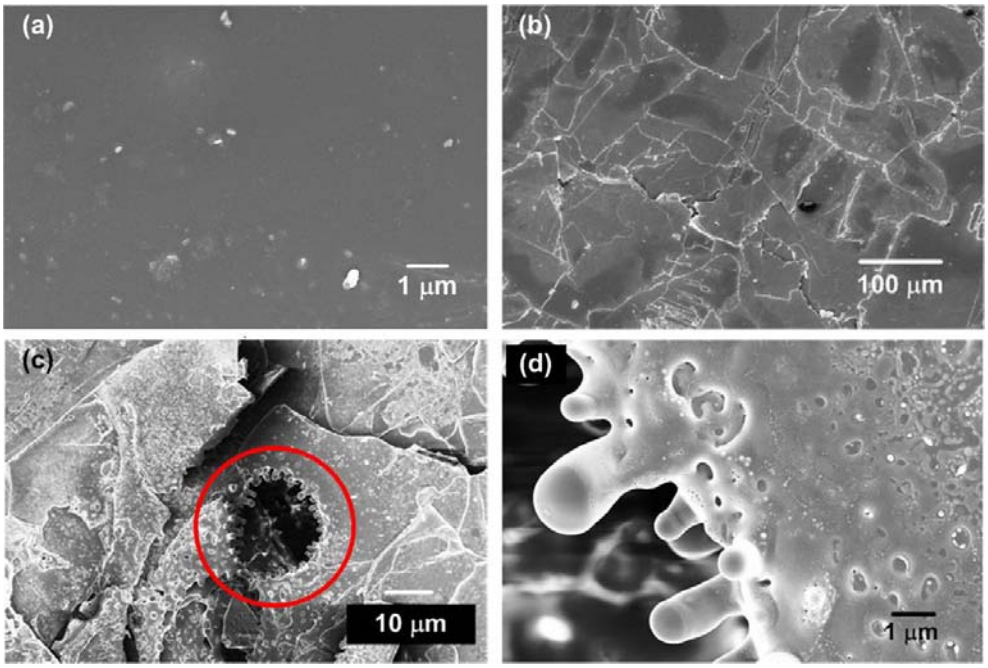

Figure 4.13: SEM photographs of mica-tape before and after breakdown, subjected to steep-front unipolar voltage pulses; (a) mica virgin sample, (b) pulse aged specimen, (c) mica-tape after pulse breakdown, (d) magnified breakdown area of (c) in mica-tape.

To verify aging mechanisms described in Figure 4.13, further examination of failed stator bar groundwall insulation, described in Section 2.2.4, is carried out in the next section of this research work.

4.4.2 Visual Examination of the Failed Stator Bars

The failed stator bars, subjected to fast repetitive voltage pulses, are removed after failure. It is observed that the presence of severe PD is responsible for the deterioration in the groundwall insulation. In pulse aging, the potential area for the initial erosion is most likely between the consecutive overlaps of the mica tape [162]. Therefore, delamination between the half-lapped mica-mica layers is much faster, due to additional heating caused by the high *dV/dt* and fast switching frequency, compared to 60 Hz ac. In the groundwall

insulation, the electrical activity can also begin due to defects during the manufacturing process; for example, wrinkles in the mica tape or various weak areas at the edges of the groundwall tape [163, 164]. In addition, any defects in the bent area can cause a significant reduction in the time-to-breakdown. Similar results, as exhibited in Figure 4.14, are reported by Vogelsang [164] during breakdown studies of high voltage winding insulations.

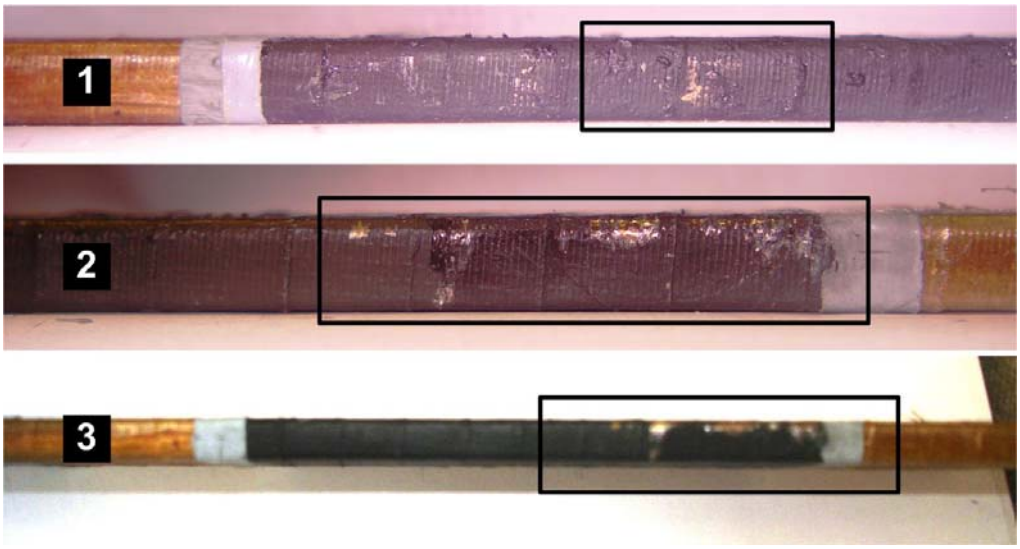

Figure 4.14: Degradation of the edges and bent areas in three different stator bars (top view).

Also, during pulse aging, clear signs of physical erosion are observed on the surface of groundwall mica tape due to enhanced PD activity [165]. In short, such a mechanism likely causes an increase in the total number of defects with time. They can be distributed randomly in the stator winding insulation system and affect the long-term performance of the motors. Also, voids, generated at the interface sites of the mica-mica layer, are linked to the horizontal cracks that are observed during the aging process (see Figure 4.15). Moreover, the occurrence of PD activity in the delamination or cracks, which exist as gaps or voids, can also chemically deteriorate the groundwall insulation [44]. However, in the case of 60 Hz ac aging, if in any part of the groundwall insulation the impregnation is improper or gaps exist between the groundwall and the copper stator bar, the PD activity become more intense in that local area, causing a localized breakdown.

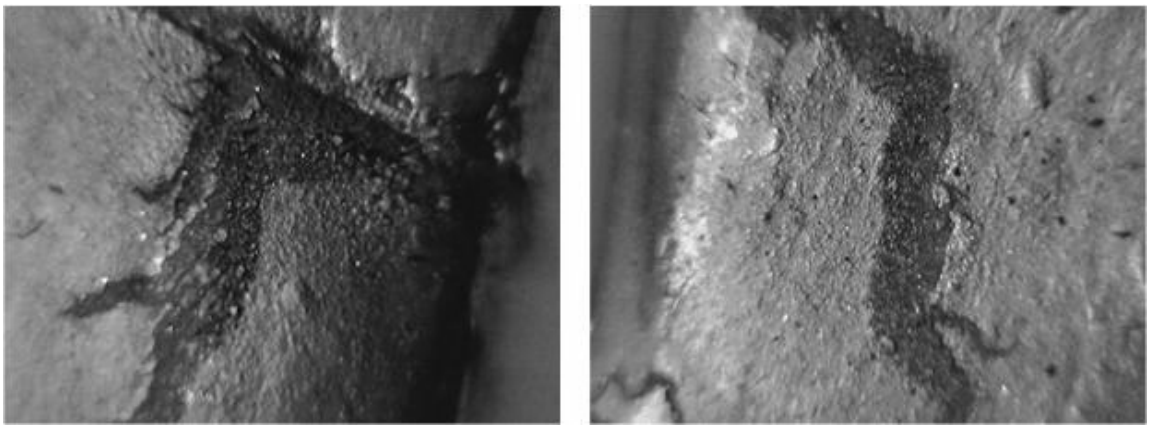

Figure 4.15: Damaged areas in the groundwall insulation after the steep-front pulse aging in the stator bar.

4.4.3 Mechanisms of the Failure in Groundwall Stator Bars

As described in Section 3.5.1, hot spots develop in the stator coils, when PWM-VSC waveforms are applied. Thus, the operational temperatures are usually higher in motors and are detrimentally affected by fast repetitive voltage pulses and high frequency components. A visual examination of failed stator bars, in Section 4.5.2 reveals that the high temperature effect do reduce the lifecycle, and the problems mostly occur in interfaces instead of in the bulk of material. The rapid breakdown of the stator bars is therefore observed, when they are subjected to elevated temperatures under steep-front pulse voltages.

Figure 4.16 shows the effect of temperature on the dc breakdown strength, which drops as the environmental temperature increase. This rise in the temperature can strongly influence the long-term behaviour of the groundwall insulation. Figure 4.17 shows the development of hot spots, where a rise in the temperature is observed with the aging duration and ultimately failures are observed in the same area. Therefore, based on the analysis in Figures 4.16 and 4.17, the breakdown of the groundwall insulation can be readily described as follows: the occurrence of hot spots, due to fast switching frequencies and localized dielectric heating. Both hot spots and dielectric heating then leads to lack of the resin between the two interfaces of mica layers. Consequently, it is

expected that during the operation of motors; especially, when fed by PWM-VSC, the generated heat can cause gaps or may increase the size of the defect by the migration of the epoxy resin through consecutive over-laps. As soon as, a cavity or defect develops, the increased electric field due to the high *dV/dt* causes PD in the defected area, which, in turn, causes a further increase in the local temperature, as depicted in Figure 4.23. This high temperature expedites the PD erosion and can eventually cause the premature failure of the groundwall insulation.

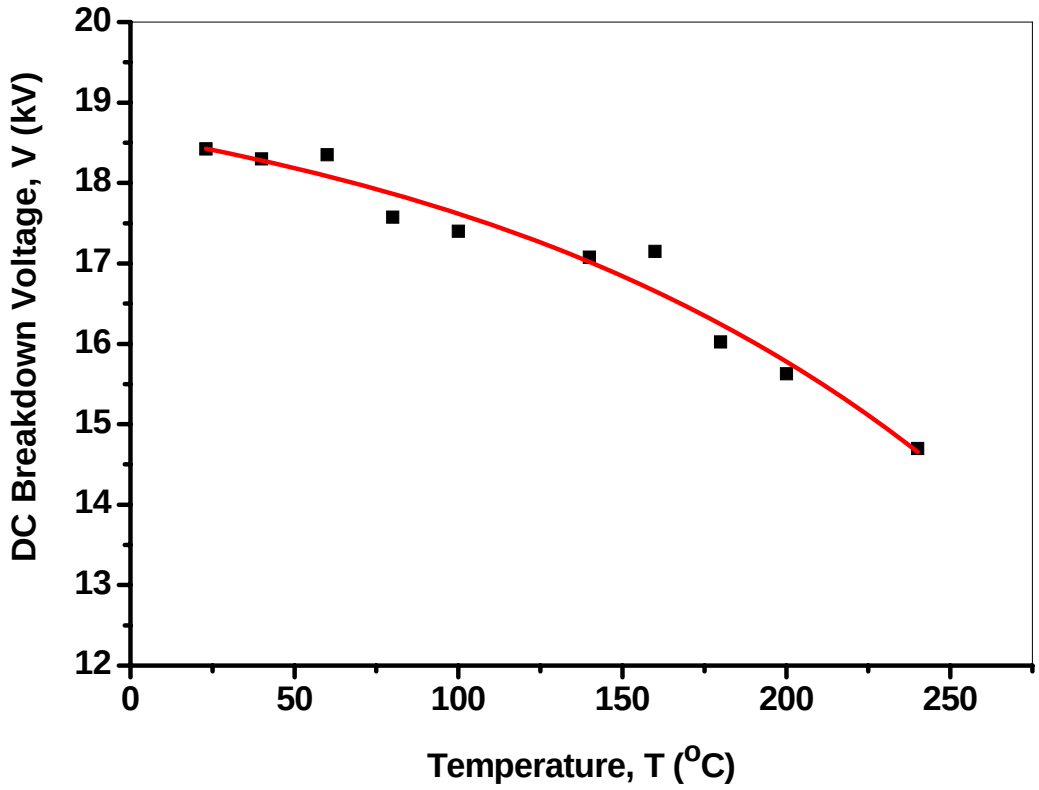

Figure 4.16: DC breakdown voltage versus temperature for VPI groundwall stator bar specimens having single layer of mica-tape.

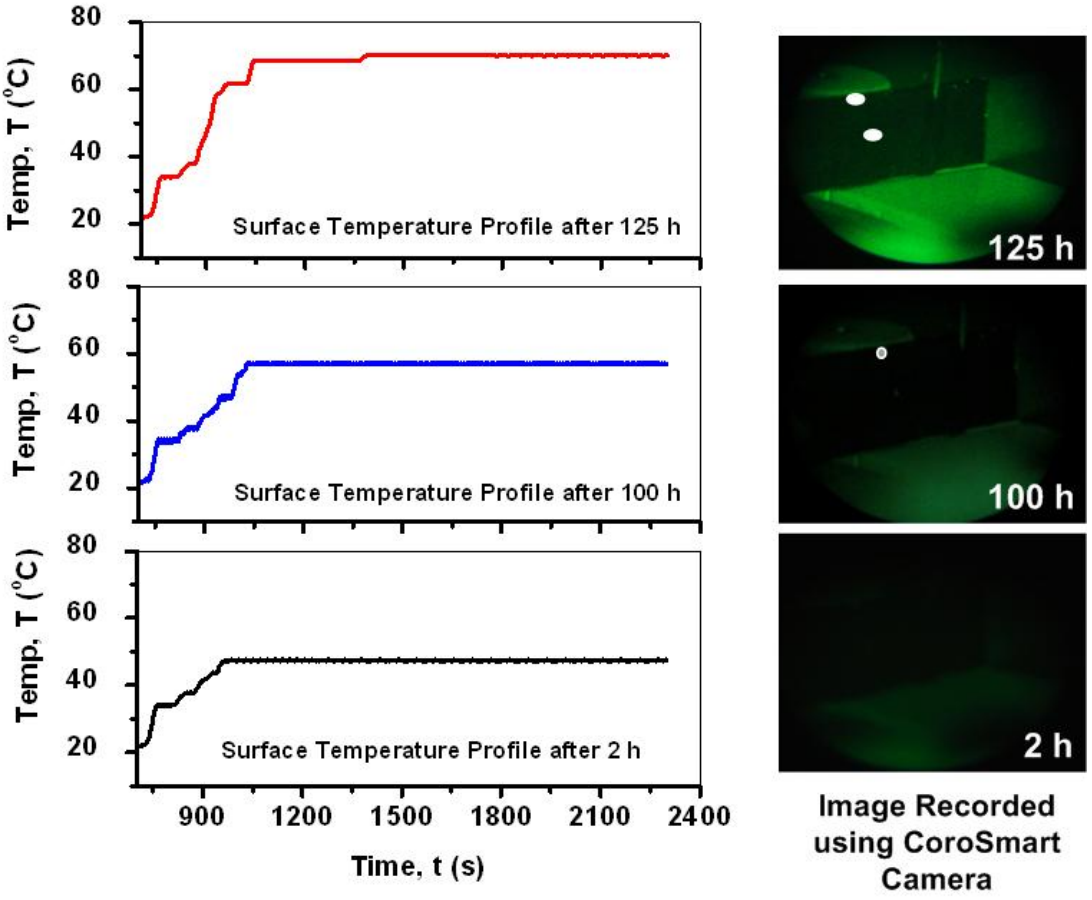

Figure 4.17: Surface temperature profiles for the stator bar groundwall insulation tested under pulse aging of 5 kV peak at 3 kHz and normal ambient temperature.

The groundwall aging investigation clearly predicts that the failure time depends on the stresses that the motor is exposed to during normal operation. The presence of both thermal and electrical stresses produces synergetic effects, leading to delamination, cracking, embitterment, or depolymerisation of the insulation system. With the 60 Hz ac aging, no hot spots are observed; therefore, the dominant mechanism is believed to be more electrical than thermal. However, the degradation mechanism caused by electrical aging, becomes much faster in the presence of hot spots, when the PWM-VSC is used. Thus, the thermal mechanism strictly controls the life expectancy of groundwall insulation, which is confirmed by the results, presented in Figure 3.26.

Overall, the analysis of stator bars determines that the manufacturing quality of high voltage winding insulations plays a major role towards microscopic properties and therefore time-to-failure. Operation at high temperature levels or hot spots in the insulation should therefore be avoided or minimised. Such temperature becomes more critical, if they are close or above the glass transition temperature of the epoxy resin. In order to extend lifetime, more attention is needed in the actual manufacturing process, which includes the taping process, material selection so as the materials are made free of defects and the VPI process. The adjustment in the resin viscosity also plays an important role to get a good penetration between the lapped layers. This adjustment should be done in such a manner that the flow-out of resin does not occur upon removal of the coils from the VPI tank. In the end, it is strongly suggested that the motor manufacturers should collaborate with both pertinent industries and research institutes for the design and development of new superior materials, along with the improved VPI techniques, especially for PWM-VSC applications.

Chapter 5 Conclusions and Suggestions for Future Work

5.1 Summary

In form-wound stator coils, both groundwall and inter-turn insulations are essential parts in medium and high voltage motors. For that reason, their optimum design is especially important, when they are subjected to pulse width modulated (PWM) voltage source converter (VSC) waveforms. In PWM-VSC, the high *dV/dt* and fast switching of pulses can strongly influence the integrity of both groundwall and inter-turn insulation. In order to investigate the problems caused due to voltage level, switching frequency, and operation temperature, both experimental and numerical analysis were carried out. From this work, different types of degradation mechanisms in stator coil insulation were identified and possible solutions to reduce the adverse effects of fast pulses from PWM-VSC are additionally proposed.

In the present state-of-the-art, the enamelled wires available for form-wound stator coils are meant to operate, mostly, at power frequency (60 Hz) voltages. During the enamelling process, to acquire the necessary thickness to meet the electrical, thermal, and abrasion specifications, the magnet wire passes through the coating applicator as many as 12 times. This layer-by-layer coating, which results in multiple polymer-to-polymer interfaces, is oven-cured after each pass. For the filled magnet wires, which are more resistant to corona, an additional coating is applied, resulting in a more complex and multi-layer insulation. The multi-layer insulation, which exits in the form of polymer-to-polymer interfaces, the accumulation of space charges, indeed occurs between the layers, leading to an unwanted stress modification. Both space charge accumulation and PD erosion can initiate turn insulation degradation, and eventually, the premature failure of the stator winding insulation system. In this regard, an experimental investigation of both conventional and laboratory developed wires clearly shows that the total stored charge in

the bulk of the insulation increases significantly as the number of insulation layers increases on the wire. It is postulated that increasing the number of layers on the magnet wire, increases the number of traps thereby the concentration of trapped charge increases with the number of insulation layers.

During the normal operation of motors under PWM-VSC, the accumulation of space charge occurs not only by electrode injection inside the insulation bulk, but also by surface PD activity. The cumulative work investigating the relationships between the release of the stored charge and aging time has therefore lead to the development of an empirical space charge model, which estimates the relative stored charge at any particular aging duration in magnet wire enamels. The estimation of the developed charge concentration using prescribed logarithmic approach and through experimental work is additionally found convenient for the quantification of coil inter-turn stress distribution. To validate the influence of stored charge on inter-turn stresses, the numerical analysis using FEM established that the electric field perturbations inside the wire insulation are significantly affected by the developed charge concentration and can begin turn insulation degradation by initiating damages to the magnet wire coating. This can eventually lead to the premature failure of the stator insulation systems.

To further enhance the performance of magnet wire coatings, the nanofiller technology has had a major impact to upgrade and diversify the material properties; including, discharge resistance, the matching of the coefficient of the thermal expansion, thermal conductivity enhancement, mechanical reinforcement, and abrasion resistance. During the past decade, the manufacture of magnet wires having fillers with a uniform coating has received great attention due to the growing use of PWM-VSC. In such devices, the repetition rate of the IGBT pulses increases substantially with much severe stresses, and can be as large as 20 kHz with rate of rise of several kV/μs. As a result, the presence of fillers in the material then forms a line of defence to limit the erosion process and prevent further degradation of the insulating material. In this work, to make the motor magnet wires less susceptible to high *dV/dt*, more resistant to PD, and for reduced space charge effects, a possible solution with new enamels, by adding inorganic nanofillers is suggested. The results clearly showed that the wire specimens with SiO_2

nanofillers have better performance compared to Al_2O_3 and TiO_2. In specimens with SiO_2, significantly low surface roughness and improved dielectric strength is achieved after accelerated aging under pulse and high frequency voltage waveforms.

In a stator coil, the main insulation also identified as groundwall, the use of PWM-VSC develops hot spots; therefore, the operational temperatures are usually higher in motor stator coils and are detrimentally affected by fast repetitive voltage pulses and high frequency components. After long-term aging the visual examination of failed stator bars revealed that the problem does occur in mica interfaces instead of in the bulk of material. The rapid breakdown of the stator bars is therefore observed, when they are subjected to elevated temperatures under steep-front pulse voltages. The investigation demonstrated that the breakdown of the groundwall insulation can be described in two subsequent stages. In the first stage, the occurrence of hot spots, due to fast switching frequencies and localized dielectric heating, leads to lack of the resin between the two interfaces of mica layers. As soon as, a cavity or defect develops, the increased electric field due to the high *dV/dt* causes PD in the defected area, which, in turn, causes a further increase in the local temperature. In the second stage, this high temperature expedites the PD erosion and can eventually cause the premature failure of the groundwall insulation.

The presence of both thermal and electrical stresses produces severe effects, leading to delamination, cracking, embitterment, or depolymerisation of the insulation system. In the presence of hot spots, the domination of the thermal mechanisms strictly controls the life expectancy of groundwall insulation, which strongly suggests that the motor manufacturers' should consider developing new superior materials along with the improved VPI techniques for PWM-VSC applications.

5.2 Conclusions

From the work done in this research, the following main conclusions are drawn:

- This research has shown that nanofilled enamelled wires show considerable improvement in life expectancy under PMW waveforms over conventional enamelled wires. However, the improvement occurs with fumed silica and with a relatively low filler concentration. This improvement is not evident when the concentration of filler exceeds 1% as the enamel coating becomes rough and brittle and unsuitable for magnet wire. This may be due to agglomeration of particles, which needs further investigation.

- In magnet wire coatings, a filler concentration up to one percent improves the insulation breakdown strength remarkably; however, above 1%, a decrease in the mechanical strength is observed. This reduction in the mechanical strength can be attributed to the limited number of sites for bonding in the polymers, which develops nanosize cracks around particles. These cracks become larger when the wires are flexed and become weak spots dielectrically, which can further influence the electrical properties.

- Thermally stimulated depolarization current (TSDC) spectra of magnet wire specimens under different polling conditions have shown clear evidence of charge injection and trapping in the conventional enamelled wires. It is evident that the total stored charge in the insulation bulk increases significantly as the number of insulation layers increases on the magnet wire. With increased number of insulation layers, the number of traps also increases thereby causing the higher concentration of trapped charge. Therefore, a lower number of layers with improved insulation performance and high resistance to PD should be a goal to reduce such effects.

- Numerical analysis using FEM demonstrated that space charge accumulation can significantly affect magnet wire insulation degradation. Charge stored in the insulation bulk and on insulation surface can produce electric field perturbations inside wire insulation and in the air gap between two adjacent wires, respectively. The presence of increased space charge concentration can trigger PD activity at much earlier stage due to its strong influence on the PDIV. Therefore, estimation of such electric fields using numerical methods is essential to understand its damaging effects.

- The inter-turn stress analysis for two different types of magnet wires, having different number of insulation layers and with overall similar coating thickness, showed significant reduction of ~48% in the maximum electric field. Therefore, it is possible to modify the inter-turn stress distribution with the reduction of number of layers from nine to four, keeping the total thickness constant. This can be attributed to a lower accumulation of space charge during the aging duration and possibly due to fewer number of trap levels.

- The accelerated degradation of the groundwall insulation demonstrated that pulse aging is much severe when compared with the power frequency (60 Hz ac) aging. A significant drop in the service life of the groundwall insulation, with reference to the switching frequency characteristic of the power source, is observed under a normal ambient temperature. In the case of PWM waveforms aging, the thermal mechanism strictly controls the life expectancy of groundwall insulation and especially becomes more critical, if they are close or above the glass transition temperature of the epoxy resin. Therefore, due to PWM waveforms, the presence of both thermal and electrical stresses produces much severe effects, leading to delamination, cracking, embitterment, or depolymerisation of the insulation system, when compared to ac aging.

- The results demonstrate that diagnostic tools, based on the temperature measurements and PD under pulse detection, can be suitably adopted in different phases of the life of inverter-fed motors to assess the quality of the insulation.

5.3 Suggestions for Future Work

In this thesis, a study that focuses on the insulation problems in form-wound stator coil is performed. For further development of new insulations and methods that can be applied as an insulation to wire and bars, following are the suggestions for the future work, in this area:

To avoid insulation problems in magnet wire enamel, fundamental understanding of dielectric properties at the nanoscale level is of great importance in the development of functional nanofilled coatings. As, the development of new and improved filled coatings was not a part of this research; therefore, magnet wire enamels filled with new nanofillers is suggested as an extension of this work. Accelerated tests, with temperature and voltage, can be used to compare the performance of these nanofillers with the conventional ones.

In this research, wire specimens with fumed silica as nanofiller showed significant improvement in life expectancy; therefore, it is recommended that such wires for inverter-fed motor applications should be considered after applying more comprehensive set of quality control tests. Since concentration of fumed silica above one percent shows some weaknesses, for example increase in roughness, which can be due to agglomeration. Several techniques are available to avoid agglomeration thereby reducing surface roughness and for improving dispersion, is a suggestion for further research.

Magnet wires having a large number of insulation layers are more susceptible to damage because of accumulation of higher charge concentration and due to occurrence of remnant polarization in each layer. In this regards, it is suggested that the manufacturers of wire investigate alternate enamels and coating application processes in an attempt to reduce the number of layers. Development of such wires will improve the life expectancy

of stator coils; especially, in applications, such as PWM-VSC, to keep the intensity of stored charge at low level.

Further investigation of the current VPI process is recommended keeping in view the process equipment, controls, coil insulation, and impregnating resin. They must all be suited to one another. In motors as the voltage rating increases, more layers of mica-paper tape are used and thus longer pressure cycle are needed for full penetration of the resin. It is suggested that tapes be developed having equivalent dielectric characteristics, while allowing a partial flow of resin directly through the material. In addition, the resin viscosity has to be further examined and should be adjusted in such a way that runoff from the stator does not occur before the start of curing process.

The inverter drive designers are employing higher voltages and faster switching devices with steeper wave fronts. Therefore, further experimental work on groundwall insulation is suggested for the establishment of a qualification scheme and standards that are suitable for a variety of different inverter system designs. In this regard, it is recommended that the effect of oscillating (bipolar) pulses on the groundwall aging requires investigation. Such type of study will be helpful for better characterization of the groundwall insulation for applications at higher temperatures and frequencies.

References

[1] Upper Peninsula Power Company, Motors: AC Induction Motors, USA, 2007.

[2] F. Blaabjerg, J. K. Pedersen, S. Rise, and H. Hansen, "A Comparative study of Energy Saving Benefits in Softstarters for Three-phase Induction Motors", IEEE Industry Applications Conference, Vo1. 1, pp. 367-374, 1995.

[3] R. H. Engelmann and W. H. Middendorf, Handbook of Electric Motors. Marcel and Dekker. NY. 1995.

[4] G. C. Stone, K. Boulter, Culber, and Dhirani. Electrical Insulation for Rotating Machines, IEEE, 2004.

[5] T. F. Lowery, "Design Considerations for Motors and Variable Speed Drives," ASHRAE J., pp. 28–32, Feb. 1999.

[6] D. Fabiani, G. C. Montanari, A. Cavallini and G. Mazzanti, " Relation Between Space Charge Accumulation and Partial Discharge Activity in Enamelled Wires Under PWM-like Voltage Waveforms", IEEE Trans. on Dielectrics and Electrical Insulation, Vol. 11, No.3, pp. 392-405, June 2004.

[7] D. Fabiani, G. C. Montanari, A. Contin, " Aging Acceleration of Insulating Materials for Electrical Machine Windings Supplied by PWM in the Presence and Absence of Partial Discharges", IEEE ICSD, Eindhoven, The Neatherlands, pp. 283-286, 2001.

[8] C. Hudon, N. Amyot, T. Lebey, P. Castelan, and N. Kandev "Testing of Low-Voltage Motor Turn Insulation Intended for PWM Applications", IEEE Transaction on Dielectrics and Electrical Insulation, Vol. 7, No. 6, pp. 783-789, Dec. 2000.

[9] D. Fabiani, and G. C. Montanari, "The Effect of Voltage Distortion on Ageing Acceleration of Insulation Systems under Partial Discharge Activity", IEEE Electrical Insulation Mag., Vol. 17, No. 3, pp. 24-33, May/June. 2001.

[10] N. Foulon, J. P. Lucas, G. Barré, R. Mailfert, J. Enon, "Investigation of the Failure Mechanism of Insulation Subjected to Repetitive Fast Voltage Surges", IEEE/EIC-EMCW Conf., pp. 401-406, Sep. 1997.

[11] J. P. Bellomo, T. Lebey, J. M. Oraison, and F. Peltier, “Electrical Aging of Stator Insulation of Low Voltage Rotating Machines Supplied by Inverters”, IEEE-ISEI, Vol. 1, pp. 210-213, June 1996.

[12] A GAMBICA/REMA Technical Report “Variable Speed Drives and Motors”, No. 1, London, UK, 2001.

[13] J. P. Bellomo, P. Castelan and T. Lebey, “The effect of Pulse Voltages on Dielectric Material Properties”, IEEE Transaction on Dielectrics and Electrical Insulation, Vol. 6, No. 1, pp. 20-26, February 1999.

[14] IEC 60034-18-41, “Evaluation and Qualification of Electrical Insulation Systems Used in Rotating Electrical Machines when Fed from Voltage Converters”, 2006.

[15] R. H. Rehder, R. E. Draper, B. J. Moore: “How Good is You Motor Insulation System?”, IEEE Electrical Insulation Magazine, Vol. 12, No. 4, pp. 8-13, July/August 1996.

[16] D. M. Hepburn, I. J. Kemp, A. J. Shields, “Mica”, IEEE Electrical Insulation Magazine, Vol. 16, No. 5, pp. 19-24, Sep-Oct. 2000.

[17] W. Grubelnik, J. Roberts, B. Koerbler, P. Marek, “A New Approach in Insulation Systems for Rotating Machines”, IEEE-EIC, pp. 97-102, 1005.

[18] W. McDermid, “Insulation Systems and Monitoring for Stator Windings of Large Rotating Machines”, IEEE Electrical Insulation Magazine, Vol. 9, No. 4, pp. 7-15, July/August 1993.

[19] A. Anton: “New Developments in Resin Rich Insulating Systems for High-voltage Rotating Machines”, Proc. of Electrical Insulation Conference and Electrical Manufacturing & Coil Winding Conference, Rosemount, Illinois, USA, pp. 607-618, Sep. 1997.

[20] R. H. Rehder, R. E. Draper, B. J. Moore: “How Good is You Motor Insulation System?”, IEEE Electrical Insulation Magazine, Vol. 12, No. 4, pp. 8-13, July/August 1996.

[21] J.A. Allison, “Understanding the need for Anti-corona materials in High Voltage Rotating Machines”, 6th International Conference on Properties and Applications of Dielectric Materials, pp. 860-863, 2000.

[22] R. Malamud, I. Cheremisov, “Anti-Corona Protection of the High Voltage Stator Windings and Semi-Conductive Materials for its Realization”, IEEE International Symposium on Electrical Insulation, pp. 32 –35, 2000.

[23] J. C. G. Wheeler, ”Effects of converter pulses on the electrical insulation in low and medium voltage motors”, IEEE Electrical Insulation Magazine, Vol. 21 , Issue 2 , pp. 22 – 29, 2005.

[24] L. Paulsson, B. Ekehov, S. Halen, T. Larsson, L. Palmqvist, A.-A. Edris, D. Kidd, A.J.F. Keri and B. Mehraban., “High-frequency impacts in a converter-based back-to-back tie; the Eagle Pass installation” IEEE Trans. on Power Delivery, Vol. 18, pp. 1410 – 1415, 2003.

[25] F. Espino, Ph.D. Thesis, “A Study of Field-Dependent Stress Grading Systems Working under Fast Rise Time Pulses”, 2006.

[26] M. K. W. Stranges, J. E. Hayward, J. H. Dymond, and R. Omranipour, “A comparative Evaluation of Various Conducting Slot Armour Materials”, IEEE EIC-EMCW Conference, pp. 599-604, Sept. 2003.

[27] Y. Shakweh, “MV Inverter Stack Topologies”, IEE Power Engineering Journal, Vol. 15, pp. 139-149, 2001.

[28] E. I. Carroll, “Power Electronics for Very High Power Applications”, IEE Power Engineering Journal, Vol. 13, pp. 81-87, 1999.

[29] B. R. Andersen, L. Xu, P.J. Horton, P. Cartwringht., “Topologies for VSC Transmission”, IEE Power Engineering Journal, Vol. 16 , Issue 3, pp. 142-150, 2002.

[30] Y. Shakweh, “Power devices for medium voltage PWM converters”, IEE Power Engineering Journal, Volume: 13 , Issue: 6 pp. 297 – 307, 1999.

[31] E. Persson, “Fast Switching Adjustable Speed Drives and Overview’, IEE Power Engineering Journal, Vol. 14, pp. 148-157, 2000.

[32] R. Teichmann, S. Bernet, “A Comparison of Three-Level Converters Versus Two-Level Converters for Low-Voltage Drives, Traction, and Utility Applications”, IEEE Trans. on Industry Applications, Vol. 41, pp. 855-865, 2005.

[33] M. Melfi, A. M. J. Sung, S. Bell, G. L. Skibinski, “Effect of Surge Voltage Risetime on the Insulation of Low-voltage Machines Fed by PWM Converters”,

IEEE Transactions on Industry Applications, Vol. 34, No. 4, pp. 766-775, Jul.-Aug. 1998.

[34] B. S. Oyegoke, "Multiconductor Transmission Line and Bewley Lattice Diagram Techniques for the Transient Inter-turn Voltages in Electrical Machine Fed from a Frequency Converter" The 10th Symposium on Electrical Apparatus and Technologies, Siela'97, 30-31 May, Plovdiv, Bulgaria, Conference Proceedings Vol. 1, pp. 251-256, 1997.

[35] G. Suresh, H. A. Toliyat, D. A. Rendussara, and P. N. Enjeti, "Predicting the Transient Effects of PWM voltage Waveform on the Stator Windings of Random Wound Induction Motors", IEEE Trans. on Industry Applications. Vol. 14. No. 1. pp. 23-30, Jan. 1999.

[36] G. Stone, S. Campbell, and S. Tetreault, "Inverter-Fed Drives: Which Motor Stators are at Risk", IEEE Industry Application Magazine, pp. 17-22, Sep/Oct. 2000.

[37] A. V. Jouanne, P. Enjetti, and W. Gray, "The Effect of Long Motor Leads on PWM Inverter Fed AC Motor Drive Systems", IEEE Conference Proceedings, pp. 592-597, 1995.

[38] A. H. Bonnett, "Analysis of the Impact of Pulse-Width Modulated Inverter Voltage Waveforms on AC induction Motors", IEEE Trans. Ind. Applicat., Vol. 32, No. 2, pp. 386-392, March 1996.

[39] B. Wu, and F. A. DeWinter, "Voltage Stress on Induction Motors in Medium-Voltage (2300-6900V) PWM GTO CSI Drives", IEEE Trans. Ind. Applicat., Vol. 12, No. 2, pp. 213-220, March 1997.

[40] E. Persson, "Transient Effects in Application of PWM Inverters to Induction Motors" IEEE Trans. Ind. Applicat., Vol. 28, No. 5, pp. 1095-1101, Sep.-Oct. 1992.

[41] E. Binder, "Techniques for Discharge Measurements in Stator Windings of Generators", CIGRE Symposium, Vienna, 1987.

[42] F. H. Kreuger. Partial Discharge Detection in High-Voltage Equipment. Butterworths. 1989.

[43] W. T. Shugg. Handbook of Electrical and Electronic Insulating Materials. IEEE Press. 1995.

[44] A. Ramme, A. V. Jouanne, A. Wallace, T. Ly, and L. Petersen, "Evaluation of Partial Discharge in Inverter Driven Medium Voltage Propulsion Coils", IEEE, pp. 1869-1873, 2003.

[45] M. Idea, "Electrical Conduction and Carrier Traps in Polymeric Materias", IEEE Transactions on Electrical Insulation, pp. 162, June. 1984.

[46] H.J. Wintle, "Unipolar Wire to Plan Corona: A Definitive Computation" IEEE Transactions on Electrical Insulation, Vol. 27, No. 2, pp. 298-308, 1992.

[47] S. U. Haq, Shesha H. Jayaram, Edward A. Cherney, and G. G. Raju, "Analysis of Space Charge and Dielectric Relaxation in Medium Voltage Magnet Wires by using Thermally Stimulated Depolarization Currents (TSDC)", ESA/IEEE-IAS/IEJ/SFE Joint Conference on Electrostatics, Vol. 2, pp. 655-664, June, 2006

[48] G. C. Stone, Ph.D. Thesis, "Aging of Epoxy Insulation by Voltage Surges", 1990.

[49] R. Bartnikas, R. M. Eichhorn, Editors "Engineering Dielectrics – Volume IIA", Chapter 3 – Conduction Processes in Polymers:, ASTM Publication 783, Philadelphia, 1983.

[50] T. J. Lewis, "The Role of Electrodes in Conduction and Breakdown in Solid Dielectrics", IEEE Transactions on Electrical Insulation, pp. June 1984.

[51] Y. Khlifi, K. Kassmi, L. Roubi, and R. Maimouni, "Modeling of Fowler-Nordheim Current of Metal/ Ultra-thin Oxide/ Semiconductor Structures", M. J. Condensed Matter, Vol. 3, No. 1, 2000.

[52] W.C. Johnson, "Electronic Transport in Insulating Films", IEEE Trans., Nuc Sci., NS-19, Vol. 6, pp. 33-40, 1972.

[53] G. Blaise and C. Le Gressus, "Charging and Flashover Induced by Surface Polarization Relaxation Process", J. Applied Phys., Vol. 69, pp. 6334-6339, 1991.

[54] J. Densley, R. Bartnikas and B. Bernstein, "Multiple Stress Aging of Solid Dielectric Extruded Dry-cured Insulation Systems for Power Transmission Cables", PES Summer Meeting, Vancouver, B.C., July 1993.

[55] H. R. Zeller, T. H. Baumann, and F. Stucki, "Microscopic Models for Ageing in Solid Dielectrics", Proc. IEEE ICPADM, pp. 13-15, 1985.

[56] Y. Weijun, “Failure Mechanism of Winding Insulations in Inverted-Fed Motors”, IEEE Electrical Insulation Magazine, pp. 18-23, 1997.

[57] T. Lebey, and S. Dinculescu, “On the Possible Impact of P.W.M Drives on Insulating Materials: A Laboratory Study”, 9th IEE-ICEM, No. 468, 1999.

[58] R. Alexandrescu, F. Dumitrache, I. Morjan, I. Sandu, M. Savoiu, I. Voicu1, C. Fleaca1 and R. Pit Icescu, “TiO2 nanosized powders by TiCl4 laser pyrolysis”, Nanotechnology, Vol. 15, pp. 537-545, 2004.

[59] N. V. Myung, J. Lim, J-P. Fleuria, M. Yun, W. West and D. Choi, “Alumina nanotemplate fabrication on silicon substrate” Nanotechnology, Vol. 15, pp. 833-838, 2004.

[60] T. Tanaka, G. C. Montanari and R. Mulhaupt, “Polymer nanocomposites as dielectrics and electrical insulation-perspectives for processing technologies, material characterization and future applications”, IEEE Transaction on Dielectrics and Electrical Insulation, Vol. 11, No. 5, pp. 763-784, August 2004.

[61] C. Hudon, N. Amyot and D. Jean, “Long term behavior of corona resistant insulation compared to standard insulation of magnet wire”, IEEE-ISEI, pp. 13-16, 2000.

[62] C. Hudon, J. N. Seguin, N. Amyot and N. Kandev, “Turn insulation aging of motors exposed to fast pulses of inverter drives” IEEE-EIC, pp. 413-417, 1997.

[63] H. Kikuchi, Y. Yukimori and S. Iyonaga, “Inverter-surge-resistance enamelled wire based on nano-composites insulating material”, Hitachi Cable Review No. 21, 2002.

[64] S. U. Haq, S. H. Jayaram, E. A. Cherney and L. C. Simon, “Partial discharge erosion of filled enamelled wires subjected to high frequency waveforms”, IEEE-ISEI, 2006.

[65] G. C. Montanari, D. Fabiani, F. Palmieri, D. Kaempfer, R. Thomann and R. Mulhaupt, “Modification of electrical properties and performance of EVA and PP insulation through nanostructure by organophilic silicates”, IEEE Transactions on Dielectrics and Electrical Insulation, Vol. 11, pp. 754-762, 2004.

[66] I. K. Nelson, J. C. Fathergill, L. A. Dissado, and W. Peasgwd, “Towards and understanding of nanometric dielectrics”, IEEE-CEIDP, pp. 295-298, October, 2002.

[67] P. C. Irwin, Y. Cao, A. Bansal and L. S. Schadler, “Thermal and mechanical properties of polyimide nanocomposites”, IEEE-CEIDP, pp. 120-123, October, 2003.

[68] R. Brütsch and P. Weyl, “A new winding for inverter drive motors”, EuroPES Conference/INSUCON, pp. 367-371, 2002.

[69] J. P. Rivenc and T. Lebey, “An overview of Electrical Properties for stress grading optimization”, IEEE Trans. DEI , Vol. 6, Num. 3, pp. 309-318, 1999.

[70] J. P. Rivenc, P. Bidan, and T. Lebey, “Stress Grading Materials: A Discussion On Lumped Elements Circuit Validity”, IEEE International Conference on Conduction an d Breakdown in Solids Dielectrics, pp. 524-527, 1998.

[71] Z. Yeo, F. Buret, L. Krahenbuhl, P. Auriol, “A Nonlinear Model for Surface Conduction”, IEEE Transactions on Magnetics , Vol. 34, Num. 5, pp. 2617-2620, 1998.

[72] Ch. Greffe, F. Gillet, J Warnant, “Contribution to the Electric Characterisation of Potential Grading Varnishes”, Elsevier Journal of Electrostatic, Vol. 48, pp. 231-243, 2000.

[73] NEMA Standards Publication MG 1, Part 30, 31 Motors and Generators, National Electrical Manufacturers Association, Rosslyn, Virginia, 2003.

[74] IEC 60034-25 TR-2004, Guide for the Design and Performance of Cage Induction Motors for Converter Supply, IEC.

[75] M. K. W. Stranges, G. C. Stone, and D. L. Bogh, “IEC 60034-18-41: A New Draft Technical Specification for Qualification and Acceptance Tests of Inverter Duty Motor Insulation”, IEEE 52nd PCIC Conference Record, pp. 297-302, 2005.

[76] D. Bogh, J. Coffee, G.C. Stone, J, Custodio, "Partial Discharge Testing on Low Voltage Motors", IEEE PCIC Conference Record, pp. 241-248. Sept 2004.

[77] M. Fenger, S. Campbell, and J. Pedersen, "Motor Winding Problems Caused by Inverter Drives", IEEE Industry Applications Magazine, pp. 22-31. July 2003.

[78] IEC 60034-18-42, "Qualification and acceptance test for type II electrical insulation systems used in rotating electrical machines fed from voltage converters", Work in progress.

[79] G. Stone, S. Campbell, and S. Tetreault, "IFD: Which Motor Stators are at Risk", IEEE Ind. App. Mag, pp. 17-22, Sep/Oct. 2000.

[80] IEEE Std. 1043: IEEE Recommended Practice for Voltage-Endurance Testing of Form-Wound Bars and Coils. 1996.

[81] IEEE Std. 1553: IEEE Trial-use Standard for Voltage-Endurance Testing of Form-Wound Coils and Bars for Hydrogenerators. 2002.

[82] Industrial Summit Technology Co: Pyre-ML® Products, 2005.

[83] Dupont Film and Fibers, 2006.

[84] NEMA Standard Publication, MW 1000-2003, Magnet Wire, 2003.

[85] R. Alexandrescu, F. Dumitrache, I. Morjan, I. Sandu, M. Savoiu, I. Voicu1, C. Fleaca1 and R. Pit Icescu, "TiO2 Nanosized Powders by TiCl4 Laser Pyrolysis", Nanotechnology, Vol. 15, pp. 537-545, 2004.

[86] S. U. Haq, S. Jayaram, and E. A. Cherney, "Performance of Nanofillers in Medium Voltage Magnet Wire Insulation under High Frequency Applications", IEEE Trans. on Dielectrics and Electrical Insulation, In-Press, 2006.

[87] N. V. Myung, J. Lim, J-P. Fleuria, M. Yun, W. West and D. Choi, "Alumina Nanotemplate Fabrication on Silicon Substrate" Nanotechnology, Vol. 15, pp. 833-838, 2004.

[88] M. Kozako, N. Fuse, Y. Ohki, T. Okamoto, and T. Tanaka, "Surface Degradation of Polyamide Nanocomposites Caused by Partial Discharge using IEC (b) Electrodes", IEEE Trans. Dielectr. Electr. Insul., Vol. 11, pp. 833-838, 2004.

[89] "IEEE Guide for the Statistical Analysis of Electrical Insulation Voltage Endurance Data", ANSI/IEEE Std. 930 1987.

[90] J. C. Forthergill, ''Estimating the Cumulative Probability of Failure Data Points to be Plotted on Weibull and Other Probability Paper'', IEEE Trans. Electr. Insul., Vol. 25, pp. 489-492, 1990.

[91] G. C. Stone and R.G. Van Heeswijk, "Parameter estimation for Weibull distribution", IEEE Transactions on Electrical Insulation, Vol. 12, No. 4, pp. 253-261, 1977.

[92] G. C. Stone, and H. Rosen, "Some Graphical Techniques for Estimating Weibull Confidence Intervals", IEEE Trans. On Reliability, pp. 362, 1984.

[93] F. J. Lawless, Statistical Models and Methods for Lifetime Data, J. Wiley and Sons, New York, 1982.

[94] L. S. Nelson, Wayne, Accelerated Testing, Statistical Models, Test Plans, and Data Analysis, John Wiley and Sons, Inc. New York, 1990.

[95] R. N. Mann, R. E. Schafer, and N. D. Singpurwalla, Methods for Statistical Analysis of Reliability and Life Data, John Wiley and Sons, Inc. New York, 1974.

[96] W. Q. Meeker, and L. A. Escobar, Statistical Methods for Reliability Data, John Wiley and Sons, Inc. New York, 1998.

[97] E. Abu-Al-Feilat, Ph.D. Thesis, "Lifetime Characteristics of Magnet Wires under High Frequency Pulsating Voltage and High Temperature", 2000.

[98] WinSMITH Weibull Software (2006), PlayTIME with SuperSMITH, 3rd ed., Fulton Findings, Torrance, CA, USA.

[99] J. P. Rivenc, P. Bidan, and T. Lebey, "Stress Grading Materials: A Discusión Lumped Elements Circuit Validity", IEEE International Conference Conduction and Breakdown in Solids Dielectrics, pp. 524-527, 1998.

[100] Comsol Multiphysics Referente Guide, AC/DC Module, 2006.

[101] J. P. Rivenc, T. Lebey, A. Loubiere, M. Biron, and J Warnant "A Discussion of Current-Voltage and Surface Potential Measurements to Test Stress Grading Materials", J. Physics D: Appl. Phys. 31, pp. 2612-2621, 1998.

[102] Y. K. Lee, and S. P. Muraka, "Study on Electrical Characteristics of Fluorinated Polyimide Film", Jornal of Material Sciences Vol. 33, pp. 4105-4109, 1998.

[103] G. Lupo, C. Petrarca, L. Engiziano, V Tucci, M. Vitelli, "Numerical Evaluation of the Electrical Field in Cable Terminations Equipped with Nonlinear Grading Materials", IEEE Annual Report CEIDP, pp. 585-588, 1998.

[104] K. Weeber, M. Shutt, J. Dymond, R. Rehder, "Finite Element Field Analysis Of Nonuniform Surface Contamination On High Voltage Windings Of Electric Machines", Annual Report CEIDP IEEE, pp 40-43, 1996.

[105] H. El-Kishky, B. S. Nindra, M. Abdel-Salam, E. Williams, "Experience with Development and Evaluation of Corona-Suppression Systems for HV Rotating Machines", IEEE Trans. On Dielectric and Electric Insulation, Vol. 9, Num. 4, pp. 569-576, 2002.

[106] M. Sadiku, "Elements of Electromagnetism", Oxford University Press, 1998.

[107] Peter P. Silvester, Ronald L. Ferrari, "Finite Elements for Electrical Engineers", Cambridge University Press; 3 edition, 1996.

[108] A. E. Baker, A.M. Gully, J. C. G. Wheeler, "Finite Element Modeling of Non-liner Stress Grading Materials for Machine End Windings", IEE Conference on Power Electronics, Machines and Drivers, pp. 265-268, 2002.

[109] T. Hara, T. Naito, J. Umoto, "Time-Periodic Finite Element Method for Non-Linear Diffusion Equations", IEEE Trans. on Magnetics Vol. MAG –21, Num. 6, pp. 2261-2264, 1985.

[110] Z. Zheng and S.A. Boggs, "Efficient Solution of Transient Nonlinear Field Problems", IEEE Annual Report CEIDP, pp. 130-133, 2002.

[111] P. Braunlich, Thermally stimulated relaxations in solids (Topics in Applied Physics Vol. 37) (Berlin: Springer), 1979.

[112] E. Neagu and R. Neagu, "The Determination of Relaxation Parameters and Their Distributions using Thermally Stimulated Discharge Current Measurements", J. Phys. D: Appl. Phys. 35, 2002, pp. 8–2303.

[113] C. Bucci, and R. Fieschi, "Ionic Thermocurrents in Dielectrics", Phys. Rev. 148, pp. 816-823, 1966.

[114] S. W. McKeever and E. Lilley, "Thermally Stimulated Polarization and Depolarization Currents (TSPC and TSDC) in LiF: Mg2+ (TLD-100), J. Phys. C: Solid State Phys., 14, 1981, pp. 3547-3555.

[115] R. J. Fleming, "Thermally stimulated conductivity and luminescence in organic polymers", IEEE Transaction on Electrical Insulation, Vol. 24, No. 3, Jun. 1989, pp. 523-532.

[116] M. A. Sussi, and G. Raju, “Depolarization Current in Corona Charged Aromatic Polyamides”, 3rd Int. Conf. On Properties and Application of Dielectric Materials, 12, 1991.

[117] IRIS Power LP, User Manual PD Alert, 2006.

[118] ThermoCAMTM Operator’s Manual, 2001.

[119] Gorur G. Raju, Dielectrics in Electric Fields. Marcel and Dekker, 2003.

[120] DTI Product Brief on High Voltage Pulse Modulators, 2006.

[121] IEC Std. 62068: Evaluation of Electric Stresses Produced by Repetitive Impulses. Part 1: General methods of evaluation of electrical endurance (IEC 98-160 CDV). Part 2: State of the art report (62068-2 (2001-08)).

[122] J. A. Oliver and G. Stone, “Implications for the Amplification of Adjustable Speed Drive Electronic to Motor Stator Winding Insulation”, IEEE Elect. Insul. Mag. Vol. 11, pp. 32-36, 1995.

[123] Y. Shakweh, “Power Devices for Medium Voltage PWM Converters”, Power Engineering Journal, pp. 297-307, Vol. 13, No. 6, Dec. 1999.

[124] F. Guastavino, G. Coletti and E. Toreloo, “Medium Term Aging Characterization of Enamelled Wires for High Frequency Applications”, IEEE Trans. Dielectrics and Electrical Insulation, Vol. 12, pp. 524-529, June 2005.

[125] IEC TR 60034-18-32, “Rotating electrical machines - Part 18: Functional evaluation of insulation systems - Section 32: Test procedures for form-wound windings - Electrical evaluation of insulation systems used in machines up to and including 50 MVA and 15 kV”, 1995.

[126] G. Raju, A. Katebian and S. Z. Jafri, “Breakdown Voltages of Polymers in the Temperature Range 23oC-250oC”, IEEE Trans. Dielectr. Electr. Insul., Vol. 10, pp. 117-127, 2003.

[127] W. G. Cochran, and G. W. Snedecor, Statistical Methods, Iowa State, 6th ed., 1976.

[128] S. U. Haq, S. Jayaram, and E. A. Cherney, "Evaluation of Medium Voltage Enamelled Wire Exposed to Fast Repetitive Voltage Pulses”, IEEE Transactions on Dielectrics and Electrical Insulation, Accepted, In-Press, 2007.

[129] S. U. Haq, and G. G. Raju, "DC Breakdown Characteristics of High Temperature Polymer Films", IEEE Transactions on Dielectrics and Electrical Insulation, Vol. 13, No. 4, Aug. 2007.

[130] J. P. Bellomo, S. Dinculescu, T. Lebey, "Lifetime of Convencional and Corona Resistant Enamels", IEEE Intern. Sympos. Electr. Insul. (ISEI), pp. 173-176, 1998.

[131] F. P. Espino-Cortes, Y. Montasser, S. H. Jayaram, E. A. Cherney and L. C. Simon, "Study of stress grading systems working under fast rise time pulses", IEEE Intern. Sympos. Electr. Insul. (ISEI), pp. 380-383, 2006.

[132] M. Kozako, R. Kido, T. Imai, T. Ozaki, T. Shimizu and T. Tanaka, "Surface roughness change of epoxy/TiO2 nanocomposites due to partial discharges", International Symposium on Electrical Insulating Materials (ISEIM), pp. 661-664, 2005.

[133] M. A. Sussi, Ph.D. Thesis, "Charge Storage and Decay in High Temperature Insulating Materials", 1992.

[134] E. Neagu and D. K. Gupta, "Thermally Stimulated Discharge Current Studies of Corona-Charged Tefzel", IEEE Trans. Electr. Insul., Vol. 24, No. 3, pp. 489-494, 1989.

[135] S. U. Haq, Shesha H. Jayaram, E. A. Cherney and G. Raju, "Charge Injection into Enamelled Wires Studied by Thermally Stimulated Depolarization Current (TSDC)", IEEE-CEIDP, pp. 515-518, 2005.

[136] M. Fu, G. Chen, X. Liu, "Space Charge Behaviour in LDPE after AC Electrical Ageing" Proceedings of the 2004 IEEE Intern. Conf. Solid Dielectrics, ICSD, Vol. 1, pp. 217-220, 2004.

[137] P. Braunlich, Thermally Stimulated Relaxations in Solids, (Topics in Applied Physics Vol. 37), Berlin: Springer, 1979.

[138] L. Ming, E. Martensson, F. Salen, K. Johansson, H. Eriksson, O. Koponen, and S. Paakkonen, "Effects of Repetitive Voltages on Surface Temperature Increase at End Corona Protection Region of High Voltage Motors", 10th INSUCON Conference, pp. 105-108, 2006.

[139] A. H. Bonnet, “A comparison Between Insulation Systems Available for PWM-Inverter-Fed Motors”, IEEE Transactions on Industry Applications, Vol. 33, No. 5, pp. 1331-1341, 1997.

[140] M. J. Melfi, "Low Voltage PWM Inverter Fed Motor Insulation Issues", IEEE PCIC Conference Record, pp. 137-142. Sept 2004.

[141] G. Stone, S. Campbell, S. Tetreault, “INVERTER-FED DRIVES: Which Motor Stators Are at Risk?”, IEEE Ind. Application Magazine, Vol. 6, Issue 5, pp. 17-22, 2000.

[142] M. Kaufhold, G. Borner, and M. Eberhardt, “Failure Mechanism of the Interturn Insulation of Low Voltage Electric Machines Fed by Pulse-Controlled Inverters” IEEE Electr. Insul. Mag., Vol. 12, No. 5, pp. 9-16, 1996.

[143] J. Lewiner, “Evolution of Experimental Techniques for the Study of the Electrical Properties on Insulating Materials”, IEEE Trans. Elect. Insul., Vol. E1-21, No. 3, pp. 351-360, 1986.

[144] Y. Zhang, J. Lewiner, and C. Alquier, “Evidence of Strong Correlation between Space Charge Build-up and Breakdown in Cable Insulation”, IEEE Trans. Dielectr. Electr. Insul., Vol. 3, No. 6, pp. 778-783, 1991.

[145] W. Khachen, and J. R. Laghari, “Polypropyline for High Voltage High Frequency Airborne Applications”, IEEE-ISEI, pp. 80-83, 1990.

[146] K. Zhou, G. Wu, T. Deng, and J. Wu, “Aging Time Effect on PD and Space Charge Behavior in Magnet Wire Ander High PWM Voltajes”, IEEE-ISEI, pp. 159-162, 2006.

[147] D. Fabiani, Accelerated Degradation of AC-Motor Winding Insulation due to Voltage Waveforms Generated by Adjustable Speed Drives, Ph.D. Thesis, University of Bologna, Bologna, Italy, 2002, published by Gedit Edizioni, Bologna, Italy, May 2003.

[148] R. Busch, F. Pohlmann and K. Muller, ‘‘The Influence of Several Environmental Conditions on the Partial Discharge Characteristics and on the Lifetime of Magnet Wires under Invertir Pulse Operation’’, IEEE ISEIM, Himeji, Japan, pp. 645-648, 2001.

[149] T. Jing, Surface charge accumulation in SF6 , Ph.D. Thesis, Delft University Press, Delft, The Netherlands, 1993.

[150] M. Takashima, K. Soda and T. Takada, ‘‘Measurement of Electric Charges at the Interface Between Two Dielectric Layers Using an Electro-acoustic Transducer Technique’’, IEEE Trans. Electr. Insul., Vol. 23, pp. 287-295, 1988.

[151] A. A. Alagiriswamy, K. S. Narayan and G. Raju, “Relaxation Processes in Aromatic Polyamide”, J. Phys. D: Appl. Phys., Vol. 35, pp. 2850-2856, 2002.

[152] E. R. Neagu, J. N. Marat-Mendes, D. K. Das-Gupta, R. M. Neagu, and R. Igreja, “Analysis of the Thermally Stimulated Discharge Current Around Glass-Rubber Transition Temperature in Polyethylene Terephthalate”, Vol. 82, No. 5, pp. 2488-2496, 1997.

[153] R. H. Partridge, Radiation Chemistry of Macromolecules, Vol. 1, ed. M. Dole (New York: Academic) pp. 193-222, 1972.

[154] C. Pientschke, R. Steihausen, A. Kouvatov, H. T. Langhammer, and H. Beige, “Section G: Theory and Modelling, Equivalent Circuit Modelling of the Time-Dependent Poling Behaviour of Ferroelectric Multilayer Structures, Feroelectronics”, No. 319, pp. 180-191, 2005.

[155] G. Raju, Waterloo, Canada, “Personal Communication”, 2006.

[156] G. F. J. Garlick and A. F. Gibson, Proc. Phys. Soc., 60, 1948, 574.

[157] N. Fuse, M. Kozako, T. Tanaka, S. Murase and Y. Ohki, “Possible mechanism of superior partial-discharge resistance of polyimide nanocomposites”, IEEE Conf. Electr. Insul. Dielectr. Phenomena (CEIDP), pp. 322-325, 2004.

[158] M. Kozako, R. Kido, N. Fuse, Y. Ohki, T. Okamoto and T. Tanaka, “Differences in Surface Degradation due to Partial Discharges Between Polyamide Nanocomposites and Microcomposites”, IEEE Conf. Electr. Insul. Dielectr. Phenomena (CEIDP), pp. 398-401, 2004.

[159] A. H. El-Hag, L. C. Simon, S. H. Jayaram, and E. A. Cherney, “Erosion Resistance of Nanofilled Silicone Rubber”, IEEE Trans. Dielectr. Electr. Insul., Vol. 13, pp. 122-128, 2006.

[160] C. Chauvet and C. Laurent, “Weibull Statistics in Short-term Dielectric Breakdown of Thin Polyethylene Films”, IEEE Trans. Electr. Insul., Vol. 28, pp. 18-29, 1993.

[161] L. M. Rux, Ph. D. Thesis, The physical phenomena associated with stator winding insulation condition as detected by the ramped direct high-voltage method, 2004.

[162] A. H. Bonnet, “A comparison Between Insulation Systems Available for PWM-Inverter-Fed Motors”, IEEE Transactions on Industry Applications, Vol. 33, No. 5, pp. 1331-1341, 1997.

[163] M. L. Miller, “Achieving high voltage dielectric breakdown of turbine generator stator coils using capacitors”, IEEE Conference on Electrical Insulation and Dielectric Phenomena, Vol. 1, pp. 339-340, 1998.

[164] D. I. R. Vogelsang, Ph.D. Thesis, Time to Breakdown of High Voltage Winding Insulations with Respect to Microscopic Properties and Manufacturing Qualities, 2004.

[165] J. H. Dymond, N. Stranges, K. Younsi, J. E. Hayward, “Stator Winding Failures: Contamination, Surface Discharge, Tracking”, IEEE Transactions on Industry Applications, Vol. 38, No. 2, pp. 577-583, 2002.

Appendix A: Inter-Turn Model

This section addresses the problems, associated with the inter-turn electric stress of the coils, subjected to PWM-VSC waveforms. For a 4.0 kV_{L-L} form-wound coil, as depicted in Figure A1, the magnet wire has a rectangular shape with smooth and continuous corners, bearing width of 6.51 mm, and a thickness of 2.22 mm. As has been discussed earlier, a SEM illustration of coating on magnet wire is given in Figure A2 for reader convenience. The coating on the magnet wire consists of multiple layers, forming polymer-to-polymer interface. Each layer has a thickness of ~5 μm, which constitutes a total coating thickness of ~40 μm on the magnet wire. This coating thickness varies, depending on the wire type and its application.

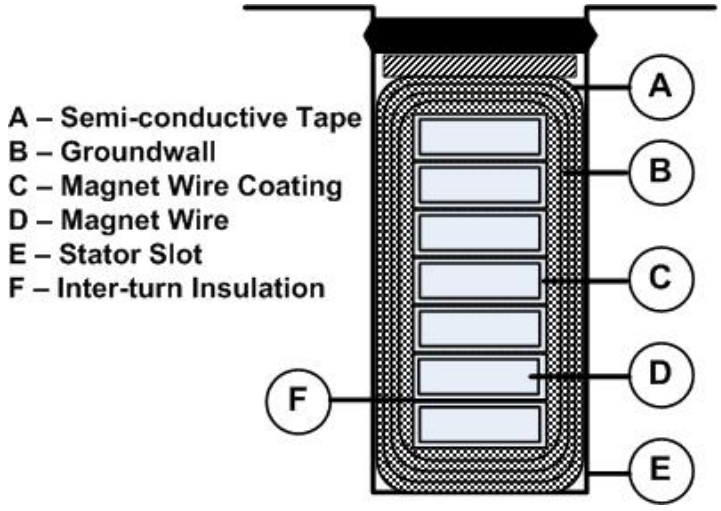

Figure A1: Different insulation systems on a form-wound coil.

Evidences have been provided in the literature regarding the accumulation of space charges in insulation internal and external interfaces, leading to the distortion of the electric field [147,148,149,150]. The accumulation of space charge occurs not only by electrode injection inside the insulation bulk, but also by surface PD activity [147]. The enamelled wires that are exposed to PWM-VSC waveforms can create internal defects between coating interfaces. This process can cause delamination of the insulation, and even peeling

of the insulation from the polyimide layer, which goes through the deterioration process caused due to PD and space charge accumulation.

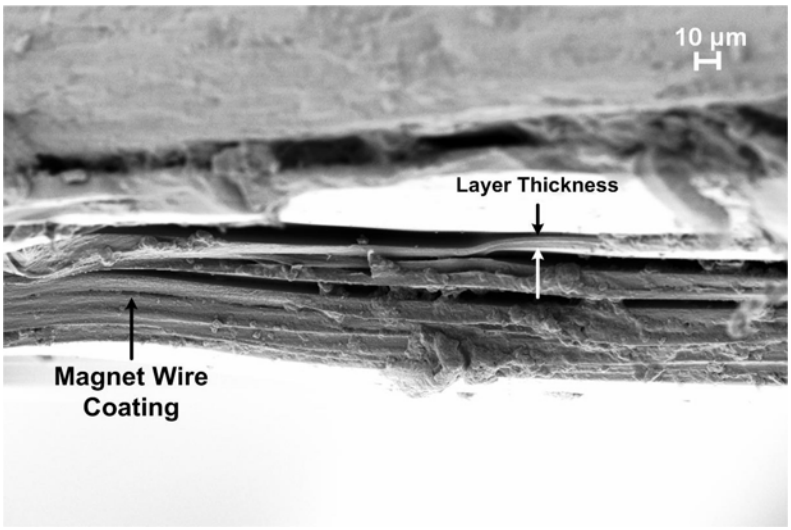

Figure A2: Microscopic picture of a commercial magnet wire S_1 (Mag: 900x).

A1. Numerical Analysis

To analyze the affect of stored charge under the PWM-VSC, the transient FEM with time dependent solver is adopted to analyze the effect of the fast rise time pulses on the inter-turn model, as shown in Figure A3. This model is based on the cross-section shown in Figure A1-(F). In the analysis, to observe the influence of time dependent polling behaviour on electric fields in multilayer insulation system, the coating insulation is considered as polyimide. In addition, no nonlinearities in the material properties and remnant polarizations are considered. Thus, the values of polarization are given in advance in FEM sub-domain menu, during the electric field calculation. In all cases, the bottom conductor is set to zero potential, which is equivalent to a grounded electrode. The voltages with different rise times of 40, 100 and 500 ns are applied, respectively, to the top electrode and considered as transient voltages with steep-fronts, as shown in Figure A4.

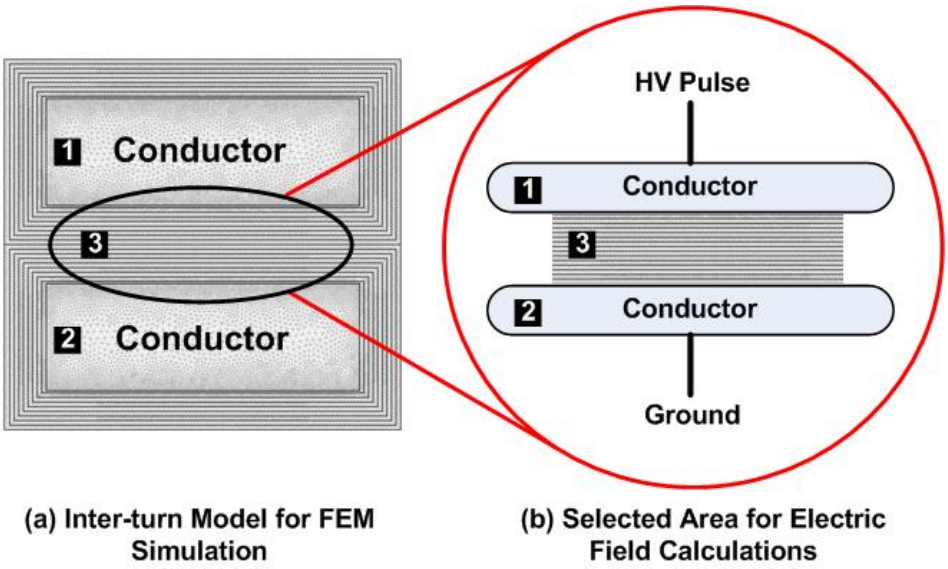

Figure A3: Stator inter-turn model along with the selected area for space charge influenced field calculation; (1) and (2) represent magnet wires, and (3) shows polyimide based multilayer insulation system between consecutive wires.

In order to estimate the electric field perturbation in multiple layers, the derivation of the polarization at different time intervals using constant stress approach is included by using FEM sub-domain menu. The dielectric displacement caused after different aging durations in a magnet wire, is given as [154]:

$$D_x = \varepsilon_o E_x + P_x, (x = 1,2...n) \tag{A1}$$

where x represents different time intervals, ε_o is the permittivity of free space, E is the electric field strength and P is the electric polarization.

The current density J consists of conductive current and the displacement current. TSDC peaks shown in Figure 3.12 are utilized to determine the current densities. At different time intervals, the current density J is composed of:

$$J = J_1 = J_2 = \sigma_1 E_1 + D_1 = \sigma_2 E_2 + D_2 .....J_x = \sigma_x E_x + D_x \tag{A2}$$

The conductivities σ_x are first approximation considered constant with respect to the electric field strength. The combination of Equation (A1) and (A2) will yield the

polarization. Finally, by knowing the parameters listed in Table A1, the field distribution through the multilayer structure can so be calculated for different test conditions.

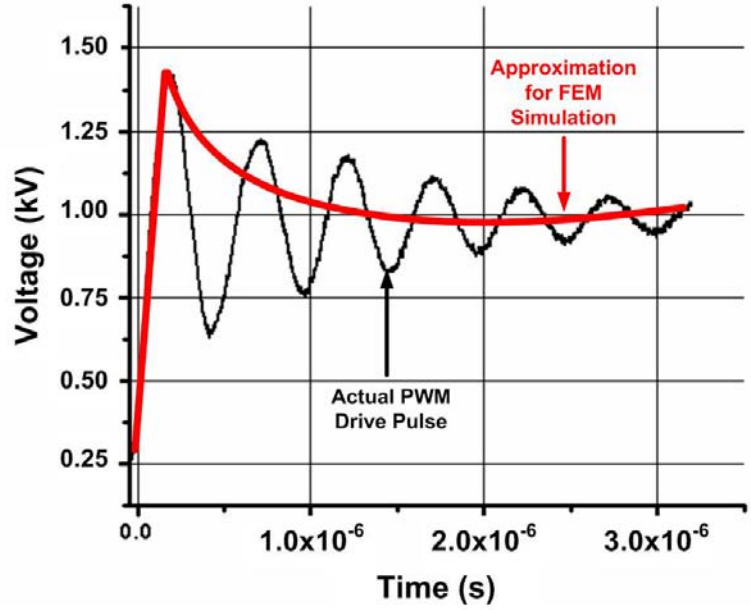

Figure A4: Approximation of measured PWM drive pulse voltage waveform, considered for the transient FEM simulations.

Table A1. Polyimide coated magnet wire (S_1) electrical and physical constants, and parameters for numerical analysis.

Constants and Parameters	Value
Magnet Wire Dimensions (WxD)	6.15x2.22 mm
Number of Coating Layers on Magnet Wire	9
Individual Layer Thickness	~5-7 μm
Time Dependent Polarization	0-172800 s
Dielectric Strength, *E*	345×10^6 [V/m]
Dielectric Constant @ 1 MHz	3.2
Electrical Conductivity, σ	3.4×10^{-15} S/m

The simulation results, illustrated in Figure A5, demonstrate a significant effect on the inter-turn stress due to space charge injection and accumulation with time. For a steep-front voltage pulses with different rise times, increase in the stress distribution are observed with aging duration, which can considerably affect the PDIV [147,148]. However, due to the saturation in the charge concentration, the space charge influenced field is also affected. The gradual increase in the electric field can begin inter-turn insulation degradation by initiating damages to the magnet wire coating, which are in the form of a polymer-to-polymer interface, and eventually the premature failure of the stator insulation can occur.

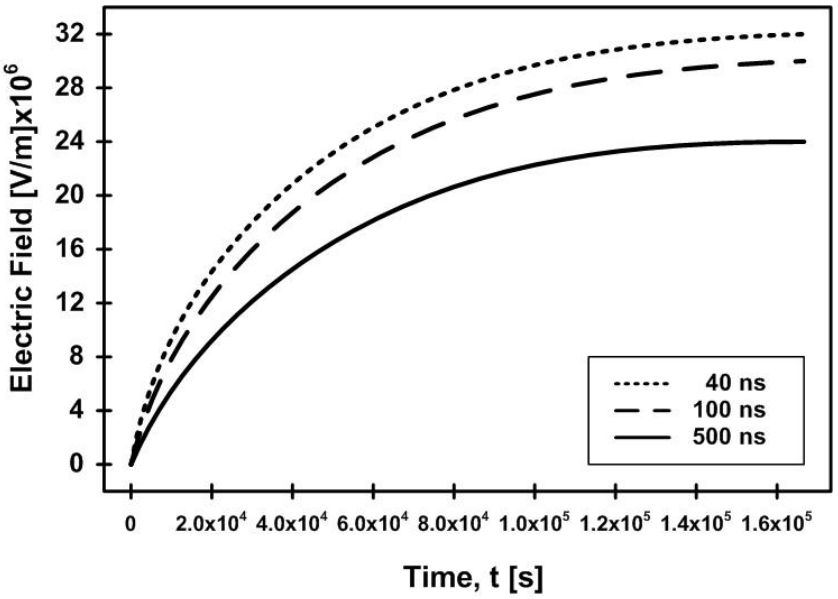

Figure A5: Form-wound stator intern-turn electric field behaviour with time due to space charge accumulation for pulse voltages with different rise times.

Furthermore, the analysis for inter-turn stress was repeated for two different types of magnet wires, having different number of insulation layers, keeping the overall coating thickness constant. The results are illustrated in Figure A6, which confirmed a significant reduction of ~48% in the maximum electric field, for the magnet wire having four layers. This can be attributed to a lower accumulation of space charge during the aging duration and possibly due to fewer number of trap levels. Therefore, the results strongly suggest that a lesser number of insulation layers should be a future goal for the wire manufacturers, to achieve maximum reliability.

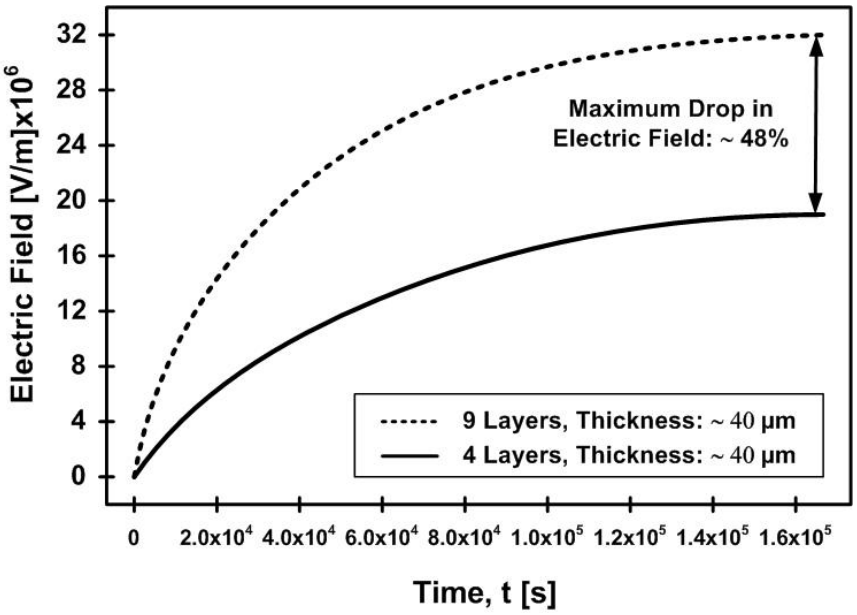

Figure A6: Form-wound stator intern-turn electric field behaviour by reducing the number of layers and keeping the coating thickness constant on magnet wire, for pulse rise time 40 ns.

A2. Influence of Pulse Rise Time

The analysis, illustrated in Figure A7, further demonstrates that the electric field perturbation in the wire insulation can be affected considerably by the supply waveform; especially, with the pulse voltage rise time. As an example, the inter-turn field distribution profile is plotted in Figure A7 by keeping the maximum polarization behaviour constant in the FEM sub-domain. The summarized results clearly indicate that the inter-turn stress decreases significantly as the pulse voltage rise time value increases. A pulse rise time as high as 500 ns reveals quite a large value for the inter-turn stress; whereas, for the value of $t_{rise} \geq 5$ µs, no space charge accumulation effect on the inter-turn stress is observed, and the field remains constant, after this threshold value.

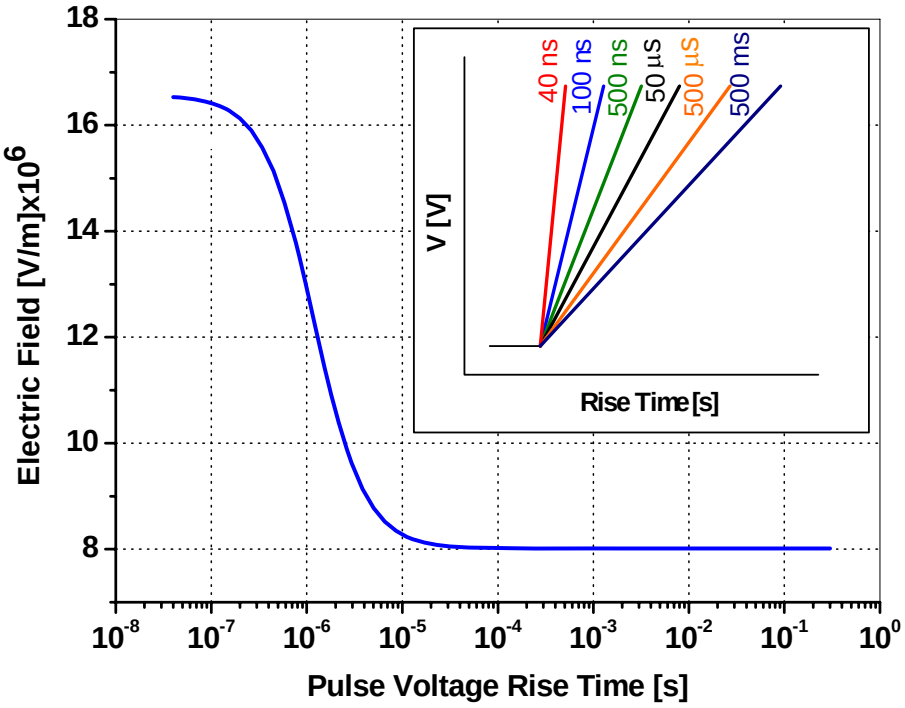

Figure A7: Effect of the pulse voltage rise time on the inter-turn stress distribution.

The investigation based on FEM simulation reveals that the intensity of stored charge is not sufficient to understand the degradation mechanisms. It is also essential to know the influence of stored charge on the electric field distribution inside thin multilayer systems, to understand its damaging effects. Magnet wires having higher number of layers are more susceptible to damage due to accumulation of higher charge concentration and occurrence of remnant polarization in each layer, as describe earlier in Figure A6. In applications, such as PWM-VSC, care should be taken in the selection of wire type to keep the intensity of stored charge at low level, which is vital for the safe operation of the induction motor.

Appendix B: Space Charge Measurements using Pulse Electroacoustic (PEA)

To confirm the charge trapping and injection in the bulk of multi-layer magnet wire coatings, specimens of wire S_1 and S_2 were sent to TECHIMP in Bologna, Italy. To confirm the existence of space charge, pulsed electroacoustic (PEA) technique is used. In this technique, for measurement of space charge, a short electric pulse is applied across the magnet wire specimen. The applied pulse field induces a perturbing force density on the coating material in the presence of resident charges. This force causes the charge to move slightly. This movement generates an acoustic wave that is related to the charge distribution in the specimen. A significant increase in the charge accumulation for magnet wire specimens S_1 and S_2 were observed for durations of 10 to 5000 s. Results for magnet wire specimen S_2 are depicted in Figures B1 and B2.

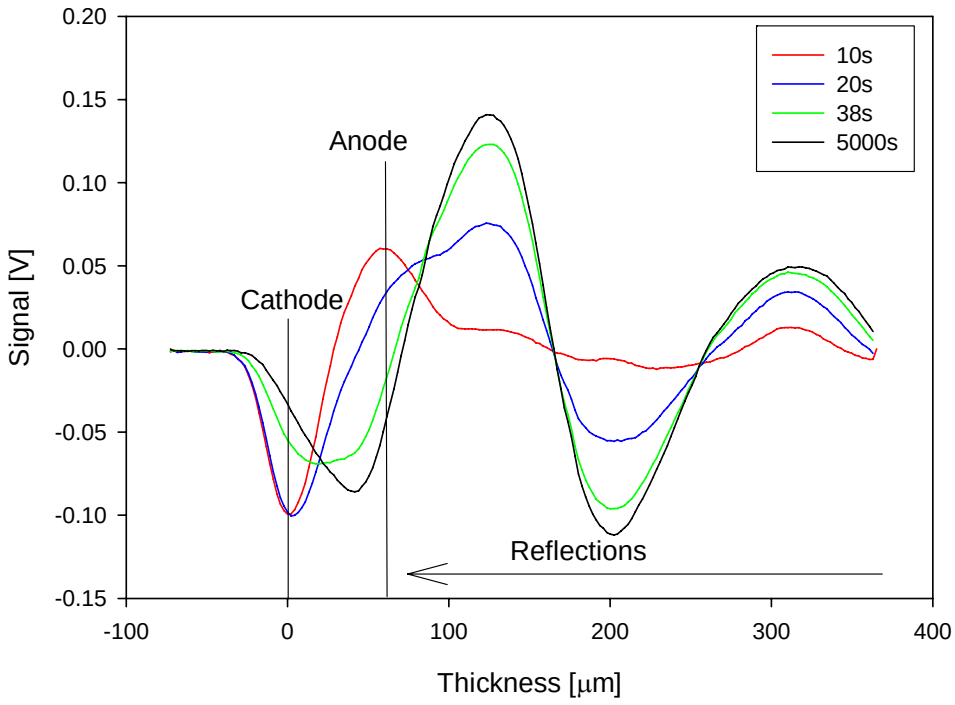

Figure B1: Charge profiles obtained at different polling time for magnet wire S_2 (applied voltage: 1500 V).

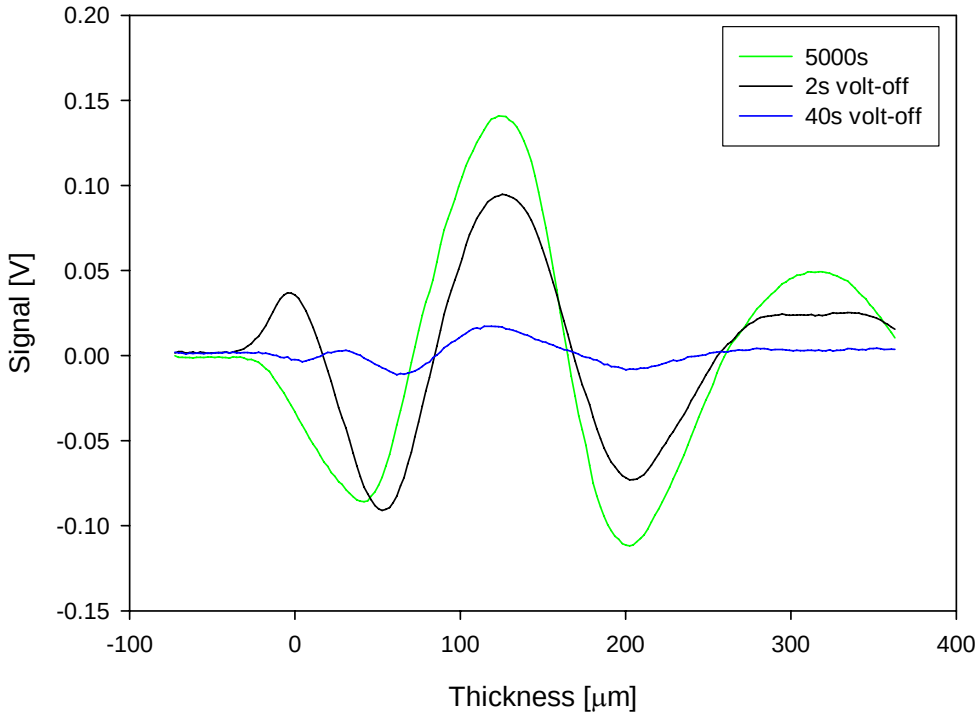

Figure B2: Polarisation and depolarisation (volt-off) charge profiles for magnet wire S_2 (applied voltage 1500 V).

Appendix C: List of Publications

C1 Papers in Refereed Journals

1. S. Ul Haq, Shesha H. Jayaram, and Edward A. Cherney, "Performance of Nanofillers in Medium Voltage Magnet Wire Insulation under High Frequency Applications", IEEE Transactions on Dielectrics and Electrical Insulation, Vol. 14, No. 2, pp. 417-426, 2007.
2. S. Ul Haq, Shesha H. Jayaram, and Edward A. Cherney, "Evaluation of Medium Voltage Enamelled Wire Exposed to Fast Repetitive Voltage Pulses" IEEE Transactions on Dielectrics and Electrical Insulation, Vol. 14, No. 1, pp. 194-903, 2007.
3. S. Ul Haq, Shesha H. Jayaram, and Edward A. Cherney, "Space Charge Accumulation in Induction Motor Magnet Wire: A New Measurement Approach", IEEE Transaction on Energy Conversion, Vol. 22, No. 2, April-June, 2007.
4. S. Ul Haq, and Gorur G. Raju, "DC Breakdown Characteristics of High Temperature Polymer Films", IEEE Transactions on Dielectrics and Electrical Insulation, Vol. 13, No. 4, pp. 917-926, 2006.
5. S. Ul Haq, Shesha H. Jayaram, Edward A. Cherney, and Gorur G. Raju, "Analysis of Space Charge and Dielectric Relaxation in Medium Voltage Magnet Wires by using Thermally Stimulated Depolarization Currents (TSDC)", Selected for Journal of Electrostatics, Submitted, 2006.

C2 Papers in Refereed Conferences

1. S. Ul Haq, Shesha H. Jayaram, and Edward A. Cherney, "Experimental Study of Space Charge Influenced Field in Motor Enamelled Wires", Electrostatics Society of America, Annual Meeting, June, 2007.
2. S. Ul Haq, Shesha H. Jayaram, and Edward A. Cherney "Insulation Problems in Medium Voltage Stator Coils under Fast Repetitive Voltage Pulses", 53rd IEEE Pulp and Paper Industry Technology Conference, June, 2007.
3. S. Ul Haq, Shesha H. Jayaram, and Edward A. Cherney, "Evaluation of Medium Voltage Stator Bar Groundwall Insulation under Inverter-Fed Pulses", IEEE CEIDP, pp. 465-468, Oct. 2006.
4. S. Ul Haq, Shesha H. Jayaram, and Edward A. Cherney, and Gorur G. Raju, "Analysis of Space Charge and Dielectric Relaxation in Medium Voltage Magnet Wires by using Thermally Stimulated Depolarization Currents (TSDC)", ESA/IEEE-IAS/IEJ/SFE Joint Conference on Electrostatics, Vol. 2, pp. 655-664, June, 2006
5. S. Ul Haq, Shesha H. Jayaram, Edward A. Cherney and L. C. Simon, "Partial Discharge Erosion in Filled Enameled Wires Subjected to High Frequency Waveforms", IEEE International Symposium in Electrical Insulation ISEI, Toronto, Ontario, pp. 396-399, June, 2006.
6. S. Ul Haq, Shesha H. Jayaram, and Edward A. Cherney, Aging Characterization of Medium Voltage Groundwall Insulation Intended for PWM Applications", IEEE International Symposium in Electrical Insulation ISEI, Toronto, Ontario, pp. 143-146, June, 2006.
7. S. Ul-Haq, Shesha H. Jayaram, Edward A. Cherney, and Gorur G. Raju, "Charge Injection into Enamelled Wires Studied by Thermally Stimulated Depolarization Current (TSDC)", IEEE CEIDP, pp. 515-518, Oct. 2005.

8. S. Ul Haq, Shesha H. Jayaram, and Edward A. Cherney "Evaluation of Medium Voltage Groundwall Insulation Exposed to High Frequency Pulse Voltages", IEEE Electrical Insulation Conference and Electrical Manufacturing Expo, pp. 194-197, Oct. 2005.
9. S. Ul Haq, Shesha H. Jayaram, and Edward A. Cherney "Degradation of Turn Insulation Subjected to Fast Repetitive Voltage Pulses", IEEE Electrical Insulation Conference and Electrical Manufacturing Expo, pp. 163-166, Oct. 2005.
10. S. Ul-Haq, S. H. Jayaram, and Edward A. Cherney "Degradation of Stator Winding Insulation under Steep-Fronted Voltage Pulses", Electrostatics Society of America, Annual Meeting, pp. 160-167, June, 2004.

C3 Non-refereed Presentations

1. S. Ul Haq, "High Voltage Insulation and Pulse Power Applications Research", Presented to the Department of Electrical and Computer Engineering, University of Waterloo, Waterloo, ON, November, 2006.
2. S. Ul Haq, Shesha H. Jayaram, Edward A. Cherney "Evaluation of Medium Voltage Groundwall Insulation under Pulse Applications", CAGE Club Student Conference on High Voltage Engineering and Electrostatics, University of Western Ontario, London, ON, August, 2006.
3. S. Ul Haq, Shesha H. Jayaram, and Edward A. Cherney, "Microscopic Analysis of Nanoparticles Distribution and Performance in Magnet Wire Coatings", Ontario Nano Symposium, University of Waterloo, Ontario, page. 16, May 2006.
4. S. Ul Haq, "Role of Nanofillers in Medium Voltage Magnet Wires Intended for PWM Applications", Graduate Talks, Department of Electrical and Computer Engineering, University of Waterloo, Waterloo, ON, July, 2006.

5. S. Ul Haq, Shesha H. Jayaram, and Edward A. Cherney, "Short-Term Aging Test Technique for Medium Voltage Enamelled Wires" 6th Annual Graduate Student Research Conference, University of Waterloo, Waterloo, Ontario, April, 2006.

6. S. Ul Haq, "A Study on Insulation Problems in Drive Fed Medium Voltage Induction Motors", Presented at General Electric Peterborough, ON, Canada, January, 2006.

7. S. Ul Haq, Shesha H. Jayaram, Edward A. Cherney "Evaluation of Medium Voltage Magnet Wires with Single and Multi-Layer Insulation under High Frequency Waveforms", CAGE Club Student Conference on High Voltage Engineering and Electrostatics, McMaster University, ON, August, 2005.

8. S. Ul Haq, Shesha H. Jayaram, Edward A. Cherney, "Evaluation of Inverter-Duty Motor Insulation System using Partial Discharge and Space Charge Measurements", 5th Annual Graduate Student Research Conference, University of Waterloo, Waterloo, Ontario, April, 2005.

9. S. Ul Haq, Shesha H. Jayaram, Edward A. Cherney "Insulation Aging in Form Wound Stator Winding Exposed to Inverter Drives", CAGE Club Student Conference on High Voltage Engineering and Electrostatics, University of Toronto, Toronto, ON, August, 2004.

10. S. Ul Haq and M. Kazerani, "Energy Management Strategy in Hybrid Electric Vehicles (HEVs)", 4th Annual Graduate Student Research Conference, University of Waterloo, Waterloo, Ontario, March 31-April 2nd, 2004.